Complexity of the 2009 L'Aquila earthquake causative fault system (Abruzzi Apennines, Italy) and effects on the Middle Aterno Quaternary basin arrangement

Pucci, S. [1]*, F. Villani[2], R. Civico[1], D. Di Naccio[2], M. Porreca[3,1], L. Benedetti[4], A. Gueli[5], G. Stella[5], P. Baccheschi[1], D. Pantosti[1]

[1] Istituto Nazionale di Geofisica e Vulcanologia, Via di Vigna Murata 605, 00143 Rome, Italy, e-mail: stefano.pucci@ingv.it

[2] Istituto Nazionale di Geofisica e Vulcanologia, Viale Crispi 43, 67100 L'Aquila, Italy

[3] Dipartimento di Fisica e Geologia, Università degli Studi di Perugia, Piazza dell'Università 1, 00143 Perugia, Italy,

[4] Aix-Marseille Université, CEREGE CNRS-IRD UMR 34, Aix en Provence, France.

[5] PH3DRA labs, Dipartimento di Fisica e Astronomia dell'Università & INFN CT, via Santa Sofia 64, 95123 Catania, Italy

*Corresponding author

Keywords: Quaternary extensional basin; continental stratigraphy; alluvial fan; earthquake; central Apennines; Active tectonics

Abstract

An Mw 6.1, devastating earthquake, on April 6, 2009, struck the Middle Aterno Valley (Abruzzi Apennines, Italy) due to the activation of a poorly known normal fault system. Structural analysis of the fault population and investigation of the relationships with the Quaternary continental deposits through integrated field and laboratory techniques were conducted in order to reconstruct the long-term, tectono-sedimentary evolution of the basin and hypothesize the size of the fault segment.

A polyphasic evolution of the Middle Aterno Valley is characterized by a conjugate, ~E-W- and ~N-S-striking fault system, during the early stage of basin development, and by a dip-slip, NW-striking fault system in a later phase.

The old conjugate fault system controlled the generation of the largest sedimentary traps in the area and is responsible for the horst and graben structures within the basin. During the Early Pleistocene the E-W and N-S system reactivated with dip-slip kinematics. This gave rise to intra-basin bedrock highs and a significant syn-tectonic deposition, causing variable thickness and hiatuses of the continental infill.

Subsequently, since the end of the Early Pleistocene, with the inception of the NW-striking fault system, several NW-strands linked into longer splays and their activity migrated toward a leading segment affecting the Paganica-San Demetrio basin: the Paganica-San Demetrio fault alignment.

The findings from this work constrain and are consistent with the subsurface basin geometry inferred from previous geophysical investigations. Notably, two major elements of the ~E-W- and ~N-S-striking faults likely act as transfer to the nearby stepping active fault systems or form the boundaries, as geometric complexities, that limit the Paganica-San Demetrio fault segment overall length to 19±3 km. The resulting size of the leading fault segment is coherent with the extent of the 6 April 2009 L'Aquila earthquake causative fault.

The positive match between the geologic long-term and coseismic images of the 2009 seismogenic fault highlights that the comprehensive reconstruction of the deformation history offers a unique contribution to the understanding faults seismic potential.

1. Introduction

On April 6, 2009, a strong earthquake (Mw 6.1 according to: Pondrelli et al., 2010; Scognamiglio et al., 2010; Herrmann et al., 2011) struck the Middle Aterno Valley (Abruzzi Apennines, Italy) and was

felt in a wide area of central Italy (Fig. 1). Due to its shallow hypocentral depth (~9 km) and proximity to the historical town of L'Aquila (population of about 70,000), this earthquake caused heavy damage in a 500 km^2 area, resulted in 309 fatalities, thousands of injured and tens of thousands homeless.

The seismic source parameters derived from the analysis of the last seismic 2009 event (e.g. geodetic displacement field, surface faulting pattern, high-resolution aftershocks relocation, strong motion data inversion, etc.; e.g. Atzori et al. 2009, EMERGEO Working Group 2010, Cirella et al. 2012, Valoroso et al. 2013) may not reveal the actual seismic potential of the causative fault. Often, based on the concept of characteristic earthquake model (Schwartz and Coppersmith, 1984) it is assumed that a strong earthquake is representative of the true seismic potential of the fault, assuming the fault behaviour being nearly constant in terms of magnitude. Such simplified interpretation does not take into account possible partial fault activation, non-uniform slip accumulation and possible fault interaction. Indeed, the 2009 earthquake stimulated a scientific debate on the segmentation of the causative fault, in particular on the maximum possible extent of the rupture length and on its capability to involve multiple fault systems along the Middle Aterno Valley (hereinafter MAV) (e.g. Galli et al., 2011; Lavecchia et al., 2012; Moro et al. 2013; Blumetti et al., 2013). At present, the available Holocene paleo-earthquake records (i.e. paleoseismological data) in the Apennines cannot resolve the possible complex behaviour of the overall fault structure (e.g. Galli et al., 2008; Benedetti et al., 2013; Cowie et al., 2017) and its segmentation.

Recent works following the 2009 seismic sequence (Cinti et al., 2011; Galli et al. 2011; Giaccio et al., 2012; Gori et al., 2012; Lavecchia et al., 2012; Moro et al., 2013; Villani et al., 2015; Civico et al., 2015; Blumetti et al., 2013 and 2017) propose quite different and, sometimes, conflicting interpretations of the L'Aquila earthquake causative fault-system boundaries. Detailed geological data can help to mark the permanent fault segments boundaries by identifying at the surface km-scale structural complexities able to facilitate or hamper rupture propagation (see Pizzi and Galadini, 2009; Scholz and Gupta, 2000) and act as barriers (e.g. Wesnousky, 2006 and 2008). The relationship between the geological long-term and the

coseismic fault expression well contributes to the understanding of its behaviour at depth and of the most likely factors promoting the rupture arrest. Although the 2009 earthquake represent a unique opportunity to test this approach, very few high-resolution 'classical' geological studies (e.g. Giaccio et al., 2012; Lavecchia et al., 2012) focussing on the 2009 fault segmentation were published.

The aim of this study is to provide new insights on the structural heterogeneities and on the internal organization of the fault system responsible for the 2009 L'Aquila earthquake, via a high-resolution geological investigation and to investigate the persistent, long-term segment boundaries setting to be compared with the exceptional wealth of multidisciplinary observations on the 2009 coseismic source. The understanding of the Quaternary evolution of the L'Aquila earthquake causative fault system can improve the characterization of the permanent and not-permanent segment boundaries of the fault system.

For this purpose, we analyse the role of faulting in the arrangement of the continental basin infill (Blair and Mc Pherson, 1994; Gawthorpe and Leeder, 2000; Harvey, 2002; Viseras et al., 2003; Allen and Allen, 2005) and investigate the timing of syn-sedimentary evolution during the Quaternary. We first performed a detailed structural analysis to characterize the geometry, kinematics and paleostress of the faults population, and to define the relationships between the observed fault systems through a slip-tendency and crosscut analysis. Then, we collected data on the continental depositional bodies, supported by dating, and reconstructed the relationship between the geomorphic features and deposits distribution evolution to estimate the tectonic activity of the fault systems and its Quaternary evolution. Finally, we individuated the major splays composing the fault segment and discuss its permanent boundaries to be compared with the 2009 L'Aquila earthquake coseismic deformation (both near-fault and far field).

2. Geological background

2.1 Tectonic setting

The study area is located in the axial part of the central Apennines of Italy, a Neogene northeast-verging fold-and-thrust belt (Fig. 1a). The Apennines underwent multi-phased contractional and extensional deformation (see Carminati and Doglioni, 2012 for a review). The Late Miocene-Early Pliocene compressive tectonics (Cipollari and Cosentino, 1995; Vezzani et al., 2010) affected a Meso-Cenozoic marly-carbonatic marine multi-layer, which developed into different paleogeographic domains during Jurassic extensional phases: the Umbria-Marche basinal domain to the North, and the Latium-Abruzzi platform/margin domain to the south (Ciarapica & Passeri, 2002; Butler et al., 2006, Centamore et al., 2006). The post-orogenic, Pliocene-Quaternary extensional tectonics was superimposed on this complex structural setting, reactivating older normal and thrusts faults (Tavarnelli, 1999) or pre-existing cross-structures (Chiaraluce et al., 2005; Pizzi and Galadini, 2009; Di Domenica et al., 2014). All this resulted in a complicated network of 15-35 km-long, mainly NW-SE trending and SW-dipping active normal fault systems, which accommodate 1–3 mm/a of regional extension rates (Hunstad, 2003; D'Agostino et al., 2011; Devoti et al., 2011; Carafa and Bird, 2016) along a ~N225° direction (Bagh et al., 2007; Faure Walker et al., 2010; Montone et al., 2012 and references therein). Several intramontane basins infilled with Plio-Quaternary continental deposits developed in the hangingwall of these normal faults systems (among the others: Cavinato and De Celles, 1999, Bosi et al., 2003; Galli et al., 2010; Giaccio et al., 2012; Pucci et al., 2015 and 2016; Porreca et al., 2016), among them, the MAV.

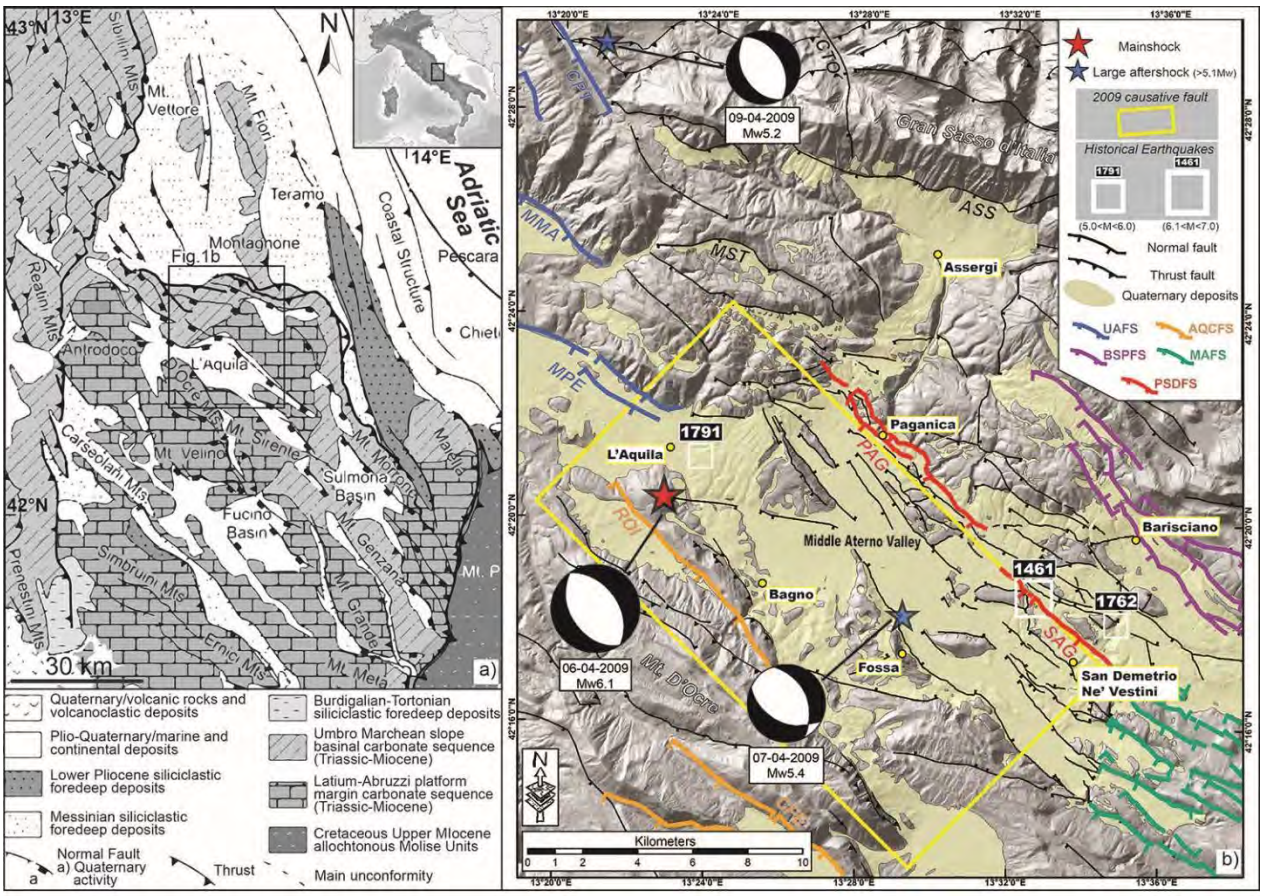

Fig. 1

Figure 1. a) Simplified geological map of the Central Apennines (modified after Di Domenica et al., 2012). The inset shows the location of the study area. b) Scheme of the spatial relationship among the fault systems of the study area. The main fault systems are coloured: Upper Aterno (UAFS - blue); Aquila-Campo Felice (AQCFS - orange); Barisciano-San Pio (BSPFS - violet); Middle Aterno (MAFS - green). The two main sections of the Paganica-San Demetrio fault system (PSDFS) are shown in red: the Paganica (PAG) and San Giovanni (SAG) faults (simplified from Civico et al., 2015). Other faults noted in the text are labelled (Capitignano Fault, CPT; Monte Marine Fault, MMA; Monte Pettino Fault, MPE; Campotosto Fault, CTF; Monte Stabiata Fault, MSF; Assergi Fault, AF; Roio Fault, ROI; Campo Felice Fault, CFE). The location of the 2009 L'Aquila seismic sequence mainshocks are shown along with their focal mechanisms (http://cnt.rm.ingv.it/tdmt). White squares indicate the historical earthquakes. The yellow box represents the average surface projection of the 2009 seismic source (see a review in Chiaraluce, 2012; Vannoli et al., 2012). DEM from 10m-resolution TIN-Italy (Tarquini et al., 2017).

2.2 The 2009 L'Aquila earthquake and its seismotectonic framework

Seismologic and geodetic data depict the Mw 6.1 April 6, 2009 mainshock causative fault as a NW–SE oriented, 14-18 km long, SW–dipping normal fault (Fig. 1b). The aftershocks sharply image the causative fault, at depths below 4 km, whereas, above, they are broadly diffused (Chiaraluce et al., 2011a; Valoroso et al., 2014, 2013). After a few days, seismicity migrated northward up to the Laga Mountains Fault System (LMFS) (Chiarabba et al., 2009), while to the south the seismic activity remained confined at the southeastern boundary of the MAV Quaternary continental basin (fig. 1b).

The 2009 coseismic ruptures reached the surface along the eastern margin of the MAV, along the NW-striking Paganica Fault (PAG), forming a 3 km-long continuous primary surface rupture with maximum throws of 0.15 m at the base of a long-term, cumulative tectonic scarp (Guerrieri et al., 2010; EMERGEO Working Group, 2010; Vittori et al., 2011). The estimate of the overall length of the surface rupture, when including also secondary breaks, is still debated among the authors, and ranges from ~13 km (Boncio et al., 2010; Gori et al., 2012) to ~20 km (Galli et al., 2009). The mainshock geodetic deformation field (Anzidei et al., 2009; Atzori et al., 2009; Papanikolaou et al., 2010; Trasatti et al., 2011) shows up to 0.25 m of coseismic subsidence in the hangingwall of the PAG, in the NW portion of the MAV and in agreement with the primary surface ruptures (Fig. 1).

Frequent upper crustal seismicity affects this sector of the mountain belt (Chiarabba et al., 2005; Bagh et al., 2007; Pondrelli et al., 2010; Rovida et al., 2016) that was repeatedly hit by destructive earthquakes also in the past, as highlighted by historical and paleoseismological records (e.g. 1461 Mw 6.5, 1703 Mw 6.7, 1762 Mw 5.5 and 1791 Mw 5.3 earthquakes -Mw = derived from macroseismic intensities; Rovida et al., 2016; Galli et al., 2010 and 2011; Cinti et al., 2011; Moro et al., 2013) (Fig. 1b).

Responsible for these large earthquakes are several active normal fault systems that dissect this part of the Apennines (Galadini and Galli, 2000; Boncio et al., 2004b; Roberts and Michetti, 2004; Galli et al., 2008; Benedetti et al., 2013, and references therein) (see Fig. 1b colour coded fault systems).

More recently, a detailed mapping and geophysical investigations of the Paganica–San Demetrio Fault-System (hereinafter PSDFS) (Improta et al., 2012; Pucci et al., 2015; Pucci et al., 2016; Civico et al., 2017) show a compound Quaternary extensional fault-system bounding the MAV, consisting of several, closely spaced NW-striking synthetic and antithetic splays(Fig. 1b). Based on those studies, the PSDFS comprises two main sections: 1) the northern section, characterized by the Paganica narrow deformation zone (about 3 km wide) with a relatively small Quaternary basin; 2) the southern section, characterized by a set of parallel, km-spaced fault splays that exhume and dissect the wider San Demetrio ne' Vestini Quaternary basin.

According to some authors, the principal collinear fault strands of the two sections (*i.e.* the PAG and the San Giovanni –SAG- faults, respectively) are hard-linked as a single, ~19 km-long segment (Cinti et al., 2011; Galli et al. 2011; Giaccio et al., 2012; Lavecchia et al., 2012; Civico et al., 2015; Blumetti et al., 2013 and 2017), conversely other authors suppose they are two independent faults (Gori et al., 2012; Moro et al., 2013) (Fig. 1b). Geomorphological, geophysical and paleoseismic trenching data support the evidence on both sectors of the PSDFS of very recent faulting affecting the continental basin infill (Cesi et al., 2010; Balasco et al., 2011; Giaccio et al., 2012; Villani et al., 2015; Pucci et al., 2016; Blumetti et al., 2017; Civico et al., 2017; Villani et al., 2017): the resulting cumulative tectonic escarpments were built up by surface-rupturing earthquakes affecting alternately either the whole PSDFS length or smaller sections (as during the 2009 earthquake) (Cinti et al. 2011). Conversely, Gori et al. (2012) and Falcucci et al. (2015), adopting a scheme earlier proposed by D'Agostino et al. (1998), consider the normal faults of the PSDFS southern section as very shallow structures, rooted on the Gran Sasso thrust, with no seismogenic role or, alternatively, as the northernmost strands of the MAFS located to the south.

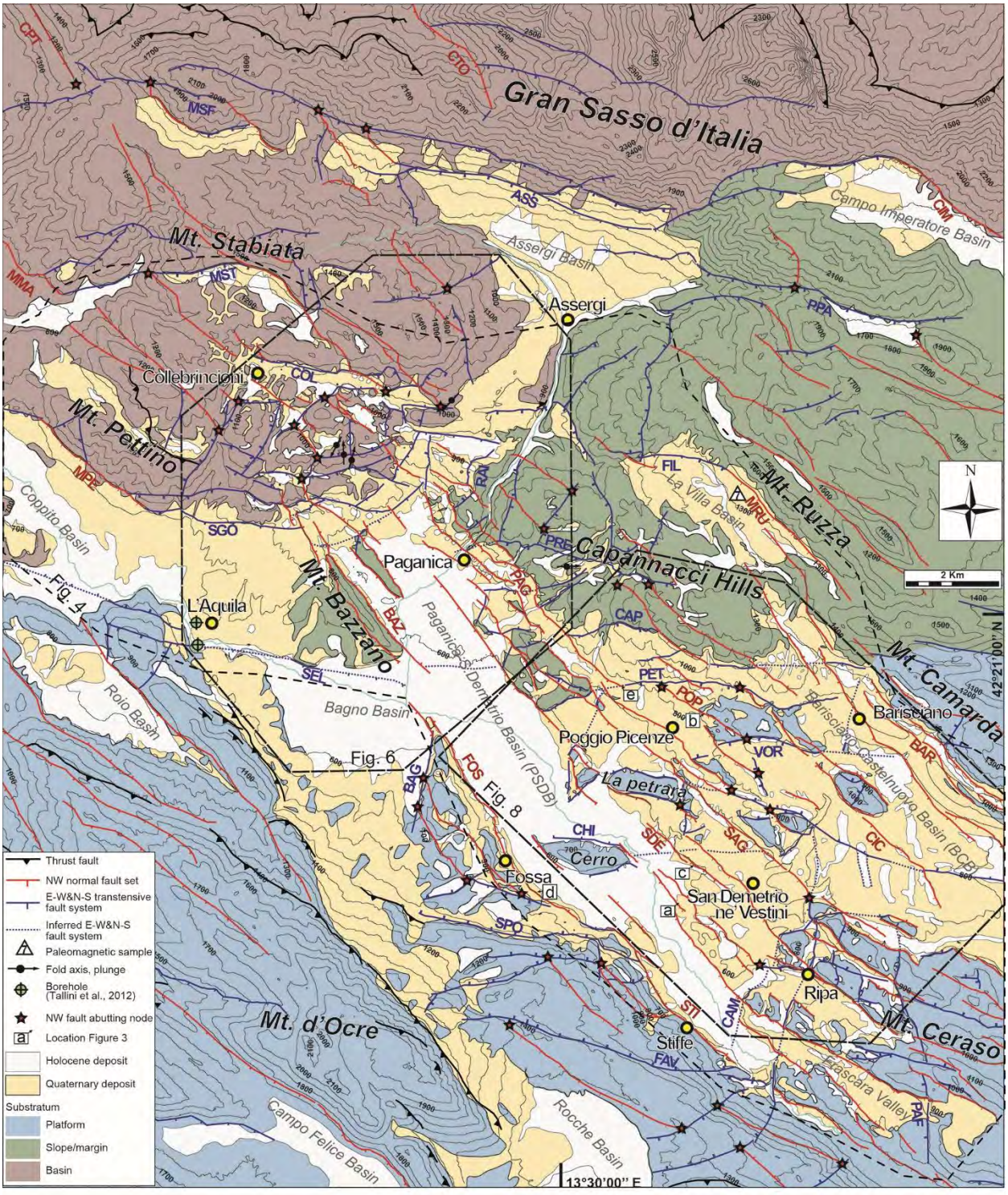
Gran Sasso d'Italia
Mt. Stabiata
Mt. Pettino
Mt. Bazzano
Mt. d'Ocre
Mt. Ruzza
Mt. Camarda
Mt. Ceraso
Capannacci Hills
Assergi
Collebrincioni
Paganica
L'Aquila
Poggio Picenze
Barisciano
La petrara
Fossa
Cerro
San Demetrio ne' Vestini
Ripa
Stiffe
Assergi Basin
Campo Imperatore Basin
La Villa Basin
Coppito Basin
Roio Basin
Bagno Basin
Paganica-San Demetrio Basin (PSDB)
Barisciano-Castelnuovo Basin (BCB)
Campo Felice Basin
Rocche Basin
Fig. 4
Fig. 6
Fig. 8
CPT
CTO
MSF
ASS
CIM
MMA
MST
PPA
COL
MPE
SGO
RAI
FIL
MRU
PRE
PAG
BAZ
CAP
SEL
PET
POP
VOR
BAR
FOS
BAG
CHI
SDE
SAG
CIC
SPO
STI
CAM
FAV
FAF
N
2 Km
42°21'00" N
13°30'00" E
Thrust fault
NW normal fault set
E-W&N-S transtensive fault system
Inferred E-W&N-S fault system
Paleomagnetic sample
Fold axis, plunge
Borehole (Tallini et al., 2012)
NW fault abutting node
Location Figure 3
Holocene deposit
Quaternary deposit
Substratum
Platform
Slope/margin
Basin

173 Fig. 2

Figure 2. Structural map of the study area (modified after Pucci et al., 2015). The NW- trending normal faults are in red, the conjugated W- and N-trending normal faults are in blue. The faults noted in the text are labelled. The three main substratum domains are also indicated with different colours (from Centamore et al., 2006). Boreholes of Tallini et al. (2012) are reported. Stars indicate the most prominent abutting nodes of NW-trending on W- or N-trending faults. The location of the presented Quaternary alluvial deposits, northern and central-southern sectors are outlined.

2.3 The Quaternary Middle Aterno (MAV) Basin

The region is characterized by intramontane tectonic depressions, hosted in the hangingwall of normal faults (Bagnaia et al., 1992; Bertini and Bosi, 1993; Santo et al., 2014). These basins are infilled by continental deposits that unconformably overlay the Meso-Cenozoic carbonate substratum (Fig. 2). Among them, the MAV is a compound Quaternary basin, WNW-ESE elongated, connected through the drainage network to several smaller, satellite basins (e.g. Assergi, Stabiata, Collebrincioni, La Villa, Frascara basins) (Fig. 1). The MAV present-day physiographic continuity, locally interrupted by some intra-basin bedrock highs (e.g. Mt. Bazzano, Mt. Cerro, La Petrara; Fig. 2), results from the coalescence of several smaller sub-basins: the Coppito, Bagno, Paganica-San Demetrio (hereinafter PSD) and the Barisciano-Castelnuovo (hereinafter BC) sub-basins (Fig. 1 and 2).

The western side of the PSD sub-basin is flanked by the Mt. Bazzano and the Fossa-Stiffe ridge, which is controlled by two aligned, NE-dipping main faults (BAZ and FOS faults). Conversely, the eastern side of the PSD and BC sub-basin is bounded by a prominent flight of fault scarps affecting the Quaternary deposits, from 550 m up to > 850 m above sea level (a.s.l.) (Fig. 2).

The Quaternary infill exhibits isolated depocentres, with a thickness up to 500-600 m-deep (Pucci et al., 2016, Civico et al., 2017), increasing from Paganica to Poggio Picenze and San Demetrio areas. It is composed of two main continental sequences with large unconformities and hiatuses (Bosi et al., 2003): 1) the L'Aquila (including the Coppito and Bagno sub-basins) and 2) the PSD and BC sub-basins units.

2.3.1 *The L'Aquila units*

Several Late Pliocene-Pleistocene, unconformity-bounded informal units have been distinguished (GE.MI.NA., 1963; Messina et al., 2001; Gruppo di Lavoro MS–AQ, 2010; Tallini et al., 2012). From the bottom to the top, they are as follows:

1) Alluvial to lacustrine sequence, 150-250 m-thick, composed of: 1a) a lower, 40-60 m thick, alluvial fan and fluvial sands, gravels, conglomerates and pelites (Amoroso et al., 2010; named "Pianola" by Bosi et al., 2003) older than 1.77 Ma (from paleomagnetic analysis and stratigraphical correlations; Messina et al., 2001); 1b) an upper, up to 200 m thick, lacustrine-palustrine clayey-sandy-lignitiferous unit (named "Scoppito-Madonna della Strada" – SMS Fm.; Bosi et al., 2003), 1.3-1.1 Ma in age (from paleo-botanic and mammal biochronological data; Magri et al., 2010; Palombo et al., 2010; Mancini et al., 2012).

2) Mass-wasting (debris-flow to rock-avalanche) breccias and calcareous gravels, up to 90 m thick, composed of variably-cemented calcareous cobbles and boulders from the basinal substratum facies. According to Tallini et al. (2012), they are partially heteropic with the uppermost levels of the SMS Fm., conversely, according to borehole data (Bertini and Bosi, 1993; Gruppo di Lavoro MS–AQ, 2010), they are locally deposited below the SMS. This unit is named "L'Aquila Breccia" in this paper (LAB Fm.) and its age is still matter of debate: according to Messina et al. (2001) it is >0.78 Ma old (from paleomagnetic analysis); GE.MI.NA. (1963) and Gruppo di Lavoro MS-AQ (2010) ascribe it to the Pliocene.

3) Complex of colluvium and alluvial terraced deposits, locally interfingered with calcareous tufa, Middle to Late Pleistocene age (Magri et al., 2010; Palombo et al., 2010; Tallini et al., 2012).

4) Alluvial and colluvial deposits, Latest Pleistocene-Holocene, mostly related to the Aterno River system.

2.3.2 *The Paganica-San Demetrio and Barisciano-Castelnuovo sub-basins*

Most of the authors (Bosi and Bertini, 1970; Bertini and Bosi, 1993; Bosi et al., 2003; Giaccio et al., 2012; Pucci et al., 2015) agree that the infill of the PSD and northern BC sub-basins, can be referred to three main unconformity-bounded units: 1) the Lower Syntheme, of fluvial-lacustrine environment (Early Pleistocene-earliest Middle Pleistocene), which represents the most voluminous and widespread Quaternary sedimentary unit in the PSD basin; 2) the Upper Syntheme, of fluvial environment (Middle Pleistocene); 3) the Late Syntheme, of fluvial-alluvial environment (Middle-Late Pleistocene to present).

The Lower Syntheme includes facies of both distal and proximal basin depositional environments that belong to a single cycle of basin infilling, from bottom to top: a) alluvial fan conglomerates and slope-derived carbonate breccias, locally well-cemented, up to 100 m thick (Valle Valiano Fm. – VVC/VVB), topped by Early Pleistocene carbonate breccias with red matrix (Fonte Vedice Fm. – FVB; D'Agostino et al., 1997); b) laminated to massive, whitish carbonate lacustrine silts, up to 100 m thick (San Nicandro Fm. - SNL), with the uppermost part being 0.78 Ma to ~1.3 Ma old (from paleomagnetic and tephra analyses; Giaccio et al., 2012); c) carbonate conglomerates with sandy matrix and rare, thin whitish clayey silt layers, locally well cemented, up to 80 m thick, of an ancient deltaic system (Vall'Orsa Fm.-VOC), and d) topset deltaic and fluvial-alluvial conglomeratic deposits (Valle dell'Inferno Fm. - VIC).

The Upper Syntheme (S. Mauro Fm. – SMA), up to 30-m thick, carved into the Lower Syntheme, is made of: a) a lower member consisting of fine-grained, well-sorted, bedded fluvial-alluvial gravels, and b) an upper member made of fluvial-alluvial silts and sands, rich in volcanoclastic material and tephra layers dated 460-350 ka (Giaccio et al., 2012).

The Late Syntheme, consists of Late Pleistocene alluvial sandy-gravel (ALP) and Holocene fluvial silty sand and gravelly sediments (Ho), mainly related to the Aterno River, and of slope debris and colluvial deposits.

3. Data collection and analysis

We conducted extensive fieldwork in the MAV, in order to refine, update, expand and analyse the Quaternary geology map of Pucci et al. (2015), where most of the subtle geomorphic features such as fault traces and the limits of Quaternary geological bodies were identified integrating classical field mapping and LiDAR derived DTM (1-m pixel size) analysis (through derivative digital maps such as shaded relief, slope, aspect, etc.).

3.1 Structural geology

We performed a detailed structural survey along the major normal faults in the MAV. The collected database including fault planes and associated slickenlines consists of more than 1200 data. The structural analysis is summarized in rose diagrams and stereoplots (Schmidt nets' lower projection) was conducted separating the bedrock fault planes data from those in Quaternary deposits. We also performed a directional analysis on the macroscopic fault traces (i.e. at the map scale), by calculating the average strike with the Linear Directional Mean tool (ArcMap ESRI ©) and weighting each fault trace according to its length, in order to avoid any bias due to the poor sampling of the shortest segments.

Kinematic data (>130 measurements) were collected in 10 different structural stations on selected outcrops. Data from the different stations were then grouped into three main subsets according to their different kinematics. For each sub-set we performed kinematic analysis through linked Bingham statistical analysis via FaultKin v.7.7.2 software of the strain tensor to obtain the long term geological extension and contraction axes (P and T) and visualize the strain tensors as synthetic focal mechanisms(full details in Marrett and Allmendinger, 1990; Allmendinger et al., 2013). We also performed a paleo-stress analysis for each fault sub-set adopting the right-dihedra method implemented in the WinTensor software v5.8.8

(Angelier and Mechler, 1979; Delvaux and Sperner, 2003). The paleo-stress inversion was performed in order to retrieve also the orientation of the three principal stress axes and their relative magnitudes.

A pervasive network of mostly dip-slip faults composed, at the macroscopic scale, of ~500 individual strands (up to ~5.6 km long) were extracted from the map of Pucci et al. (2015) (Fig. 2).

At the mesoscale (i.e. at the outcrop scale), many cemented fault mirrors on stiff pre-Quaternary bedrock crop out with frequent slickensides and rare slickenfibers or slickenlines. Conversely, faults affecting unconsolidated Quaternary deposits are expressed as a tectonic shear fabric developed in loose granular sediments, by abrupt juxtaposition of different formations, or by offset sedimentary sequences (Fig. 3).

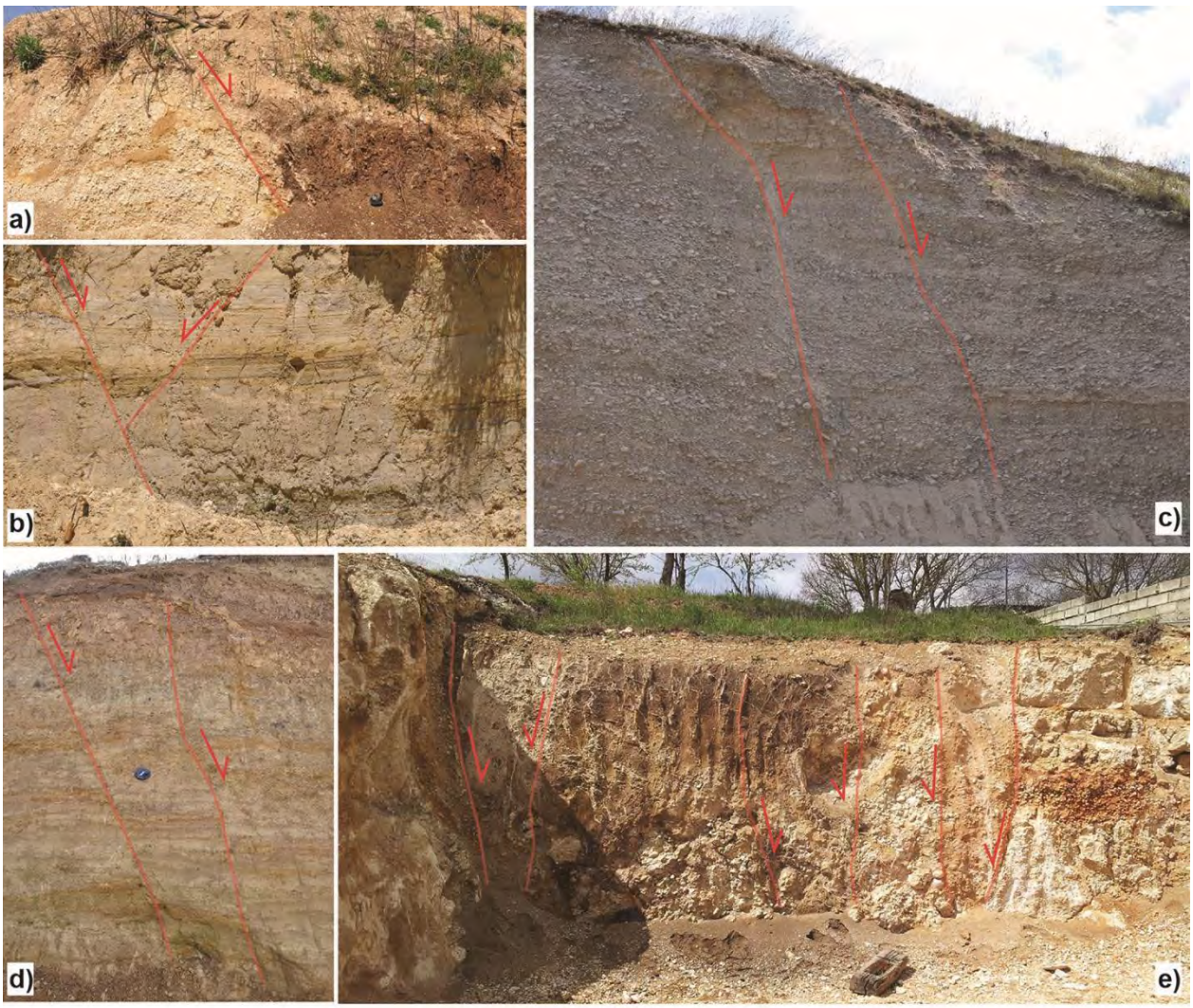

277 Fig. 3

278 **Figure 3.** Mesoscale fault expression affecting the Quaternary deposits. **a)** juxtaposition of Early-Middle Pleistocene
279 conglomerates and Middle Pleistocene silts; **b)** Andersonian conjugate faults in Early Pleistocene lacustrine deposits;
280 **c)** faulted Early-Middle Pleistocene alluvial conglomerates; **d)** faulted Late Pleistocene fluvial deposits; **e)** complex
281 fault zone forming a graben of Late Pleistocene silts between Early-Middle Pleistocene conglomerates. See Figure 2
282 for location of the outcrops.
283

284 3.1.1 *Analysis of the extensional fault systems*

285 We applied the fault directional analysis on the four sectors with different physiography, shown in
286 Figure 4a: 1) Mt. Stabiata and Mt. Pettino reliefs area, in the footwall of the UAFS Quaternary fault-system
287 (Fig. 1); 2) PSD sub-basin, including the widest outcrops of Quaternary continental deposits; 3) southern
288 boundary of the PSD sub-basin, including the Mt. Ceraso relief, in the footwall of the MAFS; 4) BC and
289 La Villa basins, in the hangingwall of the BSPF, limited to the east by the fault-bounded Mt. Ruzza and
290 Mt. Camarda ridges.
291 We recognize three main fault sets in the field both on the Meso-Cenozoic carbonate units and the
292 Quaternary continental deposits (Fig. 4): 1) a dominant fault set striking N130°-140° (hereinafter the NW
293 set, coinciding with the PSDFS *sensu* Civico et al. 2015); 2) a set striking N70°-100° (E-W set); 3) a
294 subordinate set, N170°-180° striking, nearly orthogonal to the E-W one (N-S set). The NW and E-W fault
295 sets show a prevalent SW and S dip of the fault planes, respectively.
296 The NW set is well developed all over the MAV and prevails in sectors 2, 3 and 4 as macroscopic
297 and Quaternary mesoscopic faults (Fig. 4a). In particular, in sector 2, it corresponds to the SW-and NE-
298 dipping fault sets bounding the PSD sub-basin to the east and west, respectively (PSDFS, BAZ and FOS in
299 Fig. 2). To the east, the NW-striking fault sets dissect Mt.s Ruzza and Mt. Camarda delimiting La Villa,
300 BC and San Nicandro-Prata d'Ansidonia basins, respectively (MRU, BAR e CIC faults, in the sector 4.
301 Figs. 2 and 4a). Some variation in the prevailing N130°-140° trend can be observed southward where the
302 fault traces affecting the Ceraso relief (~800-1000 m a.s.l) show a WNW-ESE bend (sector 3 in Fig. 4a).
303 Fault-slip data reveal an extensional or transtensional kinematics with dip-slip (sites 3 and 10 in Fig.4b) or
304 slightly left-lateral movement (sites 4 and 5 in Fig. 4b). Only along the San Giacomo fault (SGO), few NW-
305 trending faults have clear reverse displacement indicators.
306 The E-W set is pervasive in sector 1, showing both macroscopic and mesoscopic bedrock faults.
307 The fault planes dip south and north at high angle, bounding the L'Aquila, and Collebrincioni basins with
308 an extensional dip-slip kinematics. The mesoscopic E-W-striking bedrock faults are also predominant in

309 the PSD sub-basin (sector 2) with a mainly strike-slip kinematics (structural sites 5, 6 and 7 in Fig. 4b). The
310 majority of the E-W-trending faults are right-lateral and, subordinately left-lateral (average pitch <40°; Fig.
311 5a). We also observed the superimposition of different kinematic generations (Fig. 5b) with calcite
312 slickenfibers with mostly dip-slip motion overprinting older calcite slickenfibers showing oblique
313 kinematics. The fault planes bound the bedrock reliefs within the MAV (e.g. La Petrara and Mt. Cerro hills
314 in Fig. 2). In sector 3, the E-W-striking fault system shows a mostly dip-slip kinematic (site 9 in Fig. 4b).
315 The N-S-striking faults are the less abundant in the area. They were observed as Quaternary fault
316 in sectors 1 and 2 and as macroscopic fault traces in sector 3. They generally have a right-lateral strike-slip
317 kinematic (sites 5 and 7 in Fig. 4b), and in sector 3 their planes have high dip angle (>70°) and dip-slip
318 kinematics (site 9 in Fig. 4b).

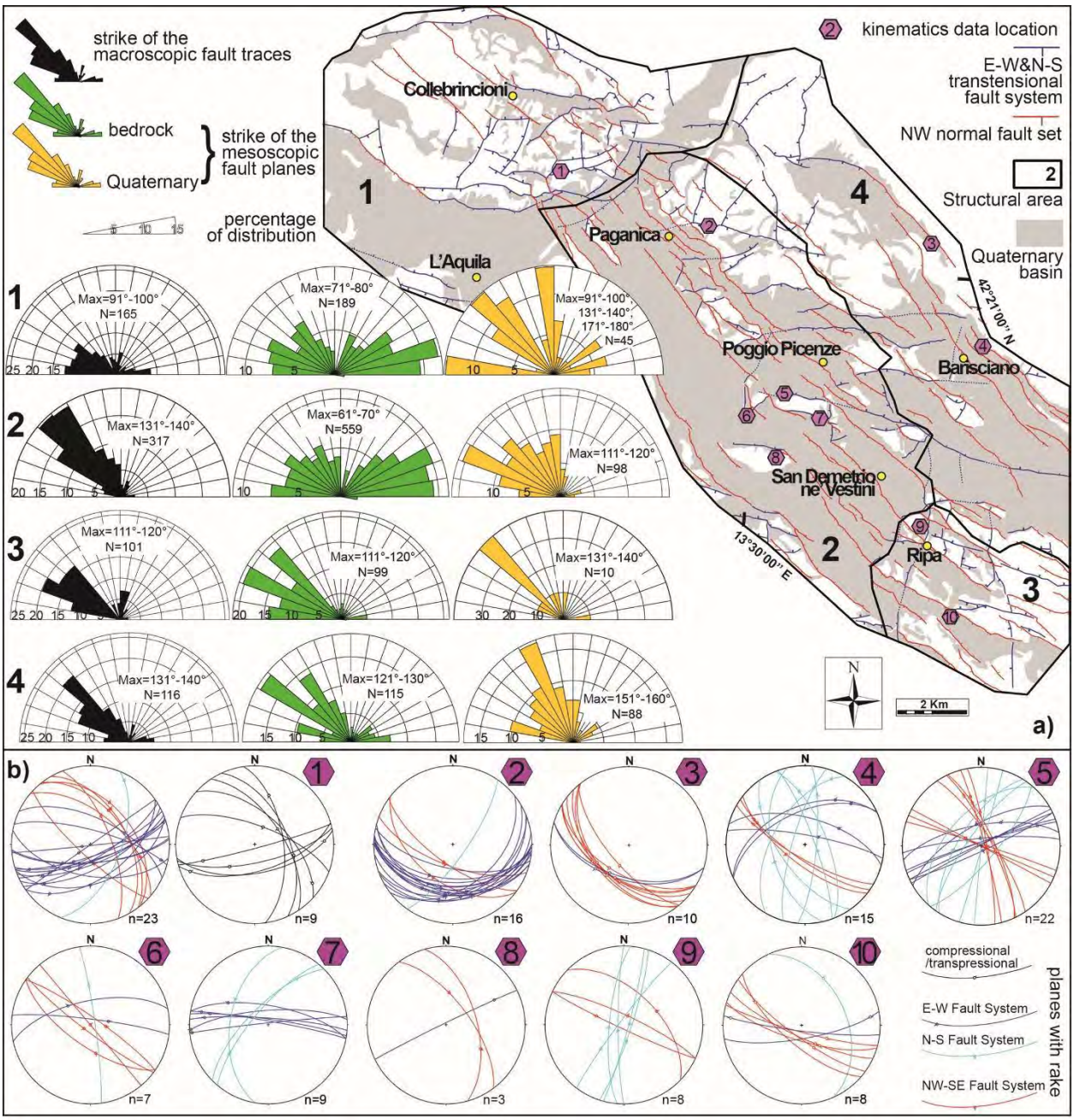

Fig. 4

Figure 4. a) Trend analysis of the fault strands. The study area is subdivided in four sectors and for each of them a rose diagram of macroscopic fault traces (black petals) and mesoscopic fault planes (yellow and green petals) are reported. Mesoscopic fault planes are subdivided in bedrock-affecting (green) and Quaternary deposits-affecting faults (yellow). **b)** Kinematic analysis of the main outcrops. For each structural station, a stereoplot of the measured fault

planes with kinematic indicators is reported (equal area Schmidt stereonet, lower hemisphere). See panel a) for locations.

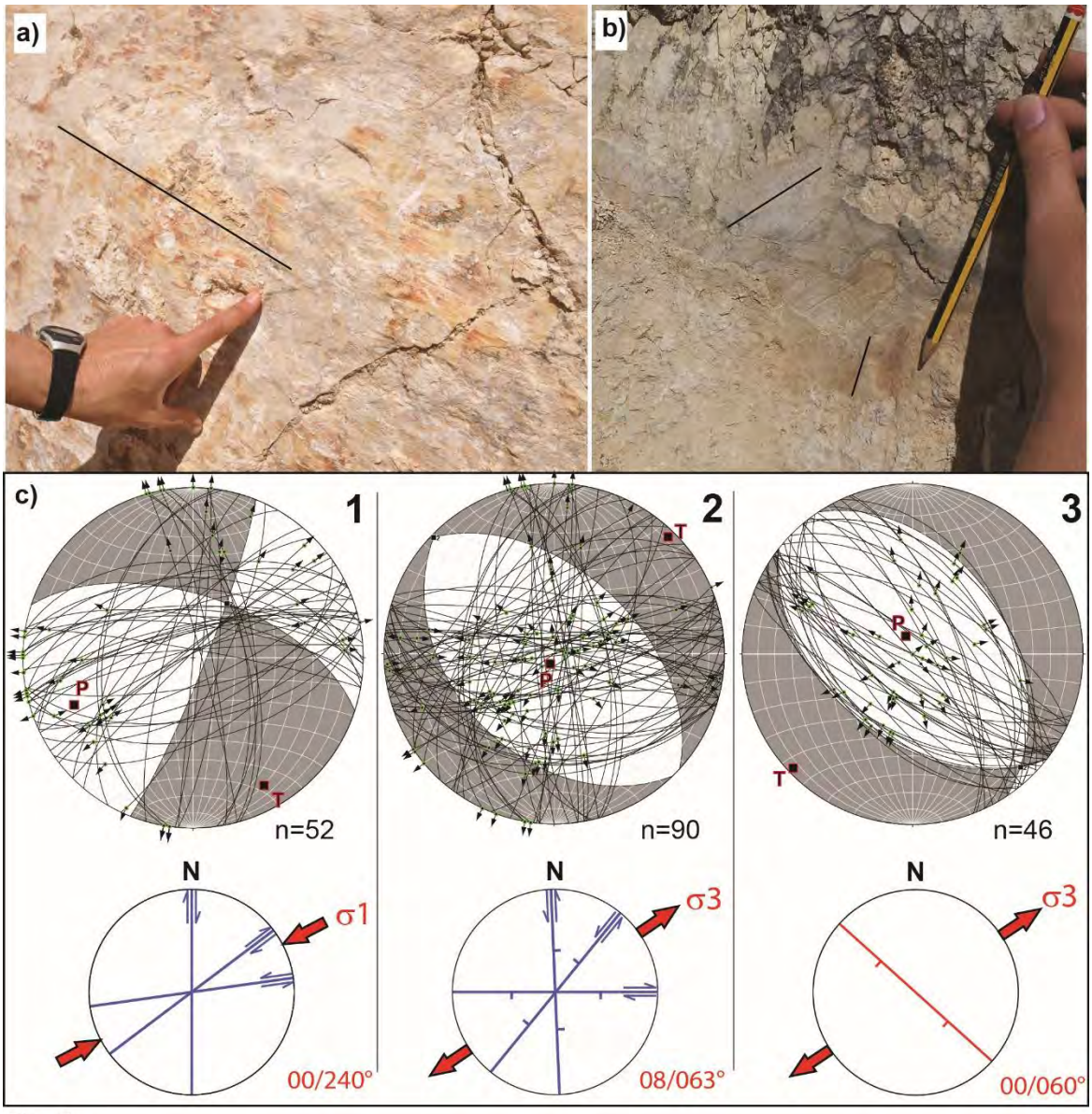

Fig. 5

Figure 5. a) Example of measured transtensional slickenfibers on E-W and N-S fault planes; **b)** Photo of a N71° striking fault plane showing an older generation of striae with right-lateral kinematics (rake 118°), overprinted by a dip-slip kinematics (rake 86°); **c)** Stereographic plots (lower hemisphere) of kinematic data along some of the main faults (see Fig. 4a for location). Small arrows indicate hangingwall slip direction. The focal mechanism obtained through linked Bingham analysis of slip vectors (Allmendinger et al., 2013, 1989) is shown, together with P and T

axes. In the lower panel, a simplified sketch of the general geometric and kinematic arrangement of each fault population is outlined. The red arrow indicates the direction of extensional (σ3) or compressional (σ1) paleostress (values in plunge and trend) (see Appendix A for details). 1) Kinematic data for a population of E-W and N-S faults compatible with a NE-directed compression. The N-S and NE-SW trending faults have right-lateral motions, whereas the E-W trending faults have a left-lateral motion; 2) Kinematic data for a sub-set of E-W and N-S faults trending. An inverted kinematics with transtensional oblique-slip motion is revealed, where N-S and NE-SW trending faults show right-lateral motions and the E-W trending faults show a left-lateral motion, compatible with a NE-directed extension; 3) Kinematic data for a population of NW-trending faults with a dominant dip-slip motion consistent with a NE-directed extension.

3.1.2 *Kinematic, paleo-stress and slip-tendency analysis of the fault-systems.*

The N-S and E-W conjugate fault sets (hereinafter E-W&N-S fault system) have kinematics with right-lateral and left-lateral strike-slip components, respectively. The obtained strain tensor highlights a sub-horizontal P-axis trending N249° and T-axis trending N151° (plot 1 in Fig. 5c), which are compatible with the regional Late Miocene-Early Pliocene NE-verging compression. The paleostress inversion results in a strike-slip regime with a N60° trending maximum horizontal compressive stress (Appendix A). Instead, the same N-S and E-W fault sets, but with left-lateral and right-lateral transtensional kinematics, respectively, indicate a nearly pure extensional strain tensor with ~vertical P-axis and a T-axis trending N44° (plot 2 in Fig. 5c). This fault subset is compatible with a normal-faulting regime causing the reactivation of pre-existing faults, with a σ3 trending N63° (Appendix A). The results therefore suggest a reactivation of the E-W&N-S fault system during the Late Pliocene-Quaternary extensional phase responsible for the formation of the NW-striking normal faults. In fact, the linked Bingham analysis of the NW set provides a near-vertical P-axis and a T-axis trending N226°, and the paleo-stress inversion results in a normal-faulting regime with the σ3 trending N60°, comparable with that computed for the E-W&N-S fault system (plot 3 in Fig. 5c; Appendix A).

We conducted a slip-tendency analysis by means of the Slip-Tendency Plug-in for Coulomb 3.3 Matlab© application (Neves et al., 2009; Toda et al., 2011) to test the slip potential of the differently oriented faults and the kinematic compatibility of the reactivated E-W&N-S fault system with the present-day extensional stress field (Morris et al., 1996) (see Appendix B for details). We adopted a simplified geometry for the analysed fault systems (Fig. B), composed of 13 NW-trending (e.g. CTO, CPT, MMA, MPE, BAR, MRU, BAZ, FOS, STI, PAG, SAG, SDE, MAFS), 11 E-W-trending (e.g. ASS, MST, SGO, COL, SEL, CAP, SPO, CHI, VOR), and 5 N-S-striking faults (e.g. RAI, BAG, CAM) (Fig. 1 and 2). The geometrical parameters of the fault system are consistent with the available geological and seismological data: dip angle of NW-, E-W- and N-S-striking systems is 50°, 60° and 70°, respectively. All the modelled fault sets highlight a significant slip potential. As expected, the NW-striking faults are the most prone to slip, followed by the E-W-trending faults (shear to normal stress ratio >0.7), while the N-S-trending faults show a low tendency to slip (shear to normal stress ratio >0.5) (Fig. B).

3.1.3 *Cross-cut relationships between different fault-systems*

At the mesoscopic scale, in several places NW-trending faults clearly cut E-W-trending faults (e.g. along the eastern border of the Mt. Cerro and the western part of La Petrara hills; Fig. 2).

Also at the macroscopic scale, the NW-striking set almost systematically crosscuts the E-W&N-S fault system (Fig. 2). Nonetheless, there are several places around the MAV where the NW-trending faults abut the E-W&N-S fault system (stars in Fig. 2), as in the following cases: the Assergi Fault (ASS), the Collebrincioni Fault (COL) and the Monte Stabiata Fault (MST), to the north; the eastern portion of the Preta Liscia Fault (PRE) and the Petogna Fault (PET), to the east; the San Panfilo d'Ocre Fault (SPO) and the Fonteavignone Fault (FAV) and nearby faults, to the south. In other cases, the E-W and the NW faults

sets appear to join with a fault bend geometry such as for Filetto (FIL) and Mt. Ruzza faults (MRU), and the ASS and the Campo Imperatore (CIM) faults (Fig. 2).

3.2 The Quaternary alluvial deposits

We produce 25 stratigraphic columns of the most significant outcrops of Quaternary units, presented with the variable-column-width technique (Miall, 2013) to refine the schemes of the stratigraphic relationships of the continental deposits and their changes along the MAV.

For each alluvial fan formation, we studied the depositional sequences and measured bedding attitude (>600 measurements) to identify: 1) the facies (classification scheme sensu Miall, 2013), the paleo-discharge directions (PDD), the conglomerate/sandstone qualitative ratio (C:S) and the maximum particle size (MPS); 2) the depositional cycles thickness; 3) the areal extent and thickness of the sedimentary body; 4) the lateral continuity of the depositional body and its degree of preservation from erosional processes, in particular the reworking by subsequent alluvial fan generations; 5) the inset relationship with other Quaternary deposits, which translates into a relative age and hierarchy of the deposition.

In order to provide a synoptic scheme of their stratigraphic and inset relationships, we analyse the depositional units and their areal distribution drawing attention to their paleo-environmental significance. The presented depositional framework is based on the description of the main outcrops and can be considered valid only for the exhumed part of the Quaternary basin: the depocentres of the basin infill may be thicker than the outcropping formations or may include unknown continental units.

We describe the results separately for the northern and central-southern areas (see Fig. 2 for location).

3.2.1 *The northern area*

Here, the gentle south-facing slope of the Mt. Bazzano carbonate ridge is draped by breccia deposits (Fig. 6), which extend southwestward with lateral continuity, separating the L'Aquila and Coppito basins. Their well-preserved top depositional surface (San Giacomo paleosurface, Fig. 6) shows an evident break in slope between San Giacomo village and L'Aquila town. We distinguish two bodies: the upper Breccia Aquilana (LAB Fm.) and the lower Megabrecce (MEB Fm.). The MEB Fm. is poorly organized and contains large olistoliths of Mesozoic basinal limestones with rock-slide facies (stratigraphic column 23 in Fig. 7) unconformably covered by a few meter-thick layer of matrix-supported clasts. Conversely, the LAB Fm. is composed of polygenic and poorly sorted, meters-thick layers of massive matrix-supported clasts, in a silty-sandy whitish matrix, showing a high-density mass wasting facies (C:S > 1, MPS > 1 m; stratigraphic column 25 in Fig. 7). The proximal facies of the MEB Fm., the dip of its depositional surface, as well as the SW-trending paleo-drainage direction (PDD), paralleling drainage incisions and the wind-gap on the San Giacomo paleosurface (Fig. 6), all suggest beheaded discharges apexes disconnected from the feeding area.

To the north, the San Giacomo paleosurface is bounded by the suspended Enzano Hills paleolandform (900-1100 m a.s.l.). The latter, moulded on bedrock, contains poorly preserved small basins with thin continental infill, displaying prominent unconformities and hiatuses (stratigraphic column 19 in Fig. 7), with ~2.5 m of a single depositional cycle of matrix-supported breccia (MEB Fm.; C:S > 2, MPS > 1 m) below ~5.0 m of decimetric layers of sandy silt and paleosoils (SMA Fm.; C:S << 1, MPS < 1 cm). These observations suggest that the erosion and exhumation processes in this area prevailed for most of the Quaternary.

The Enzano Hills paleolandform connects to the Holocene flatlands through a small and widely dissected bajada composed of SE steeply dipping (~15°) bodies of breccias (LAB Fm.), inset at 600-700 m a.s.l. between the Cesarano and San Giacomo paleosurfaces (800-900 m a.s.l.) (Fig. 6). It shows several < 2.0 m-thick layers of stratified and clast-supported, crudely bedded breccia and fine-to-coarse sand (C:S >

2, MPS < 1 m; stratigraphic column 22 in Fig. 7), and presents paleo-discharge directions to the SE, perpendicular to the flow directions of the hosting MEB Fm. (Fig. 6).

Northeast of the Paganica village, the Holocene basin is flanked by a narrow staircase of inset alluvial terraces (units ALP, SMA and VIC Fms., Fig. 6), covering a matrix-supported MEB (C:S > 1, MPS > 1 m; stratigraphic column 20 in Fig. 7) at the outlet of the Raiale River gorge. Upstream, the Raiale River gorge separates a paleolandform located at ~900 m a.s.l., on the left side, from the Cesarano depositional paleosurface (draped by the SW- and SE-flowing Cesarano Breccia, CEB Fm.), on the right side (Fig. 6). The CEB Fm. shows a lateral continuity, interrupted by a small EW-trending residual basin and a gentle SW-dipping, badly-preserved depositional surface. The CEB Fm. presents up to 1.5 m-thick layers of clast- and matrix-supported gravel, locally stratified (C:S > 2, MPS < 1 m; stratigraphic column 18 in Fig. 7), showing a more distal facies with respect to the MEB Fm..

The Camarda area, along the Raiale River gorge, is characterized by a confined body of breccias (CAB Fm.), apparently disjointed from the Paganica Quaternary basin. It is made of up to 2.5 m-thick layers of massive clast-supported, polygenic and angular gravels with abundant matrix (C:S > 2, MPS < 0.5 m), showing a proximal facies of mass-wasting deposits, or with prevalent well-sorted small angular clasts at its northern edge, suggesting a slope deposit paleo-environment. This up to 50 m-thick depositional body dips >30° and appears to be topped by the gentler alluvial bodies of the CEB Fm.

The Paganica basin is mostly infilled by the large Holocene alluvial fan fed by the Raiale River (stratigraphic column 21 in Fig. 7), which indicates a general and persistent aggradation between the Paganica and Bazzano villages.

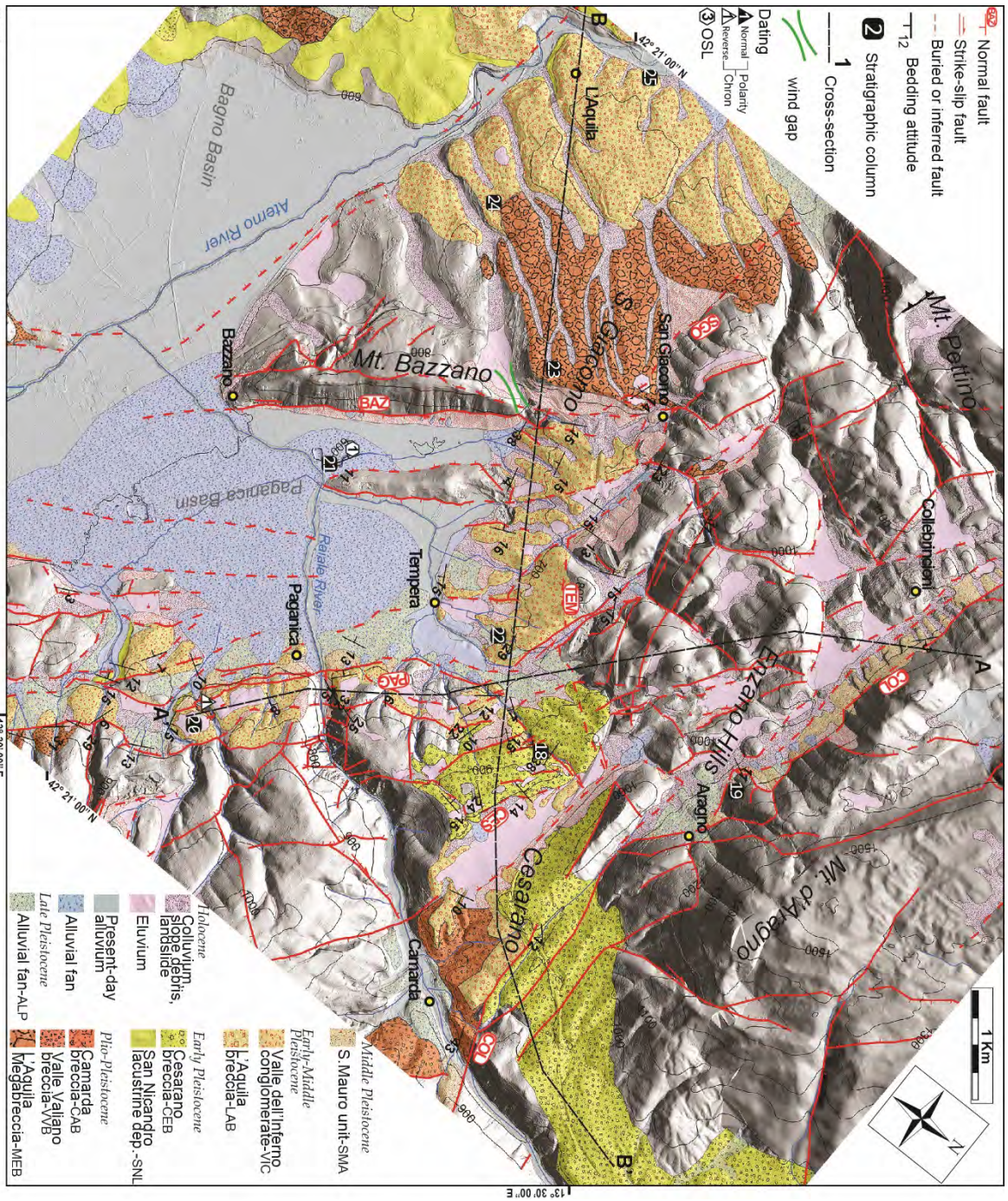

Fig. 6

446

447 **Figure 6.** Quaternary Geology map of the northern sector. Traces of the cross and longitudinal sections, along with
448 the locus of the provided stratigraphic columns and dating sites are reported. 1-m resolution hillshaded DTM from
449 LiDAR (Civico et al., 2015). See Figure 2 for location.

450

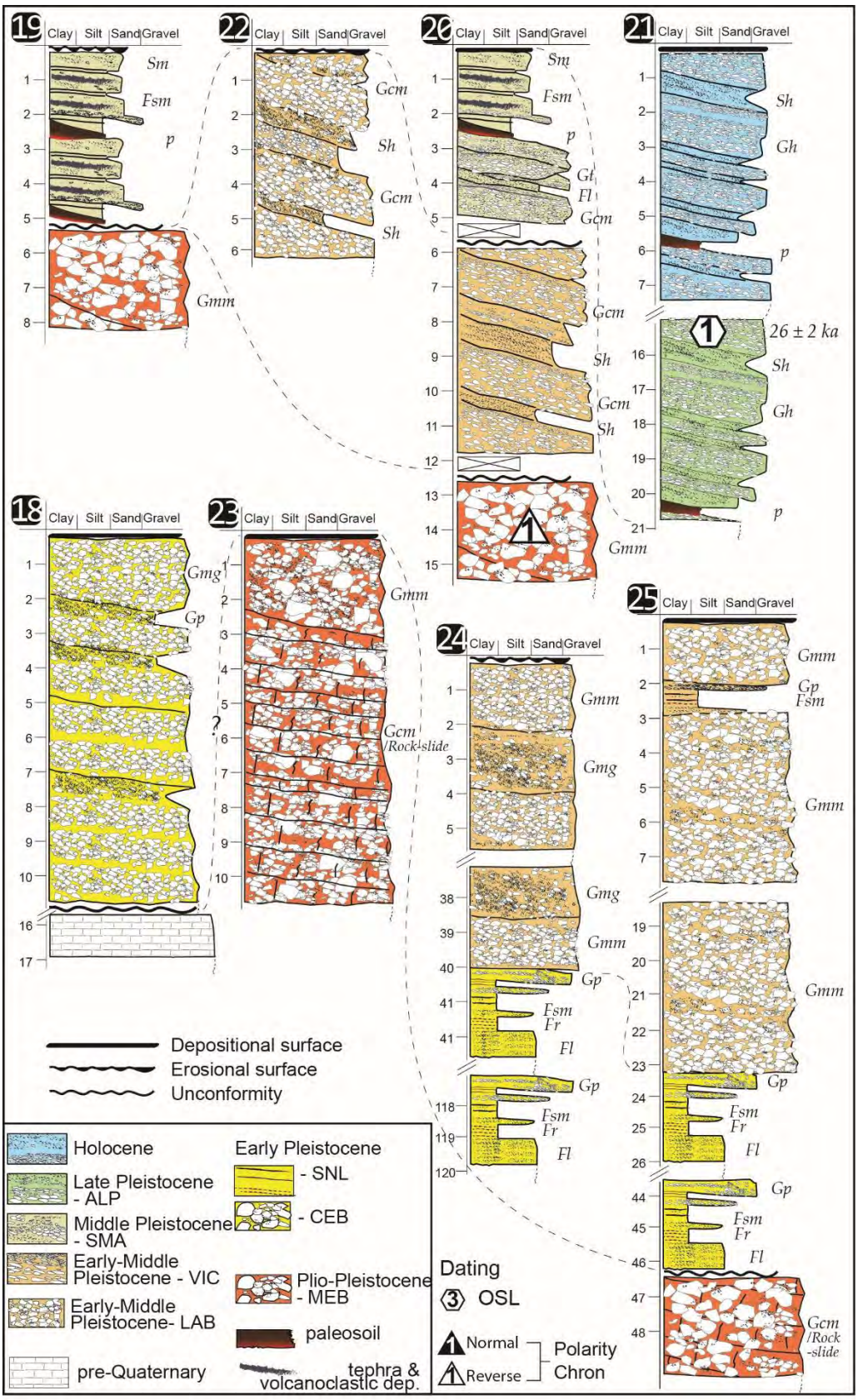
19
22
26
21
18
23
24
25
Clay
Silt
Sand
Gravel
Sm
Fsm
p
Gmm
Gcm
Sh
Gt
Fl
1
26 ± 2 ka
Gh
Gmg
Gp
?
/Rock-slide
Fr
Depositional surface
Erosional surface
Unconformity
Holocene
Late Pleistocene - ALP
Middle Pleistocene - SMA
Early-Middle Pleistocene - VIC
Early-Middle Pleistocene- LAB
pre-Quaternary
Early Pleistocene
- SNL
- CEB
Plio-Pleistocene - MEB
paleosoil
tephra & volcanoclastic dep.
Dating
3 OSL
Normal
Reverse
Polarity Chron

Fig. 7

Figure 7. Stratigraphic columns of the northern sector. Variable width refers to the lithology (Miall, 1996). Dashed line represents possible correlation of the unconformities. The recognized depositional and erosional surfaces are reported. Dated deposits are labelled. See Figure 6 for locations.

3.2.2 *The central-southern sector*

This sector (Fig. 8), marked by an evident continuity of the outcropping Quaternary continental deposits, includes the Poggio Picenze (~600-900 m a.s.l.), the San Demetrio ne' Vestini (~600-800 m a.s.l.) and the northern part of the Barisciano-Castelnuovo (BC) basins (~800-900 m a.s.l.). It is characterized by hanging and well-preserved depositional surfaces, interrupted by isolated bedrock highs (Mt. Cerro, La Petrara, San Giovanni, and Cicogna hills).

To the northeast, the Valle Vedice paleolandform (~1100 m a.s.l.) and the Capannacci Hills-Mt. Camarda reliefs (up to 1300 m a.s.l.) (Figs. 2 and 8) hang on a morphologic escarpment draped by cemented slope breccias (VVB Fm.), which grade laterally into alluvial fan facies (VVC Fm.), which are well exposed at the Valle Vedice and Valle di San Valentino outlets (Fig. 8). These breccias exhibit clast-supported and up to 2 m-thick beds (C:S >> 3, MPS < 0.3 m; stratigraphic columns 1, 2 and 5 in Fig. 9) with dips > 20°. An angular unconformity separates these breccias from the overlying Fonte Vedice breccia (FVB Fm.). The latter has a very limited lateral continuity and a well-preserved depositional surface, it is composed of a clast-supported, up to 1.0 m-thick, crudely bedded gravel (C:S > >3, MPS < 0.3 m) with low dip and reddish, residual matrix.

The Quaternary basin in the area of Barisciano-Castelnuovo-San Demetrio ne' Vestini displays the largest thickness of the infilling deposits. Here, the widespread Vall'Orsa Fm. (VOC Fm.) is characterized by clast-supported, stratified gravel layers (up to 2 m-thick) with planar cross-beds, typical of a prograding Gilbert fan delta (C:S >3, MPS < 0.2 m). The almost ubiquitous SE dip-direction of the foresets is a key distinctive marker of the VOC Fm. In the marginal parts of the basin, the VOC Fm. interfingers and is partly

heteropic with SNL (bioturbated mud-silt and sand, from massive to fine-laminated; stratigraphic columns 3, 7, and 9 in Fig. 9) and presents a marked lateral continuity in two sectors: 1) the Barisciano-Castelnuovo area, where it shows a well-preserved depositional surface; 2) the Barisciano-Poggio Picenze-San Demetrio area, where it drastically thins (and, in some cases, it directly overlays the pre-Quaternary bedrock; stratigraphic column 11 in Fig. 9). Conversely, the VOC Fm. is absent NW of the Poggio Picenze village.

The Valle dell'Inferno Fm. (VIC Fm.) is laterally continuous in the area of San Demetrio ne' Vestini and Poggio Picenze villages, where it shows widespread and well-preserved depositional surfaces (e.g. Valle Daria paleosurface; Fig. 8). It is characterized by up to 2m-thick layers of clast-supported, tabular and crudely bedded gravel with direct grading, at places alternated with decimetric fine to coarse sand, and present at the top (close to the Aterno River) cross-bedding related to minor channel fill (stratigraphic column 13 in Fig. 9). In general, this formation dips gently (2° to 15°) and thickens to the SW (stratigraphic columns 3, 6, 7 and 8 in Fig. 9). An unusual 30°-dipping bedding is limited to a narrow area between Valle dell'Inferno and San Demetrio ne' Vestini (Fig. 8). Close to Poggio Picenze, the VIC Fm. directly overlays the SNL through an evident unconformity with an interposed thick reddish paleosoil (stratigraphic column 14 in Fig. 9).

Middle-Late and Late Pleistocene alluvial fan deposits (San Mauro Fm. –SMA- and ALP) are confined in the area between the San Gregorio village, La Petrara Hill and the Petogna village. Here, a dissected Middle-Late alluvial fan (stratigraphic columns 15, Fig. 8 and Fig. 9) is composed of < 1.0 m-thick beds (C:S < 2; MPS < 0.3m) of clast-supported massive gravels, locally cross-bedded, alternating with massive sand and laminated sandy silt, with intercalated tephra and paleosoils. The inset, well-preserved Late Pleistocene alluvial fan body, fed by the Valle di San Valentino, is composed of < 0.5 m-thick depositional events of rare clast-supported gravels (C:S < 1.2; MPS < 0.2 m), locally crudely bedded or imbricated, and fine-to-coarse sand and mud (stratigraphic columns 17, Fig. 9).

Located close to the Aterno River, the largest Holocene alluvial fan depositional bodies preserve an intact depositional surface. They are composed of up to 1.0 m-thick alternating clast-supported, crudely bedded and imbricated gravels and laminated sand (fine to coarse), silt and mud with thick paleosoils.

Clear fluvial sedimentary structures are present only in the younger deposits (Middle-Late Pleistocene and Holocene), close to the present-day alluvial plain (stratigraphic columns 16, upper part of columns 9, 10 and 13; Fig. 9).

The southern limit of the PSD basin (Mt. Ceraso area, Fig. 8) is characterized by elongated, NW-SE trending bedrock ridges, spaced out with parallel suspended basin that are infilled by a thin Early Pleistocene sequence of SNL and NW-flowing VIC.

Holocene
Colluvium, slope debris, landslide
Eluvium
Present-day alluvium
Alluvial fan
Late Pleistocene
Alluvial fan-ALP
Middle Pleistocene
S.Mauro unit-SMA
Early-Middle Pleistocene
Valle dell'Inferno conglomerates-VIC
Early Pleistocene
Vall Orsa conglomerate-VOC
San Nicandro lacustrine dep.-SNL
FonteVedice breccia-FVB
Plio-Pleistocene
Valle Variano conglomerate-VVC
Valle Variano breccia-VVB
Datings
OSL
TCN
Normal
Reverse
Polarity Chron
13° 30' 00" E
13° 30' 00" E
42° 21' 00" N
42° 21' 00" N
1 Km
N
Capannacci Hills
Mt. Camarda
Poggio Picenze Basin
Aterno River
S. Demetrio Basin
Barisciano-Castelnuovo Basin
Valle Daria paleosurface
Bovacchio valley
Oprivalley
Petogna
Poggio Picenze
San Gregorio
Sant'Eusanio Forconese
San Demetrio ne'Vestini
Barisciano
Castelnuovo
Prata d'Ansidonia
Ripa
Mt. Ceraso
Cerro Hill
La Petrara Hill
S. Giovanni Hill
Cicogna Hill
Normal fault
Strike-slip fault
Buried or inferred fault
Bedding attitude
Cross-section
wind gap
paleo-drainage
Stratigraphic column

Fig. 8

510 **Figure 8.** Quaternary Geology map of the central-southern sector. Traces of the cross and longitudinal sections, along
511 with the locus of the provided stratigraphic columns are reported. 1-m resolution hillshaded DTM from LiDAR (Civico
512 et al., 2015). See Figure 2 for location.
513

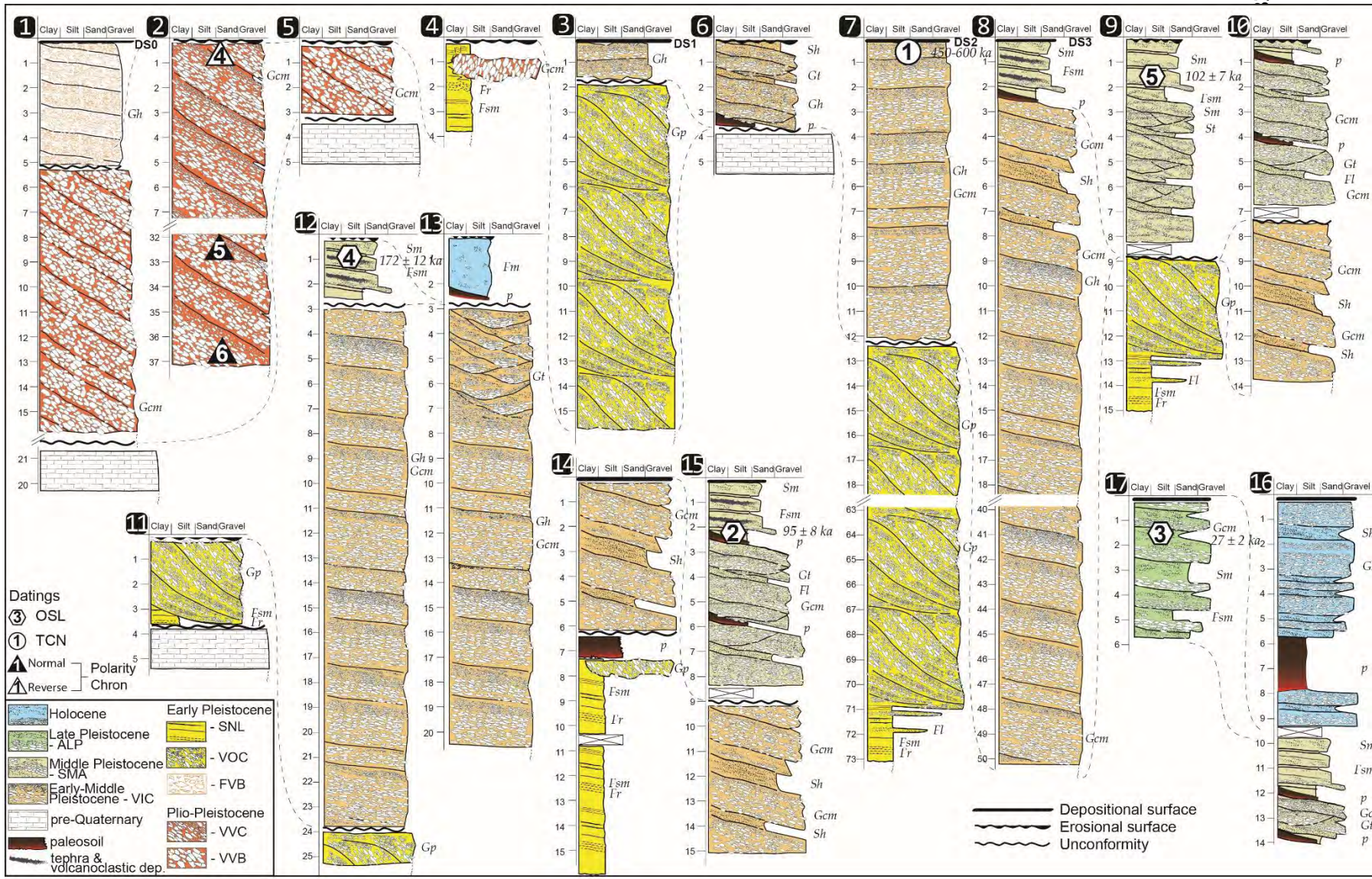
Clay Silt Sand Gravel
DS0
DS1
DS2
DS3
Gh
Gcm
Gp
Sm
Fsm
Fr
Fm
Gt
Sh
Fl
St
p
172 ± 12 ka
102 ± 7 ka
95 ± 8 ka
27 ± 2 ka
450-600 ka
Datings
OSL
TCN
Normal
Reverse
Polarity Chron
Holocene
Late Pleistocene - ALP
Middle Pleistocene - SMA
Early-Middle Pleistocene - VIC
pre-Quaternary
paleosoil
tephra & volcanoclastic dep.
Early Pleistocene
- SNL
- VOC
- FVB
Plio-Pleistocene
- VVC
- VVB
Depositional surface
Erosional surface
Unconformity

Fig. 9

Figure 9. Stratigraphic columns of the southern sector. Variable width refers to the lithology (Miall, 1996). Dashed line represents possible correlation of the unconformities. The recognized depositional and erosional surfaces are reported. Dated deposits are labelled. See Figure 8 for locations.

3.2.3 *Dating*

In order to provide age constraints to the mapped deposits, we selected 14 outcrops where we collected samples of the continental deposits. We applied the following dating methods to cover different age ranges: 1) Optical Stimulated Luminescence (OSL) (Appendix C); 2) Terrestrial Cosmonucleid (TCN) by ^{36}Cl isotope concentrations (Appendix D); and 3) paleomagnetic analysis (Appendix E).

We collected six samples for OSL dating from deposits supposed to be younger than 300 ka and composed of quarzitic fine layers (Tab. C and Figs. 6, 7, 8 and 9). Ages derive from Equivalent Dose (ED) obtained from the extracted coarse-grained (100-300 μm) quartz fraction through multiple aliquot regenerative dose technique (samples 3 and 4) and Single-Aliquot Regenerative-dose (SAR) protocol (samples 1, 2, 5, 6).

Four samples are from the SMA Fm. and two are from the ALP Fm. The oldest sample 4 is ~170 ka and comes from a thin deposit of SMA Fm. that drapes by unconformity a large alluvial fan of VIC Fm., south of La Petrara Hill at 690 m a.s.l. (Figs. 8 and 9). Samples #2, 5 and 6 are ~100 ka old and come from alluvial and fluvial facies of SMA Fm. unconformably deposited over VOC and VIC Fms. at lower elevations (650-670 m a.s.l.). Samples #1 and 3 ages are ~26 ka old and represent both buried and exposed ALP Fm. alluvial fans, respectively.

Only one site was dated through the TCN (^{36}Cl) concentration depth profile that was collected on the Valle Daria paleosurface at 900 m a.s.l. (Figs. 8 and 9) formed by the topset of VIC Fm. The modelling results of the Valle Daria paleosurface indicate that the profile is very close to steady state (i.e. exposure ages are old enough such that the concentration gains through production are balanced by the concentration

losses through radioactive decay and surface denudation, which implies that the ^{36}Cl concentration depends only on the denudation rate). The best fit of the ^{36}Cl age model is yielded with an exposure age of at least 200-600 ka, a denudation rate of 2-5 m/Ma and almost no inheritance (Fig. D). Those results suggest that the Valle Daria paleosurface formed before the interval 460 ka (given the age of the overlaying SMA Fm.) and 600 ka, assuming a very low denudation rate from its high-grade preservation.

We collected 73 samples suitable for paleomagnetic analyses from seven sites (Figs. 6, 7, 8 and 9). These are mostly located on the cemented breccia and conglomerates draping the slope bonding the NW side of the PSD sub-basin, with the exception of samples #7 located at La Villa satellite basin (Fig. 2). The samples have a natural remanence magnetization (NRM) on the order of 2.2 to 854 10E-05 A/m. Five sites show a reverse magnetic polarity and the paleomagnetic mean direction *in situ* is Dec=168.5°, Inc=-53.8°, α 95=7.9° (Fig. E1 and E2). We suggest that these reverse polarity units were deposited during the reverse Matuyama chron and then may be dated at Early Pleistocene. This is in agreement with the previous paleomagnetic studies in the area (D'Agostino et al., 1997; Messina et al., 2001). Notably, the sites #5 and 6, both located at the base of the VVC Fm., show a normal magnetic polarity and the inferred paleomagnetic mean direction *in situ* is Dec=14.6°, Inc=65.1, α95=13.8°. Conversely, sites #4 and 2, at the top of the VVB and VVC Fms., respectively, show a reverse magnetic polarity (Tab. E). In this case, the normal polarity units sampled at the base of the sequence could be ascribed to the normal Olduvai subchron (Early Pleistocene) or the older normal Gauss chron (Late Pliocene).

3.2.4 *Scheme of the stratigraphic relationships*

By integrating original data with those of the previous works discussed in Chapter 2 (Fig. 10), we constructed a synopsis of the stratigraphic framework where the stratigraphic sequences are reported as unconformity-bounded units, and the main depositional or erosional surfaces are shown.

561 The main first-order unconformity is represented by the erosional contact between the base of the
562 continental sequence and the top-bedrock. On the basis of the stratigraphic relationships, in the northern
563 sector (L'Aquila and Paganica in Fig. 10), the Megabrecce (MEB Fm.) are older than the Early Pleistocene
564 lacustrine deposits (SNL Fm.) and we hypothesize that the Middle Pleistocene L'Aquila Breccia (LAB
565 Fm.) is partly fed by the reworking of the MEB Fm. The Camarda breccia (CAB Fm.) is supposed to be
566 Plio-Pleistocene because its paleo-flow and bedding dip directions converge to an E-W oriented depocentre,
567 which is completely disconnected from the present-day morphodynamics and pre-dates the incision of the
568 Raiale River gorge (Fig. 6). The Cesarano breccia (CEB Fm.) covers with a marked angular unconformity
569 the CAB Fm. and, hence, it is supposed to be Early Pleistocene in age. Similarly, in the central-southern
570 sector (Petogna and Barisciano in Fig. 10) the inception of the deposition of the VVB and VVC Fms., which
571 drape the northeastern escarpment, is older than the Early Pleistocene deposits (SNL, VOC and VIC Fms.).
572 This is supported by fallen blocks of cemented VVB deposits that plastically deformed the SNL Fm. and
573 by paleomagnetic data (stratigraphic columns 4 and 2, respectively, in Fig. 9). The lack of Middle
574 Pleistocene tephra or matrix with volcanic minerals from the Latium volcanic districts, which were found
575 in several sites surrounding L'Aquila (Giaccio et al., 2012), provides an upper chronological constraint of
576 460 ka for the VIC Fm., confirmed by the TCN dating of its top surface (stratigraphic column 7 in Fig. 9).
577 Given the outcropping facies, the main paleo-environments can be summarized as follows: 1) Late
578 Pliocene-Early Pleistocene deposition related to slope-dominated processes at the edges and bottom of the
579 MAV basin (VVB, MEB, CEB, LAB and FVB Fms.), which locally interfingers with sparse alluvial fan
580 deposits (VVC Fm.); 2) Early Pleistocene lacustrine/palustrine deposition (SNL Fm.) that infill the irregular
581 depocentre of the MAV basin between Petogna and Barisciano; 3) Early Pleistocene alluvial fan delta
582 deposition with foresets prograding to the southeast (VOC Fm.), partially heteropic with the SNL Fm., and
583 truncated by topset (VIC Fm.), displaying the greatest geographical extent and sediment thickness of the

study area, and; 4) Middle Pleistocene fluvial (SMA Fm.) and alluvial fans (SMA, ALP and ALH Fms.) with much limited extent and relatively thin accumulations, related to the Aterno River tributaries.

In general, the sediments in the northern sector of the MAV basin (L'Aquila and Paganica sequences in Fig. 10) show a widespread and typical proximal facies, testifying the dominance of mass-wasting processes and/or rapid debris flow emplacements that persist through the Early Pleistocene. Conversely, the central and southwestern sectors of the MAV basin (Petogna, San Demetrio ne' Vestini and Barisciano sequences in Fig. 10) testify the occurrence of the largest lacustrine basin and coarse deposits exhibiting a stream-dominated transport facies.

The outcropping continental deposits clearly thickens to the southeast, with a minimum observed close to L'Aquila (~80 m) and a maximum reported in the San Demetrio ne' Vestini area (~280 m). In particular, our stratigraphic sections indicate that the exhumed Early Pleistocene depocentre is located in the San Demetrio ne' Vestini area. Conversely, the Middle-Late Pleistocene deposits are much thicker in the Petogna-Poggio Picenze area, beside the central part of the PSD sub-basin.

The presence of a rough topography during the initial stage of sedimentation is testified by the reduced thickness of Quaternary deposits onto the bedrock highs and by the widespread hiatuses affecting the lower terms (stratigraphic columns 5, 6 and 11, Fig. 9). As example, the stratigraphic column 6 (Fig. 9) located close to Colle Cicogna (Fig. 8), indicates the presence of an important bedrock high between the San Demetrio and the BC basins. Immediately SW of this high, the VIC Fm. increases in thickness and the lacustrine facies presents abundant clastic input and sedimentary structures (i.e. gravelly cross-beds of channel fills) possibly due to shallow water/shoreline environment.

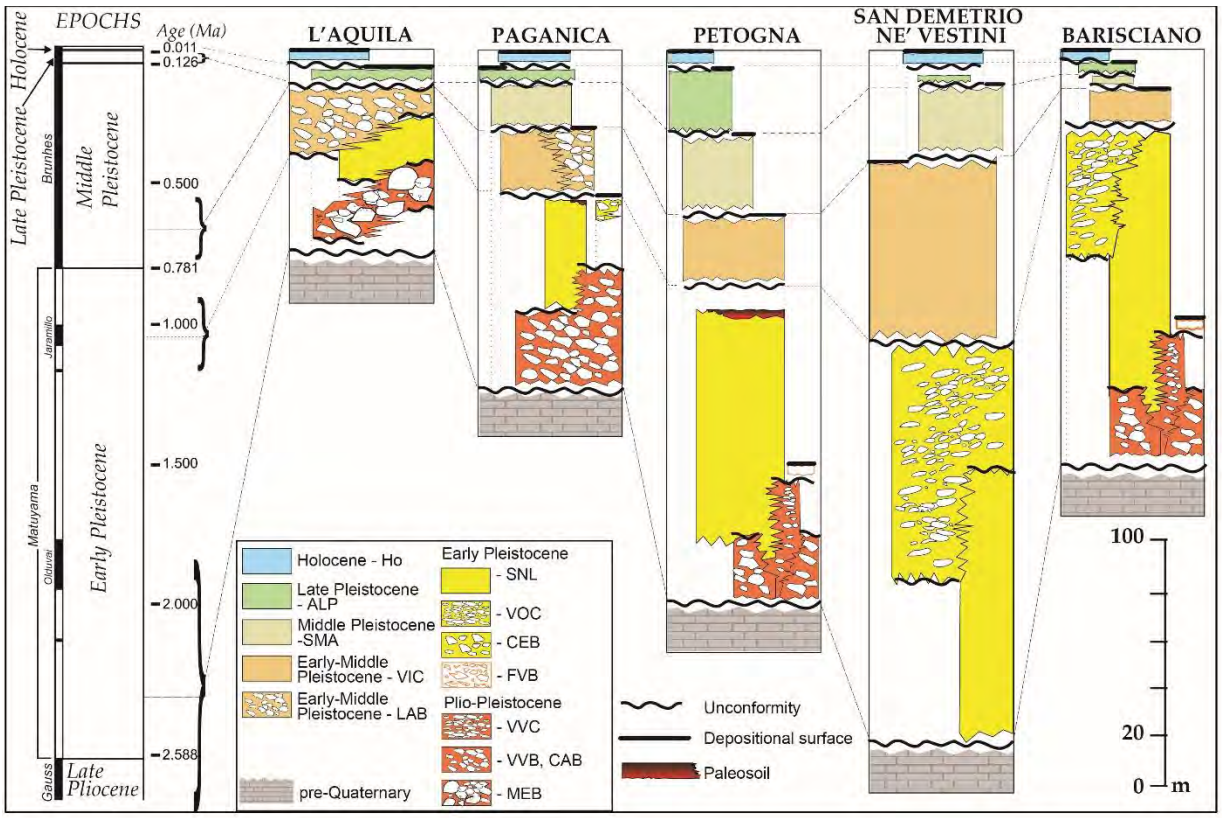

Fig. 10

Figure 10. Scheme of the reconstructed stratigraphic relationships along the L'Aquila area and the Paganica-San Demetrio and Barisciano-Castelnuovo basins. Each column is drawn with a variable width to include hiatuses. The inferred ages and thickness of the formations are reported.

3.2.5 *Morphologic relationships alluvial bodies*

In the simplified scheme of Fig. 11 we report the main top depositional and erosional surfaces of the alluvial bodies in the MAV basin and reconstruct their geomorphic relationships. These surfaces can be laterally discontinuous and locally dissected; however, we can correlate different sedimentary bodies and hypothesize their original geometry and extent. We have also studied the main paleo-flow directions (arrows in fig. 11) and the locus of entrenchment to highlight the prevailing alluvial regime (i.e. aggrading,

615 prograding or incising). This enables us to reconstruct the chrono-sequence of the alluvial fan development
616 (i.e. the distribution, localization and migration of the areas of active fan sedimentation).

617 In the northern sector of the MAV (Fig. 11a), the Holocene fan of Paganica represents the main
618 aggrading (and locally prograding) alluvial body, bounded by bad-preserved Early-Middle Pleistocene
619 terraces. Worthy to note, the high-resolution seismic tomography models by Villani et al., (2017) clearly
620 support the evidence of syn-tectonic growth and aggradation of the alluvial fan at the Raiale river outlet,
621 when crossing the PAG fault. In fact, locally, the subsurface thickness exceeds 80 m, suggesting that the
622 deposition of this alluvial fan started much earlier, probably during the Middle Pleistocene. The Holocene
623 fan of Paganica is fed by the Raiale River, which cuts a deep gorge into the bedrock after incising the
624 Cesarano depositional surface. The latter connects the Assergi and the Paganica Quaternary basins and
625 forms a paleosurface inset between the Mt. d'Aragno and the Capannacci Hills. The dissected Early-Middle
626 Pleistocene debris-flows (LAB Fm.), whose catchment drains southeastward the Enzano Hills
627 paleolandform, are inset (up to 200 m lower) between two bodies of older breccia (MEB and CEB Fms.,
628 respectively) (A in Fig. 11a), beheading the apex of the MEB Fm. body (as testified by wind gaps on the
629 Mt. Bazzano ridge; B in Fig. 11a) and interrupt the hanging Cesarano surface (C in Fig. 11a).

630 In the central-southern sector of the MAV basin, we distinguish two different areas: the Barisciano-
631 Sant'Eusanio, to the southeast, and the Petogna-Poggio Picenze, to the northwest (Fig. 11b). In the
632 Barisciano-Sant'Eusanio area, the alluvial bodies are well-preserved and occupy most of the area. Here, the
633 Early Pleistocene fan delta shows SE-prograding delta lobes with erosional surface on VOC Fm. (ES1 in
634 Fig. 11b) overlaid by the thin depositional topset of the VIC Fm. (DS2). This older alluvial body is
635 spectacularly entrenched at the Valle dell'Inferno, where a lower sequence of progressively younger
636 telescopic fans takes place (ranging from the VIC Fm. –DS3- to the Holocene fans – DS5), prograding to
637 the SW towards the Aterno River, with strong incisions into the toe zones. In the Petogna-Poggio Picenze
638 area, the Early Pleistocene fan delta (VOC Fm.) does not crop out, being its apex beheaded by the inset

Early to Middle Pleistocene alluvial bodies (D in Fig. 11b). The latter are strongly dissected and reworked by the stacked sequence of Middle to Late Pleistocene fans (E in Fig. 11b). The fan progradation appears to begin from Late Pleistocene, suggesting a later increase of sediment delivery and/or depositional (accommodation) space.

We report in Fig. 11c the rose-diagrams of the measured dip-direction of bedding surfaces and foresets of the main alluvial bodies, which we group into three main sets depending on their age: 1) Late Pliocene – Early Pleistocene; 2) Early Pleistocene; 3) Middle Pleistocene – Holocene. These rose-diagrams point out a change through time of the main flow directions. The plot of the Plio-Pleistocene alluvial bodies (1 in Fig. 11c) displays the main directions dispersed between west-southwestward and southward. The plot of the Early Pleistocene deposits (2 in Fig. 11c) displays prevalent southeastward directions, while the Early-Middle Pleistocene to Holocene alluvial bodies (3 in Fig. 11c) indicate dominant southwestward flows. Therefore, a drastic ~90° flip of flow direction occurred in the central-southern portion of the MAV basin between the Early and Middle Pleistocene.

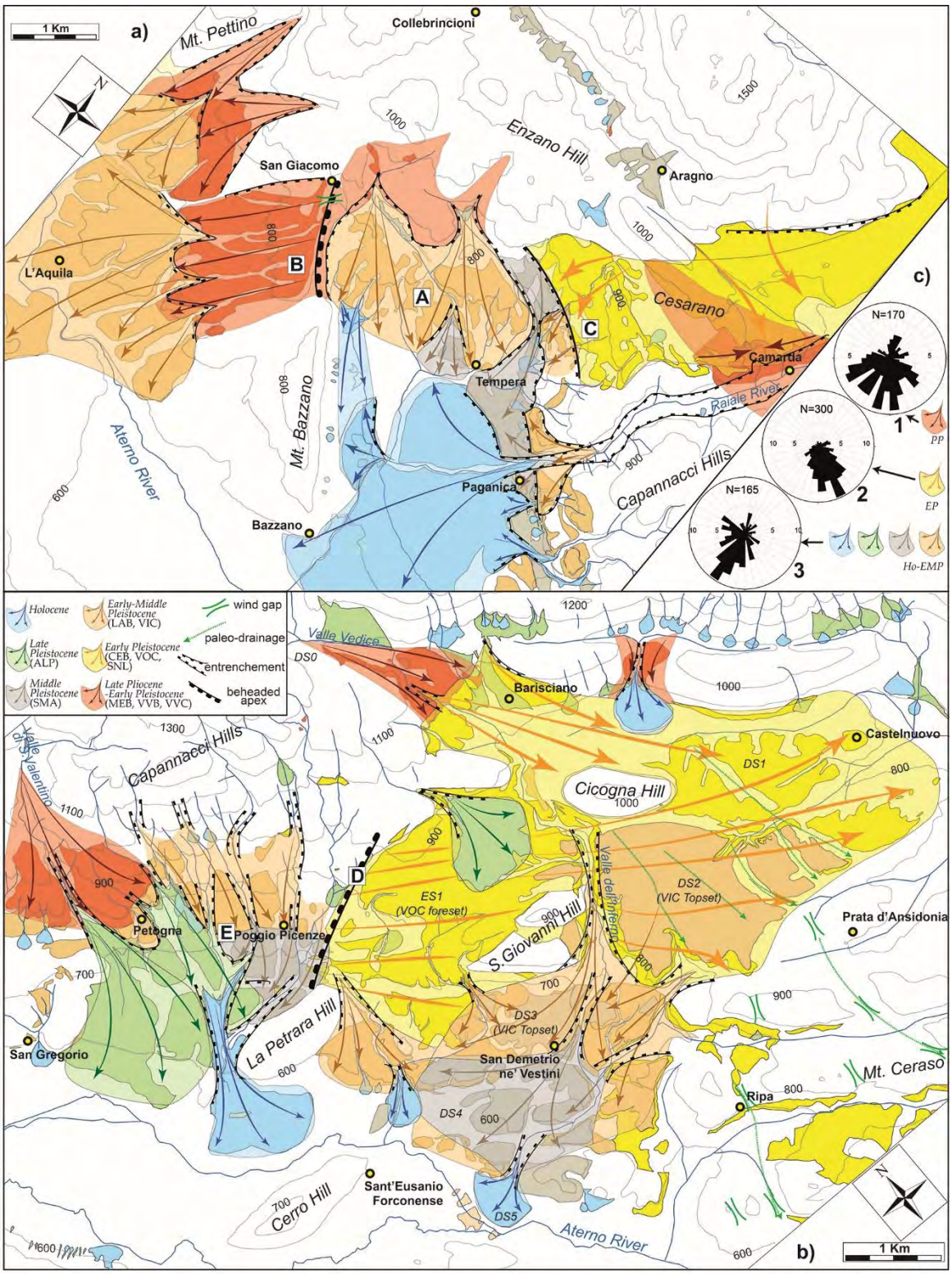
a)
1 Km
N
Mt. Pettino
Collebrincioni
Enzano Hill
Aragno
San Giacomo
L'Aquila
B
A
C
Cesarano
Camardia
Tempera
Raiale River
Mt. Bazzano
Aterno River
Paganica
Bazzano
Capannacci Hills
c)
N=170
N=300
N=165
1
2
3
PP
EP
Ho-EMP
Holocene
Early-Middle Pleistocene (LAB, VIC)
Late Pleistocene (ALP)
Early Pleistocene (CEB, VOC, SNL)
Middle Pleistocene (SMA)
Late Pliocene -Early Pleistocene (MEB, VVB, VVC)
wind gap
paleo-drainage
entrenchement
beheaded apex
Valle Vedice
DS0
Barisciano
Castelnuovo
DS1
Cicogna Hill
Valle di S.Valentino
Capannacci Hills
D
ES1 (VOC foreset)
DS2 (VIC Topset)
Valle dell'Inferno
S.Giovanni Hill
Prata d'Ansidonia
Petogna
E
Poggio Picenze
La Petrara Hill
DS3 (VIC Topset)
San Gregorio
San Demetrio ne' Vestini
Mt. Ceraso
Ripa
DS4
Sant'Eusanio Forconense
Cerro Hill
DS5
Aterno River
b)
1 Km

652 Fig. 11

Figure 11. Scheme of the inset relationships among the alluvial bodies. Light-coloured polygons represent the hypothetical original depositional body extent. Arrows indicate the discharges directions. Main body entrenchments and beheaded apexes are reported; a) Northern sector; b) Southern sector; c) Rose diagram of the depositional discharge directions for the different generations of alluvial bodies: 1) Plio-Pleistocene Fms., 2) Early Pleistocene Fm., 3) Holocene to Early/Middle Pleistocene Fms.

3.3 The interplay between faulting and the Quaternary deposition

The collected original geological, stratigraphic and morphologic data described in the previous chapters are summarized into three longitudinal and three transversal geological cross-sections (Fig. 12).

663

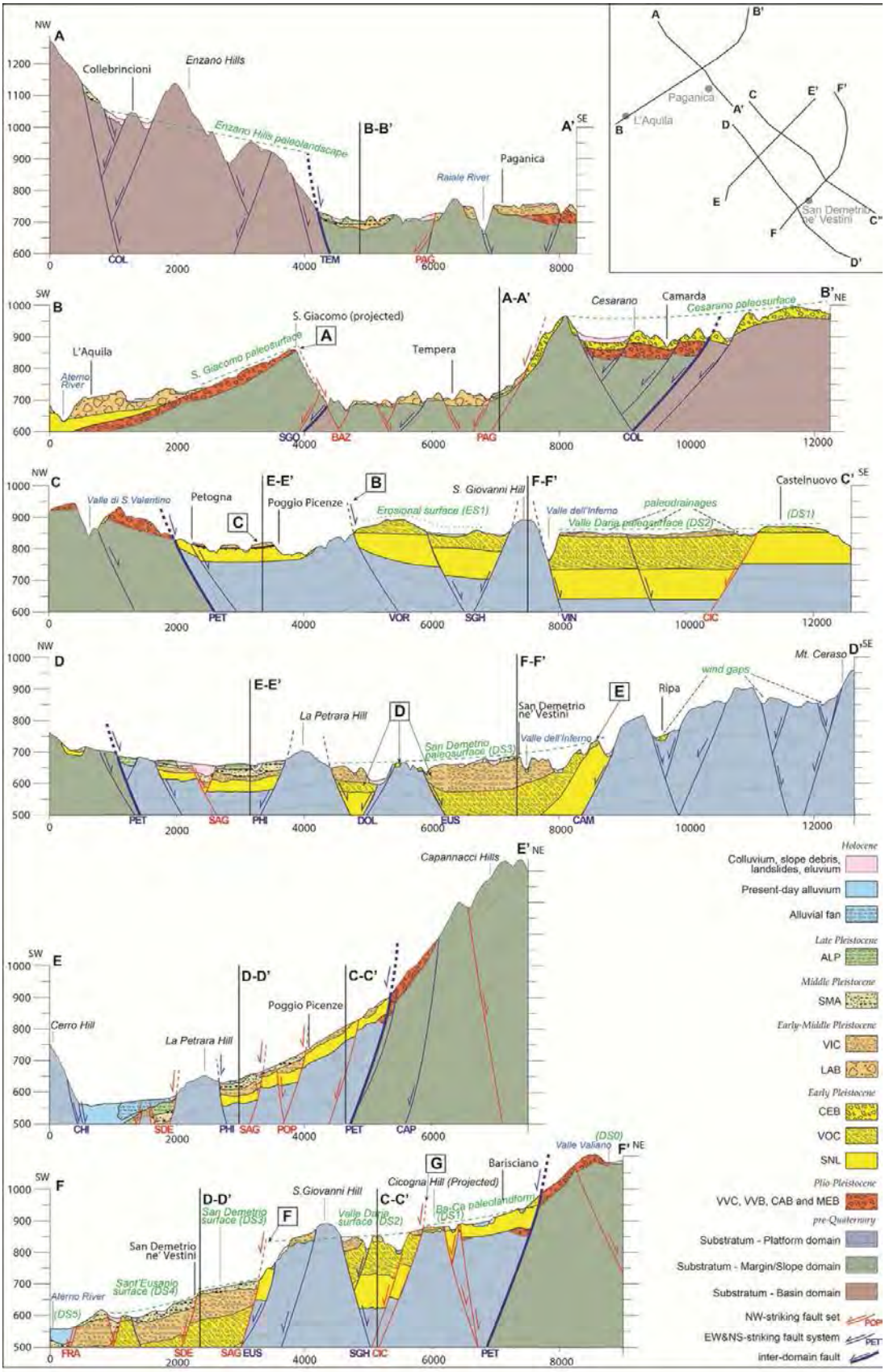
A
B-B'
A'
Collebrincioni
Enzano Hills
Enzano Hills paleolandscape
Raiale River
Paganica
B
A-A'
B'
L'Aquila
Aterno River
S. Giacomo paleosurface
S. Giacomo (projected)
Tempera
Cesarano
Camarda
Cesarano paleosurface
C
E-E'
F-F'
Valle di S. Valentino
Petogna
Poggio Picenze
Erosional surface (ES1)
S. Giovanni Hill
Valle dell'Inferno
Valle Daria paleosurface (DS2)
paleodrainages
Castelnuovo
C'
(DS1)
D
La Petrara Hill
San Demetrio paleosurface (DS3)
San Demetrio ne' Vestini
Ripa
wind gaps
Mt. Ceraso
D'
E
E'
Capannacci Hills
D-D'
C-C'
Cerro Hill
F
F'
G
Cicogna Hill (Projected)
Barisciano
Valle Valiano
(DS0)
Ba-Ca paleolandform (DS1)
Valle Daria surface (DS2)
San Demetrio surface (DS3)
Sant'Eusanio surface (DS4)
(DS5)
Holocene
Colluvium, slope debris, landslides, eluvium
Present-day alluvium
Alluvial fan
Late Pleistocene
ALP
Middle Pleistocene
SMA
Early-Middle Pleistocene
VIC
LAB
Early Pleistocene
CEB
VOC
SNL
Plio-Pleistocene
VVC, VVB, CAB and MEB
pre-Quaternary
Substratum - Platform domain
Substratum - Margin/Slope domain
Substratum - Basin domain
NW-striking fault set
EW&NS-striking fault system
inter-domain fault

Fig. 12

Figure 12. Geological cross and longitudinal sections of the Paganica-San Demetrio Basin (with vertical exaggeration 5x). Geological data are integrated with geophysical data of the substratum depth (see text for references). The inset shows the relation between section traces. See Figure 6 and 8 for detailed locations. Intersection lines among the geological sections are reported.

3.3.1 *The northern sector*

The longitudinal section A-A' (Fig. 12) shows the Enzano Hills area, bounded by the Collebrincioni Fault (COL), which preserves the envelope of a hanging SE-dipping paleo-landscape. Notably, the Tempera fault (TEM) bounds the Quaternary basin margin and additionally juxtaposes different substratum domains (hereinafter "inter-domain fault").

In the cross section B-B' (Fig. 12), the PAG sharply interrupts the Cesarano paleosurface with a vertical offset >200 m, as well as the BAZ cuts the feeding apex of the MEB Fm. (A in B-B', Fig. 12), contributing to form the graben infilled by the LAB Fm. Also, the Cesarano Fault (CES) represents an inter-domain fault affecting the Quaternary deposits, although with smaller vertical offset (~50 m).

3.3.2 *The central-southern sector*

The longitudinal section C-C' (Fig. 12) shows the inter-domain fault PET that acts as boundary of the Early-Pleistocene lacustrine basin. The parallel VOR fault downthrows the Early Pleistocene basin and allowed the southward thickening of the continental sequence (B in C-C', Fig. 12). Notably, the same fault shows a present-day topography of the hangingwall that does not seem compatible with a recent tectonic activity (i.e. landform reversal). Also, in the Poggio Picenze area, the VOC Fm. apex was eroded and replaced by the VIC Fm. Topset (C in C-C', Fig. 12), testifying a remarkable exhumation due to the footwall uplift. The San Giovanni Hill structural high is bounded by both EW- and N-S trending faults.

The longitudinal section D-D' (Fig. 12) shows the inter-domain Petogna fault (PET) acting as boundary of the Early-Pleistocene lacustrine basin. Other faults of the E-W&N-S system are responsible of

688 the horst and graben structures that affect the Quaternary basin. These structures separate continental
689 sequences with variable thickness and hiatuses (D in D-D', Fig. 12). The thickest basin, in the San Demetrio
690 ne' Vestini area, shows the progressive steepening of the angular unconformities between the depositional
691 surface (DS3), and the VIC, VOC and SNL Fms according to their increasing age (i.e. offlap growth strata,
692 *sensu* Burbank and Vergés, 1994) (E in D-D', Fig. 12).

693 The cross section E-E' (Fig. 12) shows the major splays of the NW-set (the Poggio Picenze –POP-
694 , San Giovanni –SAG- and San Demetrio -SDE- faults) that progressively down-throw the Quaternary basin
695 to the southwest with offset >50 m each. Here, both the E-W&N-S and the NW-trending faults appear to
696 control the structural highs of La Petrara and Mt. Cerro hills. The EW-trending Petogna fault (PET) affects
697 the Quaternary deposits and separates different substratum domains.

698 The cross section F-F' (Fig. 12) puts in evidence once again the E-W&N-S system that controlled
699 the structural highs (S. Giovanni and Cicogna Hills) or bounds the Early Pleistocene basin acting as
700 boundary fault (PET) (*sensu* Morley, 1995). Here, the NW-trending SAG fault produced offset of the
701 Quaternary deposits >200 m, along with considerable displacement of the San Demetrio surface (DS2) with
702 respect to the Valle Daria depositional surface (DS3) (F in F-F', Fig. 12). Differently, the Cicogna Hill fault
703 (CIC) is responsible for the irregular thickness and hiatuses of the Quaternary infill, with large offset of the
704 basin bottom (~200 m), but small offset of the top DS1 depositional surface (< 50 m) (G in F-F', Fig. 12),
705 testifying a post Early Pleistocene reduction of its activity.

706 3.3.3 *The intermountain satellite basins of the MAV basin*

707 Several strands of the E-W&N-S fault system appear to tectonically control the WNW-ESE
708 elongated Quaternary basins tributary of the MAV (i.e. intermountain satellite basins; e.g.: the Camarda,
709 Assergi, Stabiata, Collebrincioni basins, Fig. 2). Among them, the La Villa basin, in the hangingwall of
710 Filetto (FIL) and Mt. Ruzza (MRU) faults, hosts Plio-Pleistocene cemented slope breccias (VVB Fm.),

711 which typically show back-tilted attitude due to normal faulting, and coarse immature fluvial conglomerates
712 (VVC Fm.), which testify an ancient south-flowing fluvial network, pouring out into the BC sub-basin
713 through the Valle Vedice (Figs 2 and 8). Similarly, the Camarda breccia (CAB Fm.) attitude reveals the
714 presence of an old WNW-ESE elongated narrow basin, tectonically controlled and, possibly, linked to the
715 La Villa basin. This isolated old basin was subsequently: 1) infilled; 2) overlaid by the deposits of the proto-
716 Raiale valley that connected the Assergi and Paganica basins; 3) dissected by the Raiale River (Fig. 11a;
717 cross section B-B' in Fig. 12).
718
719
720 ## 4. Discussion
721 ### 4.1 The role of the inherited geological structures
722 Both primary E-W and secondary N-S-trending faults appear to be reactivated during multiple
723 tectonic phases driving the structural evolution of the Middle Aterno Valley basin (MAV). Episodes of
724 tectonic inversions are elsewhere documented in the Apennines and seem to play a key role in both
725 structural evolution and nucleation of earthquakes (Pace et al., 2002; Collettini et al., 2005; Pizzi and
726 Galadini, 2009; Lavecchia et al., 2012; Di Domenica et al., 2014).
727 The E-W&N-S system is mainly composed of conjugate strike-slip faults developed during the
728 Late Miocene-Early Pliocene compressional phase. Later, this system was reactivated with prevailing dip-
729 slip component, in response to the NE-directed Quaternary extensional stress field responsible for the NW-
730 trending faulting onset. In fact, the observed fault-slip data and the predicted slip-tendency kinematics of
731 the inverted fault planes indicate that major rotations in extension direction are not required to explain the
732 observed fault pattern (as example, see Pizzi and Galadini, 2009 and Reeve et al., 2015). Also Lavecchia et
733 al. (2012) report a full kinematic compatibility of the E-W-trending Mt. Stabiata fault (MST) with the

734 Paganica San Demetrio Fault System (PSDFS). Additionally, our paleomagnetic data from the oldest
735 continental deposits rule out the occurrence of significant rotations along vertical axes in the study area in
736 the last 2.5 Ma (Appendix E).

737 Some major E-W-trending fault (i.e. inter-domain faults) acted during the pre-thrusting Meso-
738 Cenozoic extensional phase, allowing the evolution of the substratum into different paleogeographic
739 environments. Then, during the Late Miocene-Early Pliocene compressive tectonics, they probably
740 reactivated as E-W&N-S system conjugate strike-slip faults (e.g. Pizzi and Galadini, 2009). These inter-
741 domain faults appear to control also the basin northern edge (e.g. San Giacomo -SGO- and Petogna -PET-
742 faults in Fig. 2) during the Quaternary extensional tectonic phase.

743

744

745 **4.2 Relationships between different fault-systems**

746 The NW-trending faults frequently cut the E-W&N-S ones along the Quaternary Paganica-San
747 Demetrio sub-basin (PSD). For example, the NW- Bazzano fault (BAZ) cuts the E-W- SGO fault in the
748 northern sector of the MAV (Fig. 6; A in cross section B-B' of Fig. 12). At the beginning of the extensional
749 phase, the south-dipping SGO normal fault juxtaposed the Miocene sandstones to the Jurassic formations
750 of the margin/slope carbonatic domain. Later on, during the Quaternary, the BAZ fault down-threw the
751 northeastern block, cut the SGO fault and created the accommodation space for the L'Aquila Breccias (LAB
752 Fm.).

753 Also, in the southeastern sector, the cross section F-F' shows the NW-San Giovanni fault (SAG)
754 that crosscuts the E-W- Sant'Eusanio fault (EUS) (Fig. 12). Similarly, the NW-striking Ripa (RIP) and
755 Bovacchio (BOV) faults interrupt several N-S-trending small fault strands (Fig. 8; longitudinal section D-
756 D', Fig. 12), controlling the Bovacchio and Opi Quaternary valleys and tilting the bedrock ridges of the Mt.

Ceraso area. The crosscut relationship between the two fault systems is testified by the wind gaps, carved on these ridges in coincidence of the N-S-trending faults. In fact, the wind gaps result from a SW-flowing paleo-drainage pouring out the early Middle Pleistocene Valle Daria surface, which was beheaded by the later NW-trending faults (Fig. 8 and Fig. 14a).

In many cases, the NW set abuts the E-W&N-S fault strands (stars in Fig. 2). These NW-trending faults may link into longer, double-bending fault sections via short E-W&N-S-trending strands.

Figure 13 sketches the polyphasic structural evolution of the area from the Jurassic extensional faulting to the onset and grow of the NW faults.

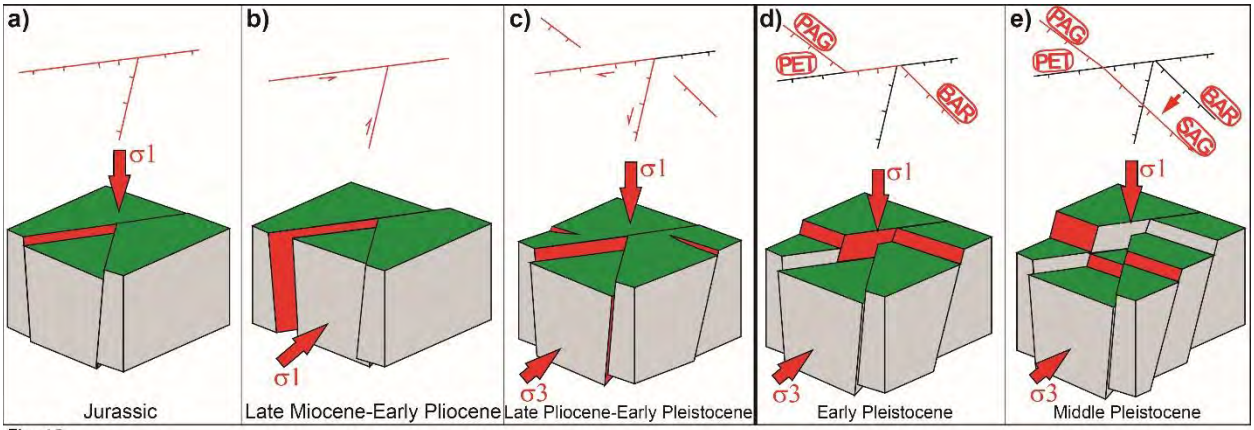

Fig. 13

Figure 13. Scheme of the fault systems evolution: **a)** Jurassic extensional faulting; **b)** Late Miocene-Early Pliocene conjugate strike-slip E-W&N-S fault system during the compressional phase; **c)** onset of the NW-trending normal and inversion of the conjugate strike-slip faults responding to the Late Pliocene-Early Pleistocene extensional stress field; **d)** Early Pleistocene NW-trending faults growth and linkage; **e)** the NW fault set bypassing the fault geometrical complexities.

4.3 Evidence for Quaternary activity of the fault-systems

The distribution and age of tectonic-controlled continental deposits provided constraints to assess the Quaternary tectonic activity of the two main fault systems (NW and the E-W&N-S).

In general, our observations indicate that the conjugate E-W&N-S fault system pre-dates almost everywhere or is coeval with the early NW-trending faults and that most of its activity lasted during the development of immature NW-trending strands (Fig. 13). The later NW-trending fault set dislocates the inherited, pre-existing complex morphology formed by the reactivated E-W&N-S system, without overprinting it completely, and their combined activity gives rise to a complex interference pattern (i.e. 3D-horst and graben of Fig. 13e) that results in prominent intra-basin highs exposing Cretaceous to Miocene carbonate rocks (e.g., San Gregorio, La Petrara, Mt. Cerro, S. Giovanni and Colle Cicogna Hills).

More in detail, the E-W&N-S extensional fault system evidences a syn-depositional tectonics in the Early Pleistocene basin, with formation of local depocentres in their hangingwall and hiatuses at their footwall (see longitudinal sections C-C' and D-D' in Fig. 12). Notably, this fault system bounds the continental basin (mostly as inter-domain fault) affecting the Plio-Early Pleistocene deposits and most of its activity is confined to the Early Pleistocene, being topographic and Middle-Late Pleistocene offsets small or negligible. On this basis, we hypothesize that the reactivation of the E-W&N-S fault system started at the beginning of the regional extensional phase (Late Pliocene), forming ~E-W oriented Quaternary basins separated by structural highs (e.g. Cerro, La Petrara and S. Giovanni hills, Fig. 8). This is in agreement with the geometry of the buried top-bedrock surface reconstructed from geophysical imaging (Pucci et al., 2016; Civico et al., 2017), which suggests: 1) an early stage of basin development promoted by the E-W&N-S fault system; 2) a southward thickening of buried depocentres; 3) a complex structure of the MAV basin, characterized by several topographic highs and lows representing horsts and depocentres, respectively.

In the southwestern sector, the NW-fault set shows the most outstanding evidence of tectonic control on landforms and Quaternary deposition: 1) syn-tectonic deposition, as testified by Early-Middle to Late Pleistocene prominent alluvial bodies progradational pattern (Figs. 11 and 14a), with the significant variation in the VIC Fm. thickness, due to local base level lowering, that progressively increases from a

few meters at DS2, to > 50 m at DS3 (stratigraphic columns 7 and 8 in Fig 9; cross section F-F' in Fig. 12; Fig. 14b); 2) hundreds of meters of topographic offset of depositional surfaces (cross section F-F' in Fig. 12; Fig. 14b and c); 3) the > 30° dip of the VIC Fm. across the San Giovanni fault (SAG) that can be explained by a later deformation between the fault blocks or due to syn-depositional tectonics (Fig. 14b and d); 4) the offlap growth strata due to syn-tectonic deposition over the relay ramp formed at the Ripa (RIP)-San Demetrio (SDE) and at the Bovacchio (BOV)-SAG faults stepover, also evidenced by Giaccio et al. (2012) (Fig. 9, longitudinal section D-D' in Fig. 13 and Fig. 14e).

Notably, the large thickness of the VIC Fm. coincides with the Early-Middle Pleistocene climatic transition (between 1.2 and 0.6 Ma), a period characterized worldwide by intense glacial phases and large alluvial fans sedimentation (Head and Gibbard, 2005; Ehlers and Gibbard, 2007). The progradational pattern indicates a high rate of sediment input, not balanced by the accommodation space generated by the basin subsidence, due to the westward migration of the Quaternary fault activity. Parallel splays, from BAR to FRA fault, progressively affects younger continental deposits, toward the present-day depocentre of the San Demetrio basin (Fig. 8), in agreement with the reconstruction proposed by Civico et al., (2017).

The earlier westward migration of the activity from MRU to PAG fault, with respect to that from BAR to Frascara (FRA) fault required an Early Pleistocene linkage of BAR fault to the left-stepping PAG fault through the E-W&N-S system (e.g. PET fault) that breached the relay ramp and formed a double fault bend bounding the PSD sub-basin deposits (Fig. 13d). Subsequently (late Early Pleistocene), the migration from BAR to SAG fault and the alignment with the PAG, allowed the fault bend bypass (Fig. 13e). A possible linkage of the SAG and the PAG, through the Poggio Picenze fault (POP), is also envisaged by Pucci et al. (2016) on the basis of geological cross sections integrated with geophysical investigation. Notably, the largest geologic offset affects the Early-Middle Pleistocene alluvial deposits and are located along the alignment PAG-POP-SAG, in coincidence with the prominent Quaternary tectonic scarps described by Civico et al., (2015). Based on the 135±15 m morphologic offset of the 450-600 yr old age

(as minimum) of the Valle Daria depositional surface (DS2; Fig. 14b), the maximum Middle Pleistocene throw rate of the SAG fault is 0.27±0.07 mm/a. This estimate, compared with the Quaternary throw rates obtained from independent approaches, is within the spread and in the average of values proposed by other authors for the same fault, and is similar to those proposed for the PAG (Fig. 15). Notably, the long/middle term throw rate estimates, although more disperse and with some outlier (e.g. Galli et al., 2010), present comparable Pleistocene-Holocene ones, suggesting a stability in the PAG and SAG activity.

The NW-trending fault set shows activity limited to the Late Pliocene-Early Pleistocene only in La Villa basin, where the Mt. Ruzza fault (MRU) controls the small thickness of VVB Fm., or in the Barisciano-Castelnuovo basin (BC), where the Barisciano fault (BAR) affects the VVB, SNL and VOC Fms. Conversely, in the northern sector of the PSD sub-basin, as evidenced also by geophysical investigations (Pucci et al., 2016; Villani et al., 2017 and Civico et al., 2017), the leading Paganica fault (PAG) controlled the basin infill with marked strain localization during the entire Pleistocene, probably after the early migration from the deactivated, eastern MRU fault.

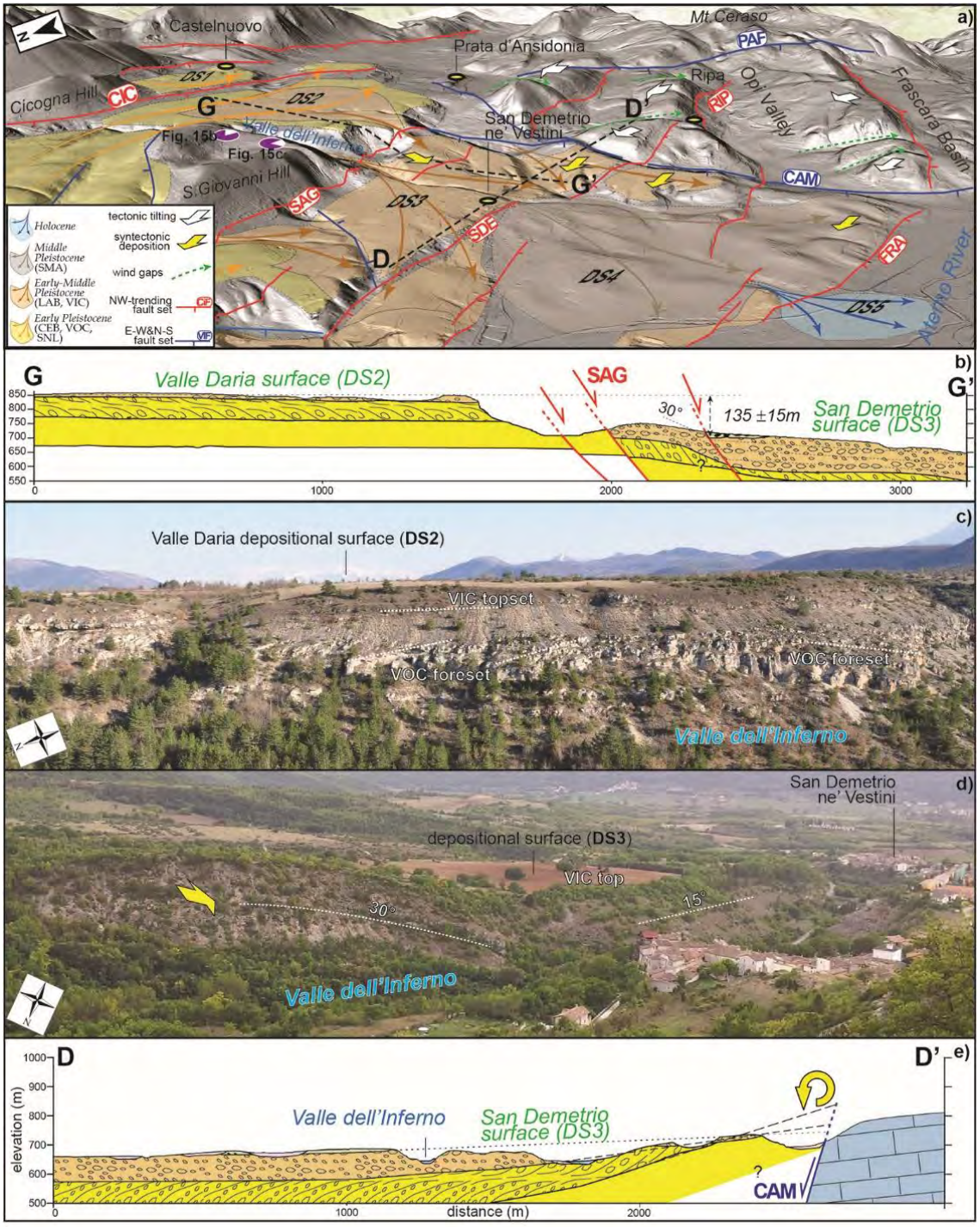

838 Fig. 14

839 **Figure 14.** a) Hillshaded DTM oblique view of the San Demetrio sub-basin morphology. Alluvial bodies (with
840 depositional and erosional surfaces) and their relationship with faulting are evidenced; b) Cross section showing the

minimum offset of the Valle Daria depositional surface. Note the attitudes tilting of the VIC bedding in proximity of the SAG fault; c) Panoramic view of the Valle Daria depositional surface (DS2) and Valle dell'Inferno outcropping sequence. The dashed white lines highlight the VOC foreset and VIC topset attitudes. See Figure 14a for location and orientation of the viewpoint; d) Panoramic view of the San Demetrio depositional surface (DS3) and Valle dell'Inferno outcropping sequence. The dashed white lines highlight the attitudes tilting of the VIC bedding; e) Cross section showing the steepening of unconformities within the relay ramp between SAG and RIP faults. See Figure 14a for location and orientation of the viewpoints.

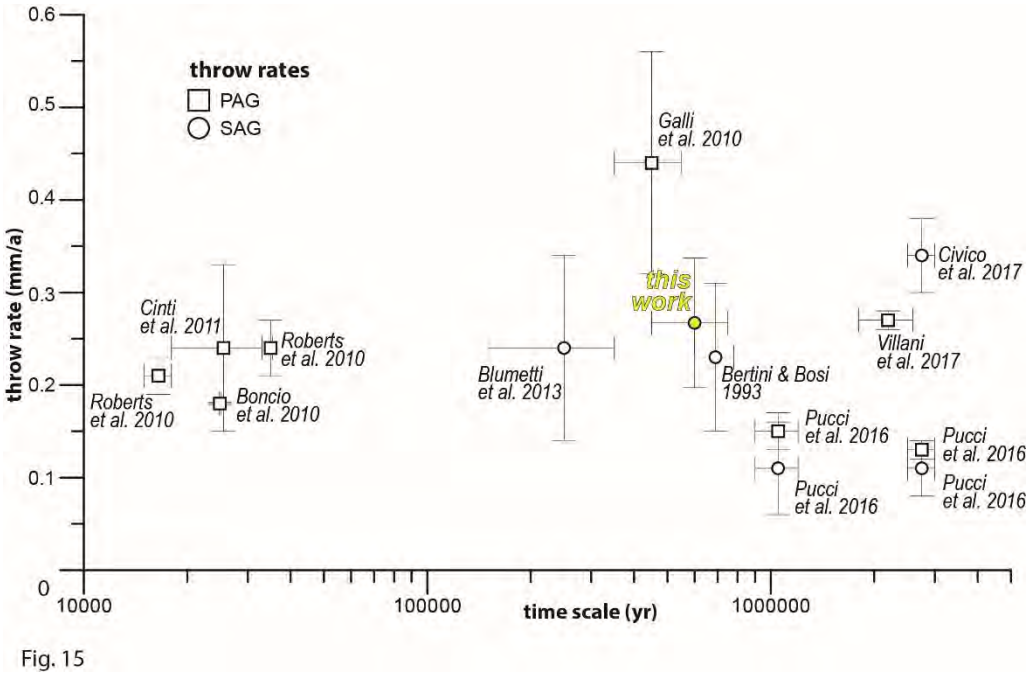

Figure 15: Comparison between throw rate estimates (with uncertainties) from the literature and this work.

4.4 Reconstruction of the Middle Aterno Valley evolution

By integrating stratigraphic and structural results, we developed a conceptual model for the Quaternary tectono-sedimentary evolution and surface expression of the MAV basin (Fig. 16), with particular emphasis on: i) the three-dimensional evolution of the basin due to the interplay of NW-and E-

W&N-S-trending fault system; and ii) the different alluvial system generations as response to tectonic vertical movements. The evolution of the MAV can be summarized as follows:

a) Late Pliocene-Early Pleistocene. During the onset of the NE-SW directed extension, the E-W&N-S-trending faults are reactivated as transtensional faults. Early sub-basins (mostly E-W trending) forms in their hangingwall, isolated by structural bedrock highs. The increase of syn-rift topographic relief triggers high-energy deposits production with mass-wasting and slope debris/breccia emplacements in dry or transport-limited conditions (MEB, VVB, CAB), and few alluvial fans due to immature drainage catchments (VVC) (Fig. 16a).

b) Early Pleistocene. The sub-basins are deepened and enlarged by the activity of the E-W&N-S-trending faults with the contribution of early NW-trending normal faults. The latter link through short E-W&N-S fault elements (BAR-PAG, via PET), deactivating some splay (e.g. MRU) (Fig. 16b). The tectonically lowered base-level promotes the development of a larger drainage catchment, with increased fluvial-dominated sediment transport (i.e. the *proto*-MAV). The result is the onset of a lacustrine environment (SNL Fm.), locally characterized by a prograding Gilbert fan delta (VOC) fed by a main SE-flowing fluvial channel (i.e. the paleo-Aterno River). The continental deposits progressively fill the depocentres forming a wide coalescing basin (Fig. 16b). Contemporaneously, a SSW-flowing drainage starts to dissect some E-W trending basins and connects the Assergi Basin with the proto-MAV through the paleo-Raiale River valley, filled by its tributaries to form the Cesarano surface (CEB).

c) Early Middle Pleistocene–Holocene. NW-trending normal faults grow by linkage (PAG and SAG, via POP) forming the PSDFS (Fig. 16c) and cross-cut E-W&N-S fault elements, enhancing the previously formed intra-basin highs forming a complex, 3D horst and graben-like style. The NW fault splays develop obliquely and overprint the Early Pleistocene physiography, disconnecting past depositional systems and producing staircase morphology of

the exhumed footwall blocks. As a result, the NW fault system controls footwall-sourced alluvial fans and induces a change in the direction of the syn-tectonic discharges that prograde to a new, narrower southwestern depocentre (Fig. 16c).

It is worth noting that, on the basis of stratigraphic relationships and dating data, the slope debris/breccia (VVB and CAB) and alluvial fans due to immature drainage catchments (VVC) are referred to a Late Pliocene-Early Pleistocene syn-rift production and are not a later lateral facies variation of VOC Fm. (see Giaccio et al., 2012). Furthermore, based on facies characteristics, our results suggest that the MEB mass-wasting deposits cannot origin from a far catastrophic detachment (see Blumetti et al., 2013; Esposito et al., 2014) but rather derives from a proximal source, favoring the preservation of rock-slide olistoliths.

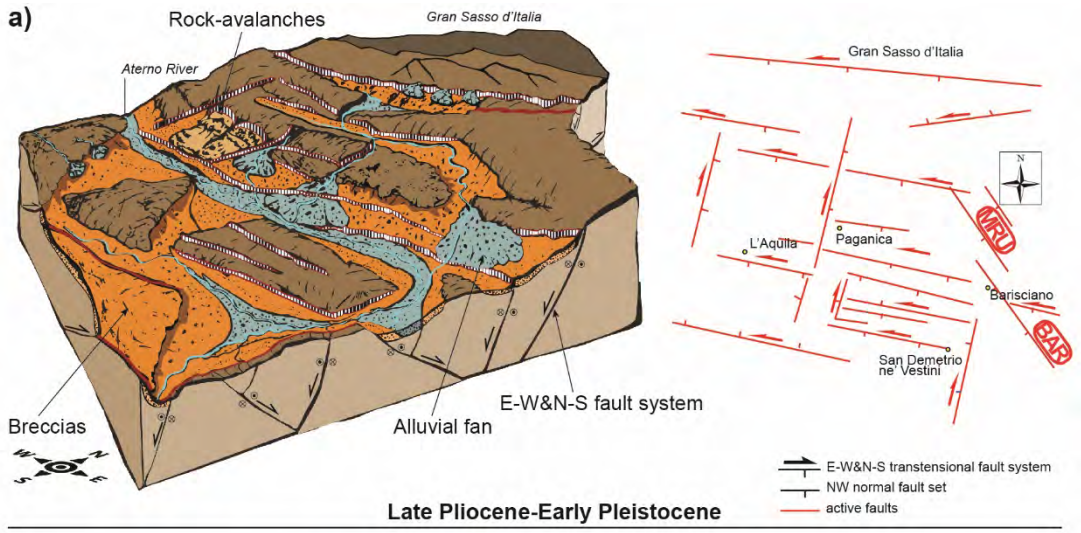
a)
Rock-avalanches
Gran Sasso d'Italia
Aterno River
Breccias
Alluvial fan
E-W&N-S fault system
Gran Sasso d'Italia
L'Aquila
Paganica
Barisciano
San Demetrio ne' Vestini
MRU
BAR
E-W&N-S transtensional fault system
NW normal fault set
active faults
Late Pliocene-Early Pleistocene

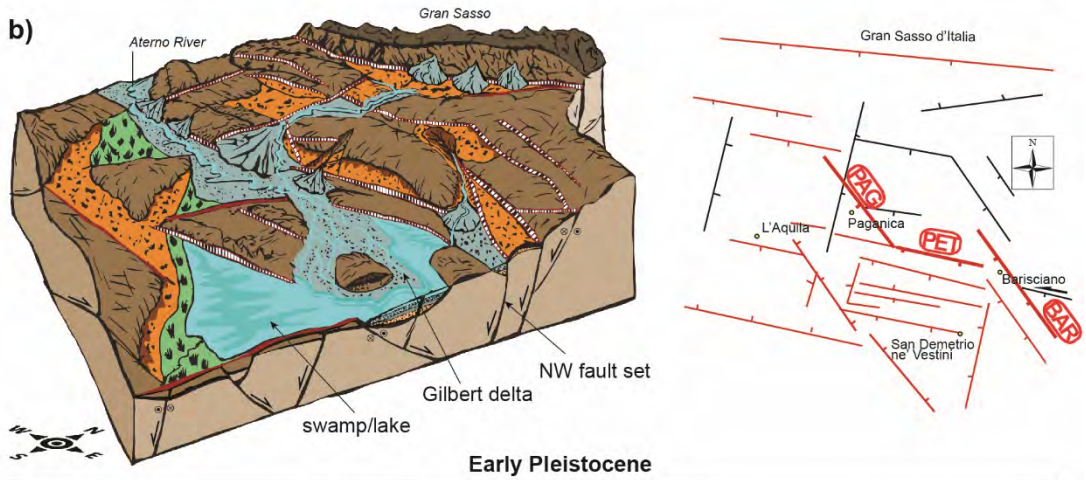
b)
Gran Sasso
Aterno River
NW fault set
Gilbert delta
swamp/lake
Gran Sasso d'Italia
L'Aquila
Paganica
Barisciano
San Demetrio ne' Vestini
PAG
PET
BAR
Early Pleistocene

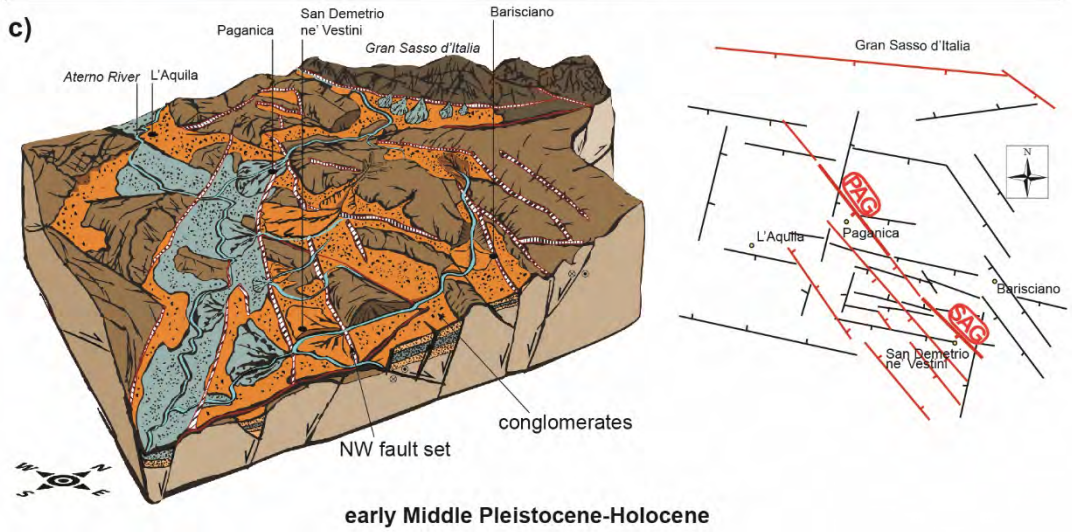
c)
Paganica
San Demetrio ne' Vestini
Barisciano
Gran Sasso d'Italia
Aterno River
L'Aquila
conglomerates
NW fault set
Gran Sasso d'Italia
L'Aquila
Paganica
Barisciano
San Demetrio ne' Vestini
PAG
SAG
early Middle Pleistocene-Holocene

Fig. 16

892 **Figure 16.** Physiographic evolution of the Middle Aterno Valley: **a)** onset of the NE-SW extension: the E-W&N-S
893 faults are reactivated as transtensional faults. Early sub-basins depocentres (mostly ~E-W trending) forms in their
894 hangingwall, isolated by structural bedrock highs; **b)** the sub-basins are tectonically deepened and enlarged. Early
895 NW-trending normal faults link to the E-W&N-S ones. Fluvial-dominated sediment transport increases and a
896 lacustrine environment takes place locally characterized by a prograding Gilbert fan delta; **c)** The NW-trending fault
897 system grows and overprints the Early Pleistocene physiography, disconnecting past depositional systems (from
898 original drawing by P. Baccheschi).
899
900

901 **4.5 Segment boundaries of the 2009 earthquake fault**

902 The 2009 L'Aquila seismic event highlighted the need to define the causative seismogenic fault
903 extent and the location of the bounding permanent barriers in the perspective of seismic risk mitigation (i.e.,
904 to define segment boundaries). The long-term expression of a fault system, in terms of geometric or
905 structural complexities, is an invaluable tool to discriminate the persistency of barriers at long time-scales
906 (10^4 to 10^6 yr), being aware that it is difficult to recognize transient dynamic barriers as coseismic ruptures
907 may occur on a small portion of the segment or jump from one segment to another, generating a much larger
908 event (Wesnousky, 2006).

909 As regards the northern extent of the fault segment responsible of the 2009 L'Aquila earthquake,
910 different interpretations are proposed: 1) on the basis of the 2009 coseismic ruptures, Falcucci et al. (2009)
911 locate the boundary at the intersection with the Mt. Stabiata fault (MST); 2) according to Lavecchia et al.,
912 (2012) the northern boundary includes also MST (Figs. 2 and 17); 3) Galli et al. (2011) and Moro et al.
913 (2013) hypothesize that the northward portion of the PAG fault may rupture together with the UAFS,
914 therefore defining a 30 km-long active segment capable of generating up to M 7 events (Fig. 2 and 17).

915 With respect to the southeastern boundary: some authors suggest it is located south of the SAG
916 fault, beyond the PAG fault (Fig. 2 and 17) (Cinti et al., 2011; Giaccio et al., 2012; Lavecchia et al., 2012;
917 Villani et al., 2015; Civico et al., 2015; Blumetti et al., 2013 and 2017), implying potential rupture lengths

ranging between 12 and 19 km. Conversely, a few authors (Gori et al., 2012; Moro et al., 2013) infer that the area between the PAG and SAG was not affected by normal faulting during the Quaternary and thus it represents a barrier between the two fault segments preventing any structural linkage and hampering rupture propagation.

Our geological data suggest that the SAG is part of the L'Aquila earthquake fault segment, linked to the PAG via POP fault to form the PSDFS starting from the early Middle Pleistocene (Fig. 17). According to some authors (Gori et al., 2012; Moro et al., 2013; Falcucci et al., 2015), the lack of obvious Quaternary offsets and the presence of outcropping interposed bedrock, represent the evidence of a permanent discontinuity that impedes the linkage of the PAG with the SAG fault, forming a barrier to the southern propagation of coseismic ruptures. Differently, we evidenced the interposed bedrock to be intra-basin structural highs (e.g. La Petrara and S. Giovanni Hills), which are remnants of the Early Pleistocene horst and graben morphology later dissected by the NW fault set.

On the basis of the reconstruction of the Quaternary evolution of the MAV, we set the main fault PSDFS segment boundaries at the tips of the PAG-SAG alignment (Fig. 17),

The northern boundary is located at the northern edge of the PSD sub-basin, where the NW-trending strands appears to be interrupted by E-W&N-S fault system. In particular, the northern propagation of the Paganica graben is hampered by the major EW-trending, inter-domain Tempera fault (TEM) (Fig. 2 and 6). Along with the SGO, the TEM fault played the role of transfer between the PAG and the left stepping Upper Aterno Fault System (UAFS) and uplifted the Enzano Hills paleolandform, as a breached relay ramp. Accordingly, the growth of the NW-trending strands crossing the Collebrincioni (COL) and MST faults, is hindered since they likely enter into the UAFS stress shadow (Fig. 2 and 17).

The southern boundary is located at the southern edge of the PSD sub-basin. Here the Mt. Ceraso ridge is affected by several aligned N-S-trending faults from the Campana fault (CAM) up to the Prata d'Ansidonia/Fontecchio fault (PAF), which shows evidence of Quaternary activity, as reported by Giaccio

et al. (2012). Although mostly cut by the NW set, these N-S-trending faults are responsible for a progressive northwest down-throwing of the Mt. Ceraso relief and possibly the PAF and CAM interrupted the SAG propagation acting as transfer fault to the right stepping Middle Aterno Fault System (MAFS) (Fig. 17). Notably, after the 2009 earthquake, in correspondence of the southeastern sector of the MAV, the crustal anisotropy of shear waves is locally characterized by a pattern of fast polarization directions with considerable divergence from the NW-striking major normal faults, and rotations of up to 90° (Baccheschi et al., 2016), which may be explained by the presence of deep NNE-striking faults (e.g. CAM and PAF) defining the structural southern boundary of the MAV.

In the proposed segmentation model, the major inherited structures of conjugate E-W&N-S fault, acting as transfer zones at the relay ramps with the nearby active fault systems, play a critical role in the definition of the segment boundaries. These boundaries can be considered pseudo-stationary up to the Late Pleistocene, providing an overall segment length of 19±3 km, in agreement with the morphotectonic long-term expression of the PSDFS pointed out by Civico et al. (2015). Under the assumption that the geological surface expression reflects the geometry and kinematics of the seismological faults and that, consequently, the observed barriers persist at depth, and, by using empirical scaling laws between fault length and earthquake size (Kanamori, 1977; Leonard, 2010), an expected maximum magnitude of up to 6.5 is estimated, in agreement with the magnitude of paleo- and historical earthquakes occurred on this fault (Cinti et al., 2011; Rovida et al., 2016; Blumetti et al., 2017, among the others). Thus, the inherited geological structures control fault boundaries and can be particularly important role in the interaction between segmented fault systems of the Central Apennines: for example, they can be activated under dynamic coseismic conditions, as highlighted by the complex rupture history of the mainshocks of the recent 2016 Amatrice-Norcia seismic sequence (among the others: Scognamiglio et al., 2018).

We note that the size of the Holocene Paganica-San Demetrio Basin (PSDB), which results from the geological long-term activity of the PSDFS, is coherent with the extent of the coseismic displacement

966 field imaged by DInSAR data (Atzori et al., 2009) (Fig. 17a). Moreover, the slip distribution at depth of the
967 L'Aquila earthquake causative fault, given by the strong motion inversion (Scognamiglio et al., 2010;
968 Cirella et al., 2012), appears to have occurred along the entire length of the PSDFS (Fig. 17b), supporting
969 the linkage of the PAG-SAG faults in one main system, with persistent boundaries. However, the
970 observations following the 2009 earthquake and the local complex structural setting envisage a high
971 variability in the slip distribution within the fault system boundaries during subsequent earthquakes. In fact,
972 the overall slip on the fault at depth during the 6 April 2009 earthquake involved a surface area much larger
973 than the shallow patch that provoked surface faulting, as envisaged by the limited length of the primary
974 coseismic ruptures, mostly confined to the northwestern part of the PSDFS. Consequently, deep slip
975 movement characterized the rupture process of the L'Aquila earthquake also on the southern part of the
976 PSDFS, whereas the surface slip deficit was undoubtedly due to the complex structural setting. Thus, the
977 pattern of long-term displacement cannot be simply the result of repeated characteristic earthquakes
978 (Schwartz & Coppersmith, 1984; Sieh, 1996). The long-term activity of the PSFDS, the throw-rates of the
979 PAG and SAG faults evaluated over different time-scales (spanning the last 2.5-3 Myr) and ranging
980 between 0.2 and 0.3 mm/yr, together with the available paleoseismic evidence (Boncio et al., 2010; Cinti
981 et al., 2011; Blumetti et al., 2017), all demonstrate that the whole section of the PSDFS ruptured the surface
982 in the past through episodic large events (M> 6.5) involving the whole segment or through smaller events
983 (M ~6) possibly with heterogeneous slip alternatively concentrated onto the PAG or the SAG fault.

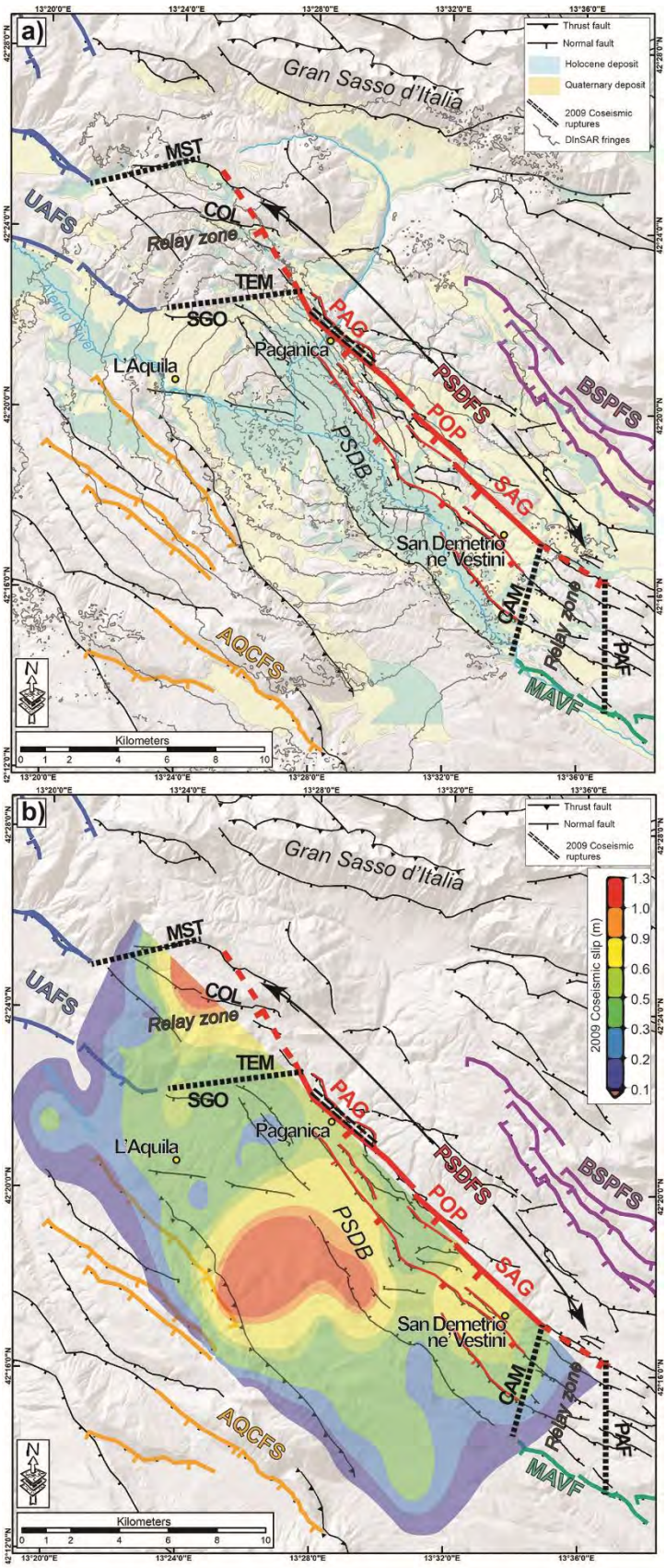
a)
Thrust fault
Normal fault
Holocene deposit
Quaternary deposit
2009 Coseismic ruptures
DInSAR fringes
Gran Sasso d'Italia
MST
UAFS
COL
Relay zone
TEM
SGO
PAG
Paganica
L'Aquila
Aterno River
PSDFS
POP
PSDB
SAG
BSPFS
San Demetrio ne' Vestini
CAM
Relay zone
PAF
MAVF
AQCFS
N
Kilometers
0 1 2 4 6 8 10
b)
Thrust fault
Normal fault
2009 Coseismic ruptures
2009 Coseismic slip (m)
1.3
1.0
0.9
0.6
0.5
0.3
0.2
0.1
Gran Sasso d'Italia
MST
UAFS
COL
Relay zone
TEM
SGO
PAG
Paganica
L'Aquila
PSDFS
POP
PSDB
SAG
BSPFS
San Demetrio ne' Vestini
CAM
Relay zone
PAF
MAVF
AQCFS
N
Kilometers
0 1 2 4 6 8 10

Fig. 17

Figure 17. Scheme of the spatial relationship among the main fault systems around the MAV and the 2009 coseismic data. The fault system are coloured: Upper Aterno (UAFS - blue); Aquila-Campo Felice (AQCFS - orange); Barisciano-San Pio (BSPFS - violet); Middle Aterno (MAFS - green); Paganica-San Demetrio (PSDFS - red). The main PSDFS segment boundaries are evidenced as E-W&N-S strands breaching relay ramps in the stepover with UAFS and MAFS. DEM from 10m-resolution TIN-Italy (Tarquini et al., 2017). **a)** Relationship between the tectonic PSDB Holocene basin and DInSAR fringes from Atzori et al. (2009); b**)** Relationship between the PSDFS and coseismic slip distribution at depth from Cirella et al. (2012).

4.6 Structural heterogeneities and earthquake rupture processes

The joint Quaternary activity of two principal fault-systems and their cross-cut/abutting relationships originate a considerable structural complexity. This structural complexity has likely driven some of the peculiarities illustrated by the geometrical and dynamic complexity of the 2009 rupture process, in particular: 1) the dispersion of rupture slip approaching the surface of the San Demetrio sector, impeding the surface faulting along the southern section of the PSDFS; 2) the multiform kinematic behaviour, with strong spatial and temporal heterogeneities during the rupture history (e.g. Cirella et al., 2012); 3) the multiple post-seismic slip patches (Cheloni et al., 2010 and 2014); 4) the large crustal volume activated imaged by aftershocks clustering on both major fault segment and subsidiary structures (Valoroso et al., 2014); 5) the composite and stepping structural arrangement of the surface rupture trace (e.g. Boncio et al., 2010).

5. Conclusions

We conducted extensive fieldwork, structural analysis of the fault population coupled with LiDAR data analysis and multi-disciplinary dating techniques, for the refinement of the stratigraphic relationships

of the Quaternary continental deposits filling the Middle Aterno Valley basin (MAV) that hosts the 2009 L'Aquila earthquake seismogenic structure.

The directional, kinematic, paleo-stress and slip-tendency analyses show the presence of a dip-slip, NW-striking fault system along with an old conjugate strike-slip fault system, ~E-W- and ~N-S-striking, that was reactivated with transtensional movement during the extensional Plio-Quaternary tectonic phase.

In concert, we reconstructed the original geometry and extension of the main alluvial bodies and the interaction between local base level lowering due to local tectonic forcing and clastic output from the mountain catchments as transient response to active faulting on the basis of: 1) an updated stratigraphic framework of the Quaternary continental sequence of the MAV, correlating different facies and thickness of the continental deposits; 2) correlations between different morphostructures. We highlighted that the tectono-sedimentary evolution of the MAV basin is driven by the interplay of NW- and E-W&N-S-trending faults. The latter controlled most of the oldest sedimentary traps of the area and are responsible for the horst and graben structures and thus of the bedrock highs and syn-tectonic deposition with variable thickness and several hiatuses of the continental infill.

Along the northern sector, the long-term subsidence of the Paganica graben, controlled by NW-trending faults, caused the drainage network to re-organize leaving wind gaps on the uplifted blocks, upraising several generations of depositional surfaces and beheaded apex/toe of Pliocene-Early Pleistocene breccia bodies, on the uplifted footwall block. Along the central-southern sector, the tectonic control on the alluvial fan evolution is represented by well-preserved alluvial bodies showing a change through time of the main flow directions with SE-prograding delta lobes of the Early Pleistocene deposits that are subject to spectacular entrenchments due to younger telescopic fans, prograding to southwest, towards the new local base level. In particular, the relationship between the geomorphic features and deposits distribution allows to infer: i) an Early Pleistocene tectonic activity for the E-W- and N-S-striking fault sets and ii) a

1033 subsequent onset and linkage of several splays of the NW-striking fault system, via E-W&N-S-trending
1034 fault sections, that in some cases evolved to bypass the interposed geometrical complexities.

1035 The distribution at the surface of the Quaternary deposits results from the interference of differently
1036 orientated fault systems and suggests a poly-phase evolution of the MAV. The geometry of the Bagno,
1037 Paganica and San Demetrio basins suggests that they possibly originated as separate basins controlled by
1038 the activity of previously isolated fault systems (the E-W&N-S fault system) during Late Pliocene-Early
1039 Pleistocene. Whereas, in a later phase, the activity of the NW fault set became predominant, with the San
1040 Giovanni (SAG) and Paganica (PAG) faults acting as leading strands in accruing most of the cumulative
1041 displacement of the Paganica-San Demetrio Fault System (PSDFS) since the end of the Early Pleistocene.
1042 In fact, the SAG fault exhibits a maximum post-450 ka throw rate (0.27±0.07 mm/a) similar to the PAG
1043 fault one and on the average of values proposed in literature for both faults, thus confirming that they are
1044 the most active strands of the PSDFS.

1045 Notably, the major elements of the E-W&N-S system that controlled the Quaternary Paganica-San
1046 Demetrio Basin (PSDB) edges during the last extensional tectonic phase, breaching the relay ramps and
1047 acting as transfer faults to the nearby stepping active fault systems, set the segment boundaries that constrain
1048 the maximum PSDFS length to 19±3 km.

1049 The size of the PSDFS as derived from its reconstruction in this study, is coherent with the extent
1050 of the 6 April 2009 L'Aquila earthquake causative fault in terms of coseismic displacement field imaged
1051 by DInSAR data (Atzori et al., 2009) and coseismic slip distribution at depth, modeled by strong motion
1052 inversion (Scognamiglio et al., 2010; Cirella et al., 2012 - Fig 17b). In this context, the limited length of
1053 the primary coseismic ruptures, reaching the surface only along the northern part of the long-term
1054 expression of the fault segment, may indicate a non-characteristic (Schwartz & Coppersmith, 1984; Sieh,
1055 1996) pattern in displacement accumulation at the surface. The joint Quaternary activity of the two principal
1056 fault-systems originated a compound fault pattern within the upper seismogenic volume: this could have

influenced the complex rupture process of the 2009 earthquake, such as dissipating the rupture slip approaching the surface of the San Demetrio sector, up to impede the surface faulting along the southern section of the PSDFS.

The wealth of studies on the 2009 L'Aquila earthquake provides a unique opportunity, not only in Italy but worldwide, to integrate multidisciplinary data and results and test geological segmentation models against true, well-documented earthquake ruptures. This test demonstrates that a comprehensive reconstruction of the long-term deformational history of active fault systems through detailed field mapping and geophysical imaging of both the Quaternary faults and basins, offers a significant contribution to the better understanding of seismogenic structures and their seismic potential.

Acknowledgements

The work was financially supported by the MIUR (Italian Ministry of Education, University and Research) project "FIRB Abruzzo - High-resolution analyses for assessing the seismic hazard and risk of the areas affected by the 6 April 2009 earthquake", ref. RBAP10ZC8K_005 and RBAP10ZC8K_007, and by Agreement INGV-DPC 2012-2021. Special thanks to Gaetano Robustelli and Ari Matmon for the valuable discussions in the field and to Francesca Di Laura, graphic Lab INGV, for the contribution in the production of the block diagrams of Figure 16. Comments and suggestions provided by the reviewers definitely helped in improving the final version of the manuscript.

References

Aitken, M. J., 1998. An introduction to optical dating: the dating of Quaternary sediments by the use of photon stimulated luminescence, Oxford Science Publications, Oxford, 267 pp.

Allen, P. A., Allen, J.R., 2005. Basin Analysis: Principls and Applications, 2nd ed. Blackwell Publishing Ltd, Oxford.

Allmendinger, R.W., Cardozo, N., Fisher, D., 2013. Structural Geology Algorithms: Vectors & Tensors. Cambridge University Press, Cambridge. doi:10.1017/S0016756812000192

Allmendinger, R.W., Gephart, J.W., Marrett, R.A., 1989. Notes on Fault Slip Analysis. Quant. Interpret. joints faults.

Amoroso, S., Di Eusebio, F., Taddei, B., Tallini, M., Totani, F., Totani, G., 2010. Campagna di indagini geologiche, geotecniche e geofisiche per lo studio della risposta sismica locale della città dell'Aquila: La stratigrafia dei sondaggi giugno-agosto 2010.

Angelier, J., Mechler, P., 1977. Sur une méthode graphique de recherche des contraintes principales également utilisable en tectonique et en séismologie: la méthode des dièdres droits. Bull. Soc. géol. France, 19, 1309–1318.

Anzidei, M., Boschi, E., Cannelli, V., Devoti, R., Esposito, A., Galvani, A., Melini, D., Pietrantonio, G., Riguzzi, F., Sepe, V., Serpelloni, E., 2009. Coseismic deformation of the destructive April 6, 2009 L'Aquila earthquake (central Italy) from GPS data. Geophys. Res. Lett. 36, 3–7. doi:10.1029/2009GL039145

Atzori, S., Hunstad, I., Chini, M., Salvi, S., Tolomei, C., Bignami, C., Stramondo, S., Trasatti, E., Antonioli, A., Boschi, E., 2009. Finite fault inversion of DInSAR coseismic displacement of the 2009 L'Aquila earthquake (central Italy). Geophys. Res. Lett. 36, 1–6. doi:10.1029/2009GL039293

Baccheschi, P., Pastori, M., Margheriti, L., Piccinini, D., 2016. Shear wave splitting of the 2009 L'Aquila seismic sequence: Fluid saturated microcracks and crustal fractures in the Abruzzi region (Central Apennines, Italy). Geophys. J. Int. 204, 1531–1549. doi:10.1093/gji/ggv536

Bagh, S., Chiaraluce, L., De Gori, P., Moretti, M., Govoni, A., Chiarabba, C., Di Bartolomeo, P., Romanelli, M., 2007. Background seismicity in the Central Apennines of Italy: The Abruzzo region case study. Tectonophysics 444, 80–92. doi:10.1016/j.tecto.2007.08.009

Bagnaia, R., D'epifanio, A., Sylos Labini, S., 1992a. Aquila and Subequan basins: an example of Quaternary evolution in Central Apennines, Italy. Quat. Nov. 2, 187–2209.

Bagnaia, R., D'Epifanio, A., Sylos Labini, S., 1992b. Aquila and Subequan basins: an example of Quaternary evolution in Central Apennines, Italy. Quat. Nov. 2, 187–209.

Balasco, M., Galli, P., Giocoli, A., Gueguen, E., Lapenna, V., Perrone, A., Piscitelli, S., Rizzo, E., Romano, G., Siniscalchi, A., Votta, M., 2011. Deep geophysical electromagnetic section across the middle Aterno Valley (central Italy): Preliminary results after the April 6, 2009 L'Aquila earthquake. Boll. di Geofis. Teor. ed Appl. 52, 443–455. doi:10.4430/bgta0028

Benedetti, L., Manighetti, I., Gaudemer, Y., Finkel, R., Malavieille, J., Pou, K., Arnold, M., Aumaître, G., Bourlès, D., Keddadouche, K., 2013. Earthquake synchrony and clustering on Fucino faults (Central Italy) as revealed from in situ 36Cl exposure dating. J. Geophys. Res. Solid Earth 118, 4948–4974. doi:10.1002/jgrb.50299

Bertini, T., Bosi, C., 1993. La tettonica quaternaria della conca di Fossa (L'Aquila). Quat. 6, 293–314.

Blair, T. C. McPherson, J. G., 1994. Alluvial fans and their natural distinction from rivers based on morphology, hydraulic processes, sedimentary processes, and facies assemblages. Journal of Sedimentary Research. 64 (3a), 450–489.

Blumetti, A.M., Guerrieri, L., Vittori, E., 2013. The primary role of the Paganica-San Demetrio fault system in the seismic landscape of the Middle Aterno Valley basin (Central Apennines). Quat. Int. 288, 183–194. doi:10.1016/j.quaint.2012.04.040

Blumetti, A. M., Di Manna, P., Comerci, V., Guerrieri, L., & Vittori, E., 2017. Paleoseismicity of the san demetrio ne'Vestini fault (L'Aquila basin, Central Italy): implications for seismic hazard. Quaternary International, 451, 129-142.

Boncio, P., Lavecchia, G., Milana, G., Rozzi, B., 2004a. Seismogenesis in Central Apennines, Italy: An integrated analysis of minor earthquake sequences and structural data in the Amatrice-Campotosto

area. Ann. Geophys. 47, 1723–1742.
Boncio, P., Lavecchia, G., Pace, B., 2004b. Defning a model of 3D seismogenic sources for Seismic Hazard Assessment applications: The case of central Apennines (Italy). J. Seismol. 8, 407–425. doi:10.1023/B:JOSE.0000038449.78801.05
Boncio, P., Pizzi, A., Brozzetti, F., Pomposo, G., Lavecchia, G., Di Naccio, D., Ferrarini, F., 2010. Coseismic ground deformation of the 6 April 2009 L'Aquila earthquake (central Italy, Mw6.3). Geophys. Res. Lett. 37, 2–7. doi:10.1029/2010GL042807
Bosi, C., Bertini, T., 1970. Geologia della Media Valle dell'Aterno. Mem. della Soc. Geol. Ital. IX, 719–777.
Bosi, C., Galadini, F., Giaccio, B., Messina, P., Sposato, A., 2003. Plio-Quaternary continental deposits in the Latium-Abruzzi Apennines: the correlation of geological events across different intermontane basins. Quat. 16, 55–76.
Bottari, C., Barbano, M. S., Pirrotta, C., Azzaro, R., Ristuccia, G., Gueli, A., 2013. Archaeological evidence for a possible first century AD earthquake in the necropolis of Abakainon (NE Sicily). Quaternary International, 316, 190-199.
Burbank, D.W., Vergés, J., 1994. Reconstruction of topography and related depositional systems during active thrusting. J. Geophys. Res. 99, 20281–20297. doi:10.1029/94JB00463
Bøtter-Jensen, L., Bulur, E., Duller, G. A. T., Murray, A. S., 2000. Advances in luminescence instrument systems. Radiation Measurements, 32, 523–528.
Butler, R.W.H., Tavarnelli, E., Grasso, M., 2006. Structural inheritance in mountain belts: An Alpine-Apennine perspective. J. Struct. Geol. 28, 1893–1908. doi:10.1016/j.jsg.2006.09.006
Braucher, R., Del Castillo, P., Siame, L., Hidy, A. J., & Bourles, D. L. (2009). Determination of both exposure time and denudation rate from an in situ-produced 10Be depth profile: A mathematical proof of uniqueness. Model sensitivity and applications to natural cases. Quaternary Geochronology, 4(1), 56-67.
Byerlee, J.D., 1978. Friction of rocks. Pure and Applied Geophysics 116, 615-626.
Calderoni, G., Di Giovambattista, R., Vannoli, P., Pucillo, S., Rovelli, A., 2012. Fault-trapped waves depict continuity of the fault system responsible for the 6 April 2009 M W 6.3 L'Aquila earthquake, central Italy. Earth Planet. Sci. Lett. 323–324, 1–8. doi:10.1016/j.epsl.2012.01.003
Carafa, M. M. C., Bird, P. (2016). Improving deformation models by discounting transient signals in geodetic data: 2. Geodetic data, stress directions, and long-term strain rates in Italy. Journal of Geophysical Research: Solid Earth, 121(7), 5557-5575. Doi: 10.1002/2016JB013038.
Carobene, L., Cirrincione, R., De Rosa, R., Gueli, A. M., Marino, S., Troja, S. O., 2006. Thermal (TL) and optical stimulated luminescence (OSL) techniques for dating Quaternary colluvial volcaniclastic sediments: An example from the Crati Basin (Northern Calabria). Quaternary International, 148 (1), 149-164.
Carminati, E., Doglioni, C., 2012. Earth-Science Reviews Alps vs. Apennines : The paradigm of a tectonically asymmetric Earth. Earth Sci. Rev. 112, 67–96. doi:10.1016/j.earscirev.2012.02.004
Cavinato, G.P., De Celles, P.G., 1999. Extensional basins in the tectonically bimodal central Apennines fold-thrust belt, Italy: Response to corner flow above a subducting slab in retrograde motion. Geology 27, 955–958. doi:10.1130/0091-7613(1999)027<0955:EBITTB>2.3.CO;2
Centamore, E., Crescenti, U., Dramis, F., Bigi, S., Fumanti, F., Rusciadelli, G., Coltorti, M., Chiocchini, M., Didaskalou, P., Mancinelli, A., Matteucci, R., Micarelli, A., Potetti, M., Pignatti, J.S., Raffi, I., Sirna, G., Conte, G., Petitta, M., 2006. Note illustrative della Carta Geologica d'Italia alla scala 1:50000, Foglio 359 L'Aquila. S.EL.CA., Firenze.
Centamore, E., Nisio, S., 2003. Effects of uplift and tilting in the Central-Northern Apennines (Italy). Quat. Int. 101–102, 93–101. doi:10.1016/S1040-6182(02)00092-7

Cesi, C., Di Filippo, M., Di Nezza, M., Ferri, F., 2010. Caratteri gravimetrici della media Valle del Fiume Aterno, in: Gruppo di Lavoro MS–AQ (Ed.), Microzonazione Sismica per La Ricostruzione Dell'area Aquilana. Regione Abruzzo – Dipartimento della Protezione Civile, L'Aquila, p. 3 vol. e Cd-.

Cheloni, D., D'Agostino, N., D'Anastasio, E., Avallone, A., Mantenuto, S., Giuliani, R., Mattone, M., Calcaterra, S., Gambino, P., Dominici, D., Radicioni, F., Fastellini, G., 2010. Coseismic and initial post-seismic slip of the 2009 Mw 6.3 L'Aquila earthquake, Italy, from GPS measurements. Geophys. J. Int. 181, 1539–1546. doi:10.1111/j.1365-246X.2010.04584.x

Cheloni, D., Giuliani, R., D'Anastasio, E., Atzori, S., Walters, R.J., Bonci, L., D'Agostino, N., Mattone, M., Calcaterra, S., Gambino, P., Deninno, F., Maseroli, R., Stefanelli, G., 2014. Coseismic and post-seismic slip of the 2009 L'Aquila (central Italy) MW6.3 earthquake and implications for seismic potential along the Campotosto fault from joint inversion of high-precision levelling, InSAR and GPS data. Tectonophysics 622, 168–185. doi:10.1016/j.tecto.2014.03.009

Chiarabba, C., Amato, A., Anselmi, M., Baccheschi, P., Bianchi, I., Cattaneo, M., Cecere, G., Chiaraluce, L., Ciaccio, M.G., De Gori, P., De Luca, G., Di Bona, M., Di Stefano, R., Faenza, L., Govoni, A., Improta, L., Lucente, F.P., Marchetti, A., Margheriti, L., Mele, F., Michelini, A., Monachesi, G., Moretti, M., Pastori, M., Piana Agostinetti, N., Piccinini, D., Roselli, P., Seccia, D., Valoroso, L., 2009. The 2009 L'Aquila (central Italy) M<inf>w</inf>6.3 earthquake: main shock and aftershocks. Geophys. Res. Lett. 36. doi:10.1029/2009GL039627

Chiarabba, C., Jovane, L., DiStefano, R., 2005. A new view of Italian seismicity using 20 years of instrumental recordings. Tectonophysics 395, 251–268. doi:10.1016/j.tecto.2004.09.013

Chiaraluce, L., 2012. Unravelling the complexity of Apenninic extensional fault systems: A review of the 2009 L'Aquila earthquake (Central Apennines, Italy). J. Struct. Geol. 42, 2–18. doi:10.1016/j.jsg.2012.06.007

Chiaraluce, L., Barchi, M., Collettini, C., Mirabella, F., Pucci, S., 2005. Connecting seismically active normal faults with Quaternary geological structures in a complex extensional environment: The Colfiorito 1997 case history (northern Apennines, Italy). Tectonics 24, 1–16.

Chiaraluce, L., Chiarabba, C., De Gori, P., Di Stefano, R., Improta, L., Piccinini, D., Schlagenhauf, A., Traversa, P., Valoroso, L., Voisin, C., 2011a. The 2009 L'Aquila (central Italy) seismic sequence. Boll. di Geofis. Teor. ed Appl. 52, 367–387. doi:10.4430/bgta0019

Chiaraluce, L., Valoroso, L., Piccinini, D., Di Stefano, R., De Gori, P., 2011b. The anatomy of the 2009 L'Aquila normal fault system (central Italy) imaged by high resolution foreshock and aftershock locations. J. Geophys. Res. Solid Earth 116, 1–25. doi:10.1029/2011JB008352

Choi, J. H., Kim, J. W., Murray, A. S., Hong, D. G., Chang, H. W., Cheonga, C. S., 2009. OSL dating of marine terrace sediments on the southeastern coast of Korea with implications for Quaternary tectonics. Quaternary International, 199 (1–2), 3-14.

Cinti, F.R., Pantosti, D., De Martini, P.M., Pucci, S., Civico, R., Pierdominici, S., Cucci, L., Brunori, C.A., Pinzi, S., Patera, A., 2011. Evidence for surface faulting events along the Paganica fault prior to the 6 April 2009 L'Aquila earthquake (central Italy). J. Geophys. Res. Solid Earth 116, 1–21. doi:10.1029/2010JB007988

Cipollari, P., Cosentino, D., 1995. Miocene unconformities in the Central Apennines: geodynamic significance and sedimentary basin evolution. Tectonophysics 252, 375–389.

Cirella, A., Piatanesi, A., Tinti, E., Chini, M., Cocco, M., 2012. Complexity of the rupture process during the 2009 L'Aquila, Italy, earthquake. Geophys. J. Int. 190, 607–621. doi:10.1111/j.1365-246X.2012.05505.x

Civico, R., Pucci, S., De Martini, P.M., Pantosti, D., 2015. Morphotectonic analysis of the long-term surface expression of the 2009 L'Aquila earthquake fault (Central Italy) using airborne LiDAR data. Tectonophysics 644, 108–121.

Civico, R., Sapia, V., Di Giulio, G., Villani, F., Pucci, S., Baccheschi, P., Amoroso, S., Cantore, L., Di Naccio, D., Hailemikael, S., Smedile, A., Vassallo, M., Marchetti, M., Pantosti, D., 2017. Geometry and evolution of a fault-controlled Quaternary basin by means of TDEM and single-station ambient vibration surveys: The example of the 2009 L'Aquila earthquake area, central Italy. J. Geophys. Res. Solid Earth 122. doi:10.1002/2016JB013451

Collettini, C., Chiaraluce, L., Pucci, S., Barchi, M.R., Cocco, M., 2005. Looking at fault reactivation matching structural geology and seismological data. J. Struct. Geol. 27, 937–942.

Cowie, P. A., Phillips, R. J., Roberts, G. P., McCaffrey, K., Zijerveld, L. J. J., Gregory, L. C., ... & Freeman, S. P. H. T. (2017). Orogen-scale uplift in the central Italian Apennines drives episodic behaviour of earthquake faults. Scientific Reports, 7, 44858.

D'Agostino, N., Speranza, F., Funiciello, R., 1997. Le Brecce Mortadella dell'Appennino Centrale: primi risultati di stratigrafia magnetica. Il Quaternario 10, 385-388.

D'Agostino, N., Chamot-Rooke, N., Funiciello, R., Jolivet, L., Speranza, F., 1998. The role of pre-existing thrust faults and topography on the styles of extension in the Gran Sasso range (central Italy). Tectonophysics 292, 229–254. doi:10.1016/S0040-1951(98)00070-5

D'Agostino, N., Mantenuto, S., D'Anastasio, E., Giuliani, R., Mattone, M., Calcaterra, S., Gambino, P., Bonci, L., 2011. Evidence for localized active extension in the central Apennines (Italy) from global positioning system observations. Geology 39, 291–294. doi:10.1130/G31796.1

Delvaux, D., Sperner, B., 2003. Stress tensor inversion from fault kinematic indicators and focal mechanism data: the tensor program. In: New Insights into Structural Interpretation and Modelling (D. Nieuwland Ed.). Geological Society, London, Special Publications, 212: 75-100

Devoti, R., Esposito, A., Pietrantonio, G., Pisani, A.R., Riguzzi, F., 2011. Evidence of large scale deformation patterns from GPS data in the Italian subduction boundary. Earth Planet. Sci. Lett. 311, 230–241. doi:10.1016/j.epsl.2011.09.034

Di Domenica, A., Petricca, P., Trippetta, F., Carminati, E., Calamita, F., 2014. Investigating fault reactivation during multiple tectonic inversions through mechanical and numerical modeling: An application to the Central-Northern Apennines of Italy. J. Struct. Geol. 67, 167–185. doi:10.1016/j.jsg.2014.07.018

Di Domenica, A., Turtù, A., Satolli, S., Calamita, F., 2012. Relationships between thrusts and normal faults in curved belts: New insight in the inversion tectonics of the Central-Northern Apennines (Italy). J. Struct. Geol. 42, 104–117. doi:10.1016/j.jsg.2012.06.008

Duller, G. A. T., 2008. Single-grain optical dating of Quaternary sediments: why aliquot size matters in luminescence dating. Boreas, 37, 589–612.

Ehlers, J., Gibbard, P.L., 2007. The extent and chronology of Cenozoic Global Glaciation. Quat. Int. 164–165, 6–20. doi:10.1016/j.quaint.2006.10.008

Esposito, C., Mugnozza, G.S., Tallini, M., Seta, M. Della, 2014. Evidence of Quaternary rock avalanches in the central Apennines : new data and interpretation of the huge clastic deposit of the L ' Aquila basin (central Apennines , Italy) 16, 12238.

Falcucci, E., Gori, S., Moro, M., Fubelli, G., Saroli, M., Chiarabba, C., Galadini, F., 2015. Deep reaching versus vertically restricted Quaternary normal faults: Implications on seismic potential assessment in tectonically active regions: Lessons from the middle Aterno valley fault system, central Italy. Tectonophysics 651, 186–198. doi:10.1016/j.tecto.2015.03.021

Falcucci, E., Gori, S., Peronace, E., Fubelli, G., Moro, M., Saroli, M., Giaccio, B., Messina, P., Naso, G., Scardia, G., Sposato, A., Voltaggio, M., Galli, P., Galadini, F., 2009. The Paganica Fault and Surface Coseismic Ruptures Caused by the 6 April 2009 Earthquake (L'Aquila, Central Italy). Seismol. Res. Lett. 80, 940–950. doi:10.1785/gssrl.80.6.940

Faure Walker, J.P., Roberts, G.P., Sammonds, P.R., Cowie, P., 2010. Comparison of earthquake strains

over 10^2 and 10^4 year timescales: Insights into variability in the seismic cycle in the central Apennines, Italy. J. Geophys. Res. Solid Earth 115, 1–26. doi:10.1029/2009JB006462
Fifield, L. K., Ophel, T. R., Allan, G. L., Bird, J. R., Davie, R. F. (1990). Accelerator mass spectrometry at the Australian National University's 14UD accelerator: experience and developments. Nuclear Instruments and Methods in Physics Research Section B: Beam Interactions with Materials and Atoms, 52 (3), 233-237.
Fuchs, M., Lang, A., 2001. OSL dating of coarse-grain fluvial quartz using single-aliquot protocols on sediments from NE-Peloponnese, Greece. Quaternary Science Reviews, 20, 783–787.
Galadini, F., Galli, P., 2000. Active Tectonics in the Central Apennines (Italy) – Input Data for Seismic Hazard Assessment. Nat. Hazards 22, 225–270. doi:10.1023/A:1008149531980
Galli, P.A.C., Giaccio, B., Messina, P., Peronace, E., Zuppi, G.M., 2011. Palaeoseismology of the L'Aquila faults (central Italy, 2009, Mw 6.3 earthquake): Implications for active fault linkage. Geophys. J. Int. 187, 1119–1134. doi:10.1111/j.1365-246X.2011.05233.x
Galli, P., Camassi, R., Azzaro, R., Bernardini, F., Castenetto, S., Molin, D., Peronace, E., Rossi, A., Vecchi, M., Tertulliani, A., 2009. Il terremoto aquilano del 6 aprile 2009: rilievo macrosismico, effetti di superficie ed implicazioni sismotettoniche. Quat.
Galli, P., Galadini, F., Pantosti, D., 2008. Twenty years of paleoseismology in Italy. Earth-Science Rev. 88, 89–117. doi:10.1016/j.earscirev.2008.01.001
Galli, P., Giaccio, B., Messina, P., 2010. The 2009 central Italy earthquake seen through 0.5 Myr-long tectonic history of the L'Aquila faults system. Quat. Sci. Rev. 29, 3768–3789. doi:10.1016/j.quascirev.2010.08.018
Gawthorpe, R.L., Leeder, M.R., 2000. Tectono-sedimentary evolution of active extensional basins. Basin Res. 12, 195–218. doi:10.1111/j.1365-2117.2000.00121.x
GE.MI.NA., 1963. Ligniti e Torbe dell'Italia Continentale. Geomineraria Nazionale, Torino.
Gerardi, F., Smedile, A., Pirrotta, C., Barbano, M. S., De Martini, P. M., Pinzi, S., Gueli, A. M., Ristuccia, G. M., Stella, G., Troja, S.O., 2012. Geological record of tsunami inundations in Pantano Morghella (southeastern Sicily) both from near and far-field sources, Natural Hazards and Earth System Sciences 12 (4), 1185-1200.
Giaccio, B., Galli, P., Messina, P., Peronace, E., Scardia, G., Sottili, G., Sposato, A., Chiarini, E., Jicha, B., Silvestri, S., 2012. Fault and basin depocentre migration over the last 2 Ma in the L'Aquila 2009 earthquake region, central Italian Apennines. Quat. Sci. Rev. 56, 69–88. doi:10.1016/j.quascirev.2012.08.016
Giunta, G., Gueli, A. M., Monaco, C., Orioli, S., Ristuccia, G. M., Stella, G., Troja, S. O., 2012. Middle-Late Pleistocene marine terraces and fault activity in the Sant'Agata di Militello coastal area (northeastern Sicily). Journals of Geodynamics, 55, 32–40.
Gruppo di Lavoro MS–AQ, 2010. Microzonazione sismica per la ricostruzione dell'area aquilana. Regione Abruzzo – Dipartimento della Protezione Civile, L'Aquila.
Guérin, G., Mercier, N., Adamiec, G., 2011. Dose-rate conversion factors: update. Ancient TL, 29, 5-8.
Gori, S., Falcucci, E., Atzori, S., Chini, M., Moro, M., Serpelloni, E., Fubelli, G., Saroli, M., Devoti, R., Stramondo, S., Galadini, F., Salvi, S., 2012. Constraining primary surface rupture length along the Paganica fault (2009 L'Aquila earthquake) with geological and geodetic (DInSAR and GPS) data. Ital. J. Geosci. 131, 359–372. doi:10.3301/IJG.2012.21.
Guerrieri, L., Baer, G., Hamiel, Y., Amit, R., Blumetti, A.M., Comerci, V., Di Manna, P., Michetti, A.M., Salamon, A., Mushkin, A., Sileo, G., Vittori, E., 2010. InSAR data as a field guide for mapping minor earthquake surface ruptures: Ground displacements along the Paganica Fault during the 6 April 2009 L'Aquila earthquake. J. Geophys. Res. Solid Earth 115. doi:10.1029/2010JB007579
Harvey, A.M., 2002. The role of base-level change in the dissection of alluvial fans: case studies from

southeast Spain and Nevada. Geomorphology, 45, 67–87. Head, M.J., Gibbard, P.L., 2005. Early-Middle Pleistocene transitions: an overview and recommendation for the defining boundary. Geol. Soc. London, Spec. Publ. 247, 1–18. doi:10.1144/GSL.SP.2005.247.01.01

Herrmann, R.B., Malagnini, L., Munafò, I., 2011. Regional moment tensors of the 2009 L'Aquila earthquake sequence. Bull. Seismol. Soc. Am. 101, 975–993. doi:10.1785/0120100184

Hunstad, I., 2003. Geodetic strain in peninsular Italy between 1875 and 2001. Geophys. Res. Lett. 30, 1–4. doi:10.1029/2002GL016447

Huntley, D. J., Godfrey-Smith, D. I., Thewalt, M. L. W., 1985. Optical dating of sediments. Nature, 313, 105-107.

Improta, L., Villani, F., Bruno, P.P., Castiello, A., Rosa, D. De, Varriale, F., Punzo, M., Brunori, C.A., Civico, R., Pierdominici, S., Berlusconi, A., Giacomuzzi, G., 2012. High-resolution controlled-source seismic tomography across the Middle Aterno basin in the epicentral area of the 2009, Mw 6.3, L'Aquila earthquake (central Apennines, Italy). Ital. J. Geosci. 131, 373–388. doi:10.3301/IJG.2011.35

Jain, M., Botter-Jensen, L., and Singhvi, A. K., 2003. Dose evaluation using multiple-aliquot quartz OSL: test of methods and a new protocol for improved accuracy and precision. Radiation Measurements 37, 67-80.

Kanamori, H., 1977. The energy release in great earthquakes, J. Geophys. Res. 82 (20), 2981–2987.

Kirschvink, J.L., 1980. The least-squares line and plane and the analysis of palaeomagnetic data. Geophysical Journal of the Royal Astronomical Society 62, 699-718.

Lavecchia, G., Ferrarini, F., Brozzetti, F., Nardis, R. De, Boncio, P., Chiaraluce, L., 2012. From surface geology to aftershock analysis: Constraints on the geometry of the L'Aquila 2009 seismogenic fault system. Ital. J. Geosci. 131, 330–347. doi:10.3301/IJG.2012.24

Le Dortz, K., Meyer, B., Sébrier, M., Nazari, H., Braucher, R., Fattahi, M., Benedetti, L., Foroutan, M., Siame, L., Bourlès, D., Talebian, M., Bateman, M. D., Ghoraishi, M., 2009. Holocene right-slip rate determined by cosmogenic and OSL dating on the Anar fault, Central Iran. Geophysical Journal International, 179(2), 700-710.

Magri, D., Rita, F. Di, Palombo, M.R., 2010. An Early Pleistocene interglacial record from an intermontane basin of central Italy (Scoppito, L'Aquila). Quat. Int. 225, 106–113. doi:10.1016/j.quaint.2009.04.005

Mancini, M., Cavuoto, G., Pandolfi, L., Petronio, C., Salari, L., Sardella, R., 2012. Coupling basin infill history and mammal biochronology in a Pleistocene intramontane basin: The case of western L'Aquila Basin (central Apennines, Italy). Quat. Int. 267, 62–77. doi:10.1016/j.quaint.2011.03.020

Marrett, R., Allmendinger, R. W., 1990. Kinematic analysis of fault-slip data. Journal of Structural Geology 12, 8, 973-986.

Mejdahl, V., 1979. Thermoluminescence dating: beta-dose attenuation in quartz grains. Archaeometry, 21, 61–72.

Murray, A. S., Wintle, A. G., 2000. Luminescence dating of quartz using an improved single-aliquot regenerative-dose protocol. Radiation Measurements, 32 (1), 57-73.

Murray, A. S., Wintle, A. G., 2003. The single aliquot regenerative dose protocol: potential for improvements in reliability. Radiation Measurements, 37, 377–381.

Messina, P., Moro, M., Speranza, F., 2001. Primi risultati di stratigrafia magnetica su alcune formazioni continentali dell'alta valle dell'Aterno (Italia centrale). Quat. 14, 167–172.

Miall, A.D., 2013. Principles of sedimentary basin analysis. Springer Science & Business Media. doi:10.1017/CBO9781107415324.004

Montone, P., Alessio, G., Alfonsi, L., Brunori, C.A., Cinti, F.R., Civico, R., Cucci, L., D'Addezio, G., DeRitis, R., Falcucci, E., Fracassi, U., Gasparini, A., Gori, S., Lisi, A., Mariano, S., Mariucci, M.T., Nappi, R., Pantosti, D., Patera, A., Pierdominici, S., Pignone, M., Pinzi, S., Pucci, S., Vannoli, P.,

Venuti, A., Villani, F., 2010. Evidence for surface rupture associated with the Mw 6.3 L'Aquila earthquake sequence of April 2009 (central Italy). Terra Nov. 22, 43–51. doi:10.1111/j.1365-3121.2009.00915.x

Montone, P., Mariucci, M.T., Pierdominici, S., 2012. The Italian present-day stress map. Geophys. J. Int. 189, 705–716. doi:10.1111/j.1365-246X.2012.05391.x

Morley, 1995. Developments in the structural geology of rifts over the last decade and their impact on hydrocarbon exploration. In: Lambiase, J.J. (Ed.), Hydrocarbon Habitat in Rift Basins, Geological Society Spec. Publ. 80, 1-32

Moro, M., Gori, S., Falcucci, E., Saroli, M., Galadini, F., Salvi, S., 2013. Historical earthquakes and variable kinematic behaviour of the 2009 L'Aquila seismic event (central Italy) causative fault, revealed by paleoseismological investigations. Tectonophysics 583, 131–144. doi:10.1016/j.tecto.2012.10.036

Morris, A., Ferrill, D.A., Henderson, D.B., Morris, A., Ferrill, D.A., Henderson, D.B., 1996. Slip-tendency analysis and fault reactivation. Geology 24, 275–278. doi:10.1130/0091-7613(1996)024<0275

Moulin A., Benedetti L., et al. (2016) The Dinaric fault system: Large-scale structure, rates of slip, and Plio-Pleistocene evolution of the transpressive northeastern boundary of the Adria microplate, Tectonics, 35, 10.1002/2016TC004188.

Neves, M.C., Paiva, L.T., Luis, J., 2009. Software for slip-tendency analysis in 3D: A plug-in for Coulomb. Comput. Geosci. 35, 2345–2352. doi:10.1016/j.cageo.2009.03.008

Pace, B., Boncio, P., Lavecchia, G., 2002. The 1984 Abruzzo earthquake (Italy): an example of seismogenic process controlled by interaction between differently oriented synkinematic faults 350, 237–254.

Palombo, M.R., Mussi, M., Agostini, S., Barbieri, M., Di Canzio, E., Di Rita, F., Fiore, I., Iacumin, P., Magri, D., Speranza, F., Tagliacozzo, A., 2010. Human peopling of Italian intramontane basins: The early Middle Pleistocene site of Pagliare di Sassa (L'Aquila, central Italy). Quat. Int. 223–224, 170–178. doi:10.1016/j.quaint.2009.10.038

Papanikolaou, I.D., Foumelis, M., Parcharidis, I., Lekkas, E.L., Fountoulis, I.G., 2010. Deformation pattern of the 6 and 7 April 2009, MW= 6.3 and MW= 5.6 earthquakes in L'Aquila (Central Italy) revealed by ground and space based observations. Nat. Hazards Earth Syst. Sci. 10, 73–87.

Pizzi, A., 2003. Plio-Quaternary uplift rates in the outer zone of the central Apennines fold-and-thrust belt, Italy. Quat. Int. 101–102, 229–237. doi:10.1016/S1040-6182(02)00105-2

Pizzi, A., Galadini, F., 2009. Pre-existing cross-structures and active fault segmentation in the northern-central Apennines (Italy). Tectonophysics 476, 304–319. doi:10.1016/j.tecto.2009.03.018

Pondrelli, S., Salimbeni, S., Morelli, A., Ekström, G., Olivieri, M., Boschi, E., 2010. Seismic moment tensors of the April 2009, L'Aquila (Central Italy), earthquake sequence. Geophys. J. Int. 180, 238–242. doi:10.1111/j.1365-246X.2009.04418.x

Porreca, M., Smedile, A., Speranza, F., Mochales Lopez, T., D'Ajello Caracciolo, F., Di Giulio, G., Vassallo, M., Villani, F., Nicolosi, I., Carluccio, R., Amoroso, S., Macrì, P., Buratti, N., Durante, F., Tallini, M., Sagnotti, L., 2016. Geological reconstruction in the area of maximum co-seismic subsidence during the 2009 Mw=6.1 L'Aquila earthquake using geophysical and borehole data. Ital. J. Geosci. 135, 350–362. doi:10.3301/IJG.2015.37

Prescott, J.R., Hutton, J.T., 1994. Cosmic ray contributions to dose rates for luminescence and ESR dating: large depths and long-term time variations. Radiation Measurements, 23, 497-500.

Pucci, S., Civico, R., Villani, F., Ricci, T., Delcher, E., Finizola, A., Sapia, V., De Martini, P.M., Pantosti, D., Barde-Cabusson, S., Brothelande, E., Gusset, R., Mezon, C., Orefice, S., Peltier, A., Poret, M., Torres, L., Suski, B., 2016. Deep electrical resistivity tomography along the tectonically active Middle Aterno Valley (2009 L'Aquila earthquake area, central Italy). Geophys. J. Int. 207, 967–982. doi:10.1093/gji/ggw308

Pucci, S., Villani, F., Civico, R., Pantosti, D., Del Carlo, P., Smedile, A., De Martini, P.M., Pons-Branchu,

E., Gueli, A., 2015. Quaternary geology of the Middle Aterno Valley, 2009 L'Aquila earthquake area (Abruzzi Apennines, Italy). J. Maps 11. doi:10.1080/17445647.2014.927128

Reeve, M.T., Bell, R.E., Duffy, O.B., Jackson, C.A.L., Sansom, E., 2015. The growth of non-colinear normal fault systems; What can we learn from 3D seismic reflection data? J. Struct. Geol. 70, 141–155. doi:10.1016/j.jsg.2014.11.007

Ristuccia, G. M., Di Stefano, A., Gueli, A. M., Monaco, C., Stella, G., Troja, S. O., 2013. OSL chronology of quaternary deposits outcropping between Mt. Etna volcano and the Catania Plain (Sicily, southern Italy). Physics and Chemistry of the Earth, 63, 36-46.

Roberts, H. M., 2006. Optical dating of coarse-silt sized quartz from loess: evaluation of equivalent dose determinations and SAR procedural checks. Radiation Measurements, 41, 923–929.

Roberts, G.P., Michetti, A.M., 2004. Spatial and temporal variations in growth rates along active normal fault systems: An example from The Lazio-Abruzzo Apennines, central Italy. J. Struct. Geol. 26, 339–376. doi:10.1016/S0191-8141(03)00103-2

Rovida A., Locati M., Camassi R., Lolli B., Gasperini P. (eds), 2016. CPTI15, the 2015 version of the Parametric Catalogue of Italian Earthquakes. Istituto Nazionale di Geofisica e Vulcanologia. doi:http://doi.org/10.6092/INGV.IT-CPTI15

Santo, A., Ascione, A., Di Crescenzo, G., Miccadei, E., Piacentini, T., Valente, E., 2014. Tectonic-geomorphological map of the middle Aterno river valley (Abruzzo, Central Italy). J. Maps 10, 365–378.

Schimmelpfennig, I., Benedetti, L., Finkel, R., Pik, R., Blard, P. H., Bourlès, D., Burnard, P., Williams, A., 2009. Sources of in-situ 36Cl in basaltic rocks. Implications for calibration of production rates. Quaternary Geochronology, 4(6), 441-461.

Schimmelpfennig, I., Benedetti, L., Garreta, V., Pik, R., Blard, P. H., Burnard, P., Bourlès, D., Finkel, R., Ammon, K., & Dunai, T., 2011. Calibration of cosmogenic 36Cl production rates from Ca and K spallation in lava flows from Mt. Etna (38° N, Italy) and Payun Matru (36° S, Argentina). Geochimica et Cosmochimica Acta, 75(10), 2611-2632.

Schlagenhauf, A., Gaudemer, Y., Benedetti, L., Manighetti, I., Palumbo, L., Schimmelpfennig, I., Finkel, R., Pou, K., 2010. Using in situ Chlorine-36 cosmonuclide to recover past earthquake histories on limestone normal fault scarps: A reappraisal of methodology and interpretations. Geophys. J. Int. 182, 36–72. doi:10.1111/j.1365-246X.2010.04622.x

Scholz, C.H., Gupta, A., 2000. Fault interactions and seismic hazard. J. Geodyn. 29, 459–467. doi:10.1016/S0264-3707(99)00040-X

Schwartz, D.P., Coppersmith, K.J., 1984. Fault behavior and characteristic earthquakes: Examples from the Wasatch and San Andreas fault zones. J. Geophys. Res. B Solid Earth 89, 5681–5698.

Scognamiglio, L., Tinti, E., Michelini, A., Dreger, D.S., Cirella, A., Cocco, M., Mazza, S., Piatanesi, A., 2010. Fast determination of moment tensors and rupture history: what has been learned from the 6 April 2009 L'Aquila earthquake sequence. Seismol. Res. Lett. 81, 892–906. doi:10.1785/gssrl.81.6.892

Scognamiglio, L., Tinti, E., Casarotti, E., Pucci, S., Villani, F., Cocco, M., Magnoni, F., Michelini, A. Dreger, D., 2018. Complex Fault Geometry and Rupture Dynamics of the Mw 6.5, 30 October 2016, Central Italy Earthquake. Journal of Geophysical Research: Solid Earth, 123(4), 2943-2964. doi: 10.1002/2018JB015603

Sharma, P., Kubik, P. W., Fehn, U., Gove, H. E., Nishiizumi, K., Elmore, D., 1990. Development of 36 Cl standards for AMS. Nuclear Instruments and Methods in Physics Research Section B: Beam Interactions with Materials and Atoms, 52(3), 410-415.

Siame, L., Bellier, O., Braucher, R., Sébrier, M., Cushing, M., Bourlès, D., Hamelin, B., Baroux, E., de Voogd, B., Raisbeck, G., Yiou, F., 2004. Local erosion rates versus active tectonics: cosmic ray

exposure modelling in Provence (southeast France). Earth and Planetary Science Letters, 220(3), 345-364.
Sieh, K., 1996. The repetition of large-earthquake ruptures. Proceedings of the National Academy of Sciences, 93(9), 3764-3771.
Stevens, T., Armitage, S. J., Lu, H., Thomas, D. S. G., 2007. Examining the potential of high sampling resolution OSL dating of Chinese loess. Quaternary Geochronology 2, 1–4, 15-22.
Stone, J. O., 2000. Air pressure and cosmogenic isotope production. J. Geophys. Res. B Solid Earth 105, B10, 23,753-23,759. doi: 10.1029/2000JB900181
Tallini, M., Cavuoto, G., Monaco, F., Del Fiore, V., Di Mancini, M., Caielli, G., Cavinato, G.P., Franco, R., De Pelosi, N., Rapolla, A., 2012. Seismic surveys integrated with geological data for in-depth investigation of Mt. Pettino active fault area (western L'Aquila basin). Ital. J. Geosci. 131, 389–402. doi:10.3301/IJG.2012.10
Tarquini S., Isola, I., Favalli, M., Mazzarini, F., Bisson, M., Pareschi, M.T., Boschi, E., 2007. TINITALY/01: a new Triangular Irregular Network of Italy, Annals of Geophysics, 50, 407-425.
Tavarnelli, E., 1999. Normal faults in thrust sheets: Pre-orogenic extension, post-orogenic extension, or both? J. Struct. Geol. 21, 1011–1018. doi:10.1016/S0191-8141(99)00034-6
Toda, S., Stein, R.S., Sevilgen, V., Lin, J., 2011. Coulomb 3.3. Graphic-rich deformation & stress-change software for earthquake, tectonic and volcano research and teaching.
Trasatti, E., Kyriakopoulos, C., Chini, M., 2011. Finite element inversion of DInSAR data from the Mw 6.3 L'Aquila earthquake, 2009 (Italy). Geophys. Res. Lett. 38, 1–6. doi:10.1029/2011GL046714
Valoroso, L., Chiaraluce, L., Collettini, C., 2014. Earthquakes and fault zone structure. Geology 42, 343–346. doi:10.1130/G35071.1
Valoroso, L., Chiaraluce, L., Piccinini, D., Di Stefano, R., Schaff, D., Waldhauser, F., 2013. Radiography of a normal fault system by 64,000 high-precision earthquake locations: The 2009 L'Aquila (central Italy) case study. J. Geophys. Res. Solid Earth 118, 1156–1176. doi:10.1002/jgrb.50130
Vannoli, P., Burrato, P., Fracassi, U., Valensise, G., 2012. A fresh look at the seismotectonics of the Abruzzi (Central Apennines) following the 6 April 2009 L ' Aquila earthquake (M w 6 . 3). Ital. J. Geosci. 131, 309–329. doi:10.3301/IJG.2012.03
Vezzani, L., Festa, A., Ghisetti, F.C., 2010. Geology and tectonic evolution of the Central-Southern Apennines, Italy. Geol. Soc. Am. Spec. Pap. 469, 1–58.
Villani, F., Improta, L., Pucci, S., Civico, R., Bruno, P.P.G., Pantosti, D., 2017. Investigating the architecture of the Paganica Fault (2009 M_w6.1 earthquake, central Italy) by integrating high-resolution multiscale refraction tomography and detailed geological mapping. Geophys. J. Int. 208. doi:10.1093/gji/ggw407
Villani, F., Pucci, S., Civico, R., De Martini, P.M., Nicolosi, I., Caracciolo, F.D.A., Carluccio, R., Di Giulio, G., Vassallo, M., Smedile, A., Pantosti, D., 2015. Imaging the structural style of an active normal fault through multidisciplinary geophysical investigation: A case study from the M<inf>W</inf> 6.1, 2009 L'Aquila earthquake region (central Italy). Geophys. J. Int. 200, 1676–1691. doi:10.1093/gji/ggu462
Viseras, C., Calvache, M. L., Soria J. M., Fernández, J., 2003. Differential features of alluvial fans controlled by tectonic or eustatic accommodation space. Examples from the Betic Cordillera, Spain. Geomorphology, 50, 1–3, 181-202
Vittori, E., di Manna, P., Blumetti, A.M., Comerci, V., Guerrieri, L., Esposito, E., Michetti, A.M., Porfido, S., Piccardi, L., Roberts, G.P., Berlusconi, A., Livio, F., Sileo, G., Wilkinson, M., McCaffrey, K.J.W., Phillips, R.J., Cowie, P.A., 2011. Surface faulting of the 6 April 2009 mw 6.3 L'Aquila earthquake in central Italy. Bull. Seismol. Soc. Am. 101, 1507–1530. doi:10.1785/0120100140
Wells, D.L., Coppersmith, K.J., 1994. New empirical relationships among magnitude, rupture length, rupture width, rupture area, and surface displacement. Bull. Seismol. Soc. Am. 84, 974–1002.

Wesnousky, S.G., 2006. Predicting the endpoints of earthquake ruptures. Nature 444, 358–360. doi:10.1038/nature05275

Wesnousky, S.G., 2008. Displacement and geometrical characteristics of earthquake surface ruptures: Issues and implications for seismic-hazard analysis and the process of earthquake rupture. Bull. Seismol. Soc. Am. 98 (4), 109-1632.

Wintle, A. G., Murray, A. S., 2000. Quartz OSL: effects of thermal treatment and their relevance to laboratory dating procedures. Radiation Measurements, 32, 387– 400.

Zijderveld, J.D.A., 1967. A.C. demagnetization of rocks: analysis of results, In: D.W. Collinson, K.M. Creer and S.K. Runcorn (eds.), Methods in Palaeomagnetism, Amsterdam, Elsevier, 254-286.

Appendix

Appendix A: Paleostress analysis

The paleo-stress inversion was (Angelier and Mechler, 1979) implemented in the WinTensor software v5.8.8 (Delvaux and Sperner, 2003) in order to retrieve the dominant faulting regime and the orientation of the three principal stress axes and their relative magnitudes.

The used improved right-dihedron method consists in the following steps. Each fault plane-slip vector pair with sense of movement defines compressional and extensional quadrants, which are plotted on the reference-counting grid net (made of 384 cells): all orientations falling in the extensional quadrants are given a counting value of 100%, while those falling in the compressional quadrants are assigned 0%. This procedure is then repeated for all fault-slip vector pairs: the counting values are summed and divided by the total number of faults. The resulting grid net of average counting values is used to define the possible orientations of σl and σ3, which correspond to the cells that have values of 0% and 100%, respectively. The stress ratio is computed through the relation R = (100 -S2val)/100, where S2val is the counting value on the reference grid closest to σ2 orientation.

The improved method also provides a counting deviation (CD, expressed in %), which is used as a compatibility criterion of fault slip data. Each fault-slip vector pair is multiplied by its weighting factor; the difference between the individual and the previously obtained average counting net is computed in order to obtain a differential counting net; the operation is repeated for all data to obtain a deviation histogram: the CD value is the average of all the differential counting grids. The compatibility of individual data with the entire data subset is estimated by the standard deviation of the individual CD values from the average of the differential counting grids: smaller standard deviations suggest high kinematic compatibility with the final average counting net.

Our subsets (Tab. A1, A2 and A3) shown in Figures A1, A2 and A3 relate to three different fault populations indicating a strike-slip regime, a re-activation through normal-faulting regime and a final normal faulting regime, respectively. The relatively large values of CD for the three datasets (>30%) are due to the oblique kinematics of the majority of the investigated faults. This denotes a quite complex kinematic evolution, with possible multiple episodes of re-activation, not easy to summarize into three discrete tectonic events.

	trend	Plunge
σ1	240	0
σ2	331	81
σ3	150	9
R	0.56	
SHmax	60	0.8
Stress regime	SS	
Data	50	

Table A1. Subset 1 results.

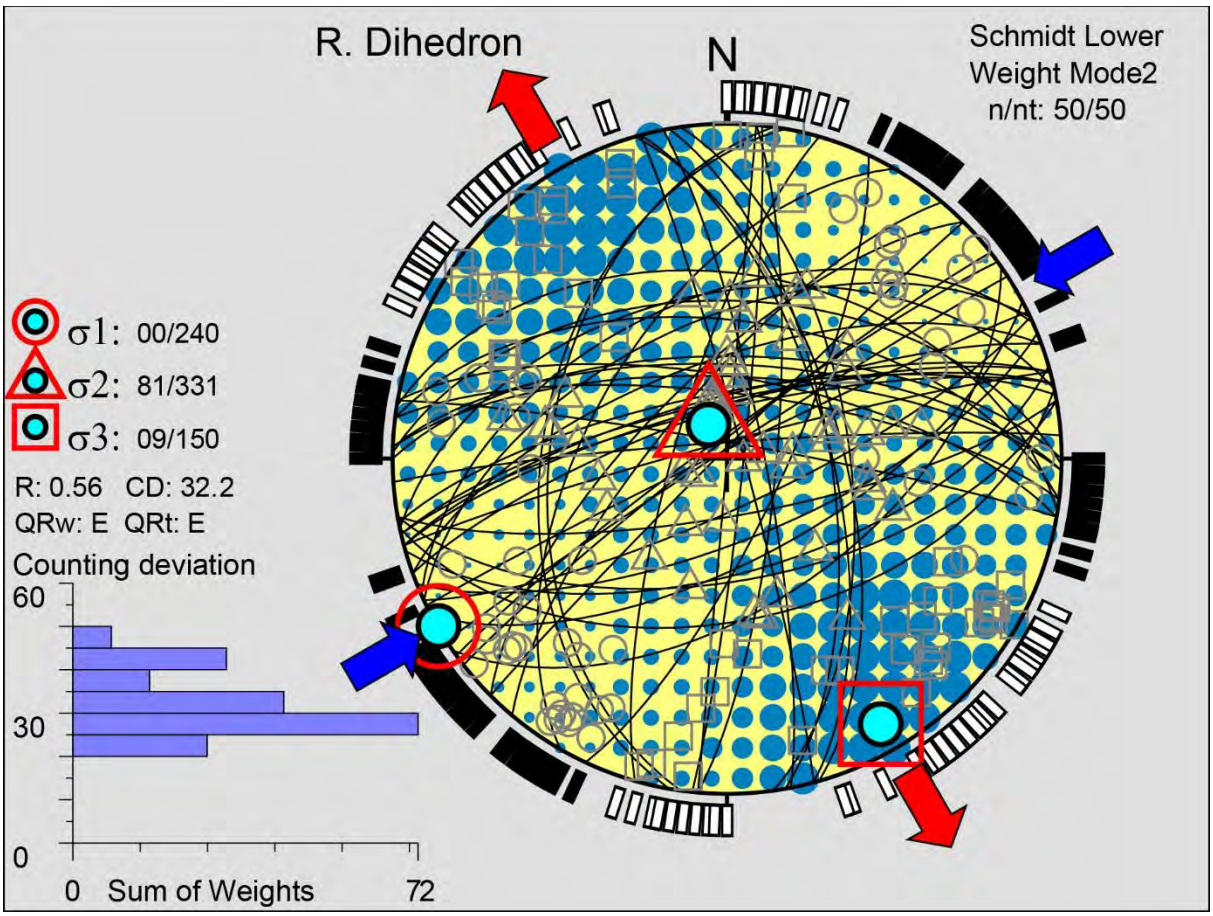

1547

1548 **Figure A1.** Fault plane-slip vector plot for Subset 1. Counting deviation (CD) and its standard deviation are

1549 reported.

	trend	Plunge
σ1	198	78
σ2	322	8
σ3	63	8
R	0.6	
SHmax	154	
Stress regime	NF	
Data	88	

1550 **Table A2.** Subset 2 results.

1551

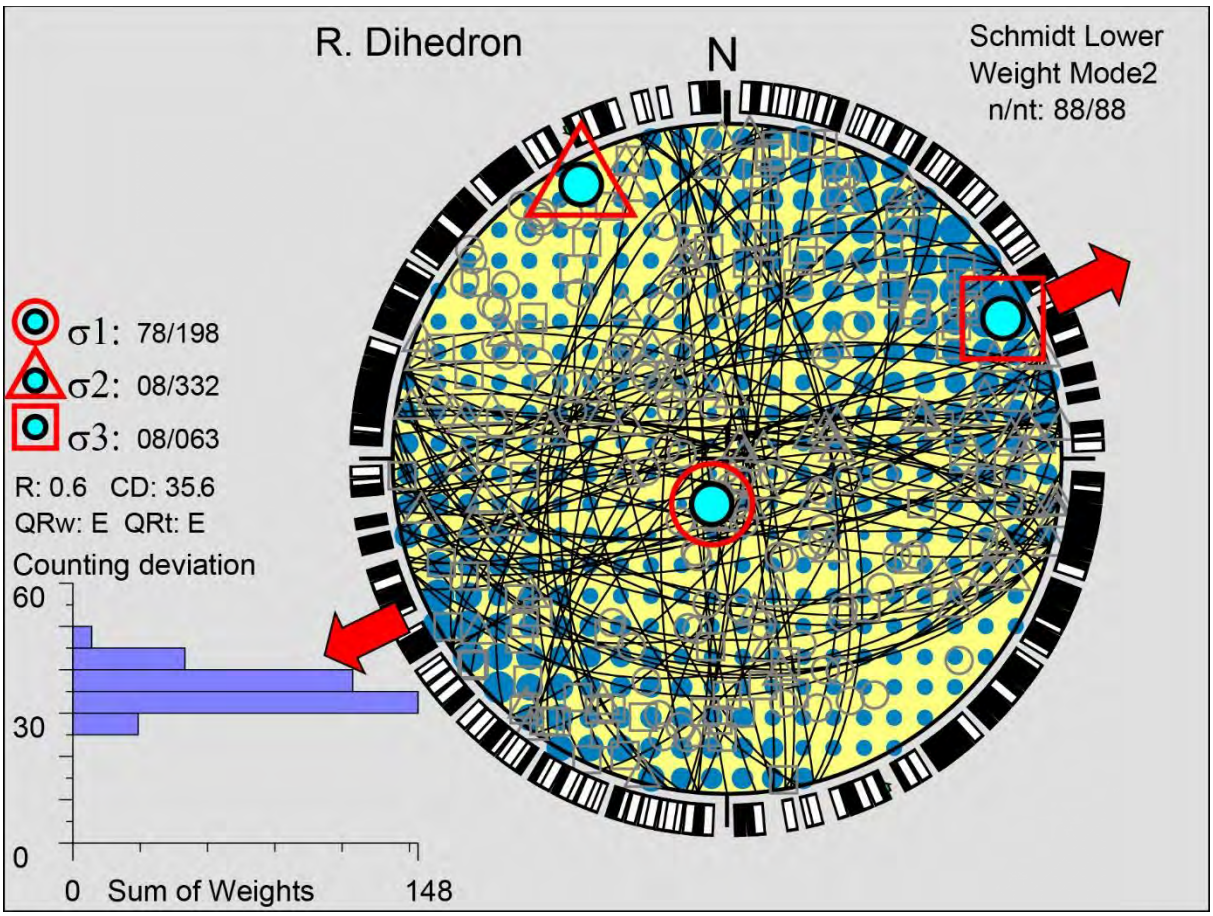

Figure A2. Fault plane-slip vector plot for Subset 2. Counting deviation (CD) and its standard deviation are reported.

	trend	Plunge
σ1	329	77
σ2	150	13
σ3	60	0
R	0.42	
SHmax	150	
Stress regime	NF	
Data	44	

Table A3. Subset 3 results.

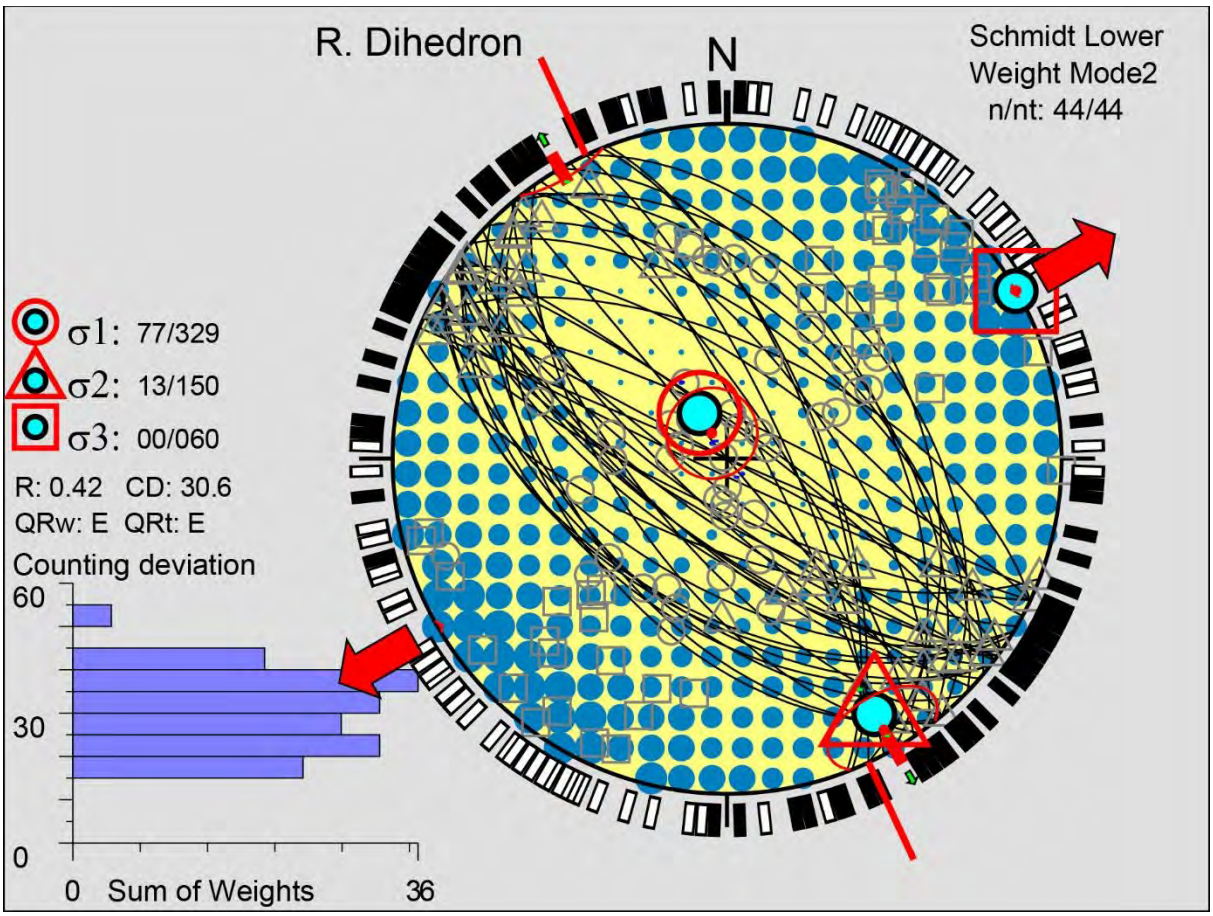

Figure A3. Fault plane-slip vector plot for Subset 3. Counting deviation (CD) and its standard deviation are reported.

Appendix B: Slip tendency analysis

According to Neves et al. (2009), the slip-tendency of a surface is defined as the ratio of the shear stress to the normal stress on that surface, evaluated in a mechanical system independent of fluid pressure and differential stress. We thus assumed the following conditions: an homogeneous stress field, with a minimum horizontal compressive stress oriented 225°N, consistent with the strain tensor from the population of the NW-trending faults (see 3.1.2) and with regional stress data (Montone et al., 2012); a principal stress difference ratio of 0.5 (Bagh et al., 2007); a fault friction coefficient of 0.6 (Byerlee, 1978). We adopted a simplified geometry for the analysed fault systems (Fig. B), characterized by planar surfaces up to 10 km deep, and the slip-tendency was calculated at 5 km of depth, which is the typical centroid depth of most crustal earthquakes in this region (Chiarabba et al., 2005). In particular, the applied fault network model is composed of 13 NW-trending (e.g. CTO, CPT, MMA, MPE, BAR, MRU, BAZ, FOS, STI, PAG, SAG, SDE, MAFS), 11 E-W-trending (e.g. ASS, MST, SGO, COL, SEL, CAP, SPO, CHI, VOR) and 5 N-

S-striking faults (e.g. RAI, BAG, CAM) (Fig. 1 and 2).

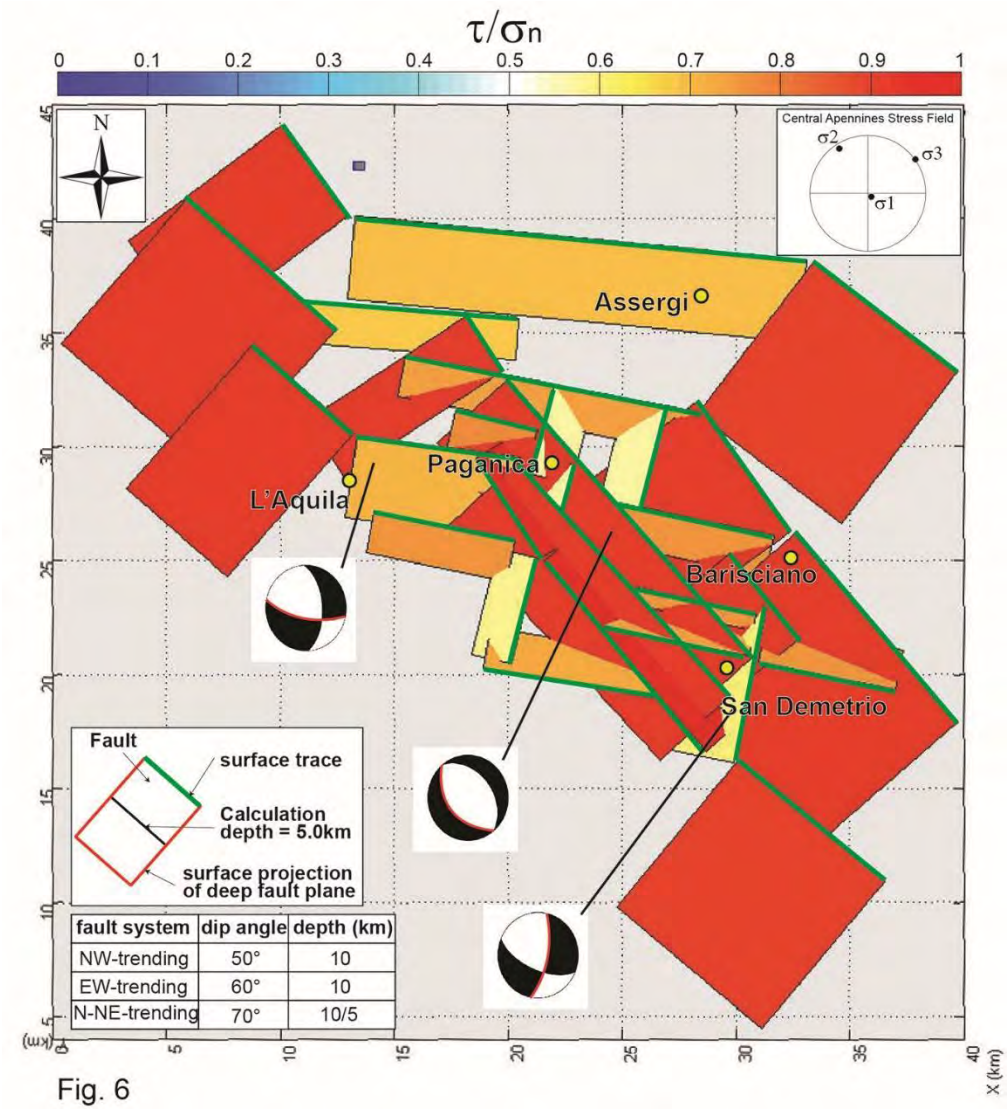

Fig. 6

Figure B. Map view of the slip-tendency analysis for the recognized fault systems (from the Coulomb 3.3 Matlab Plug-in; Neves et al., 2009; Toda et al., 2011). The modelled fault network derives from a simplified geometry of the main fault systems splays (see inset table for the applied geometrical data). The results are calculated on the fault plane at 5.0 km of depth. The axes of the present-day central Apennine extensional stress field is shown as stereographic plots (lower hemisphere) (Bagh et al., 2007). Examples of predicted focal mechanisms for the main fault trends are plotted.

Appendix C: Optical Stimulated Luminescence (OSL) dating method and results

The Optically Stimulated Luminescence (OSL) dating technique is based on the assumption that the light-sensitive signal of crystalline inclusions contained in sedimentary deposits has been zeroed during the last exposure to the sunlight. The time elapsed between this "bleaching event" and OSL measurements corresponds to the age of the sample (Huntley et al., 1985; Aitken, 1998). The OSL age (Age) is determined from the ratio of Equivalent Dose (ED) to Dose Rate (DR) (Table C), the two physical parameters related to, respectively, energy absorbed by the unit of mass of the sample (in Gray) and energy absorbed by the unit of time, generally in years (in Gy/a). The ED is the total dose accumulated since the last exposure to light, measured using luminescence signals, and DR is the quantity of the dose absorbed in a year due to the radioactivity from the sample, from its environment and from cosmic radiation.

The samples were collected by hammering opaque PVC tubes into the sediment of interest covered by a black cloth. The tubes were then placed in sealed black opaque plastic bags to prevent exposure to light and to preserve their natural moisture content. In situ measurement of humidity (by means of Field Scout TDR100 soil moisture meter) and environmental dose rate (by means of Gamma Scout, β and γ Geiger counter) were also performed.

Two samples were analysed by Steven L. Forman, at the Luminescence Dating Research Laboratory, Department of Earth and Environmental Science, University of Illinois – Chicago, USA. ED was determined by the multiple aliquot regenerative dose technique under blue light excitation (470 ± 20 nm) after infrared excitation (Jain et al., 2003). Blue emissions were measured with 3-mm-thick Schott BG-39 and one 3-mm-thick Corning 7-59 glass filters that block >90% of luminescence emitted below 390 nm and above 490 nm in front of the photomultiplier tube. The coarse-grained (100-250 μm) quartz fraction was analysed.

Four samples were analysed at the PH3DRA laboratories of INFN, Catania (Italy). A standard protocol used routinely for sediments dating was applied (Giunta et al., 2012; Ristuccia et al., 2013; Bottari

et al., 2013). ED is obtained from OSL emissions evaluated with the Single-Aliquot Regenerative-dose (SAR) protocol (Murray and Wintle, 2000; 2003) on coarse-grained quartz inclusions extracted from the sample (Fuchs and Lang, 2001; Carobene et al., 2006; Stevens et al., 2007). The DR contributions were evaluated from the sample radioactive contents while the cosmic dose rate was calculated considering the depth and the density of each sample (Prescott and Hutton, 1994). Luminescence measurements were performed on small aliquots (Duller, 2008; Gerardi et al., 2012) of quartz grains (100–300 μm) using a Risø TL-DA-15 reader equipped with an EMI9235QA photomultiplier (Bøtter -Jensen et al., 2000). The feldspar contamination was checked using IR stimulation (Choi et al., 2009) and the preheat parameters were based on test measurements (Wintle and Murray, 2000; Murray and Wintle, 2003). Only the aliquots that pass the recycling (Roberts, 2006) and recovery (Murray and Wintle, 2003) tests were considered for ED evaluation. All procedures were performed in dim red light. U, Th, Rb and K_20 content were determined by inductively coupled plasma-mass spectrometry (ICP-MS) at the Activation Laboratories Ltd., Ancaster, Ontario, Canada and used to estimate beta (D_β) and gamma (D_γ) dose contributions. Ages included a cosmic ray dose rate component from calculations of Prescott and Hutton (1994). Using the conversion factors of Guérin et al. (2011), beta attenuation factors depending on grain size (Mejdahl, 1979) and water content, the DR values were obtained.

OSL ID	Lab	Grain size (μ)	ED (Gy)	U (ppm)	Th (ppm)	K_20 (%)	H_20 (%)	cosmic(Gy/ka)	DR (Gy/ka)	Age (ka)
1	INFN	100-300	63.2 ±4.5	3.50 ±0.18	14.3 ±0.72	1.24 ±0.01		1.26 ±0.04	2.45 ±0.11	**26 ±2**
2	INFN	100-300	107.3 ±7.4	1.90 ±0.10	3.80 ±0.19	0.45 ±0.01		0.62 ±0.02	1.13 ±0.05	**95 ±8**
3	UIC	100-150	42.95 ± 2.77	2.4 ± 0.1	6.5 ± 0.1	0.76± 0.01	15 ± 5	0.18 ±0.02	1.59 ±0.08	**27 ±2**
4	UIC	150-250	348.63 ± 3.11	1.1 ± 0.1	4.4 ± 0.1	1.92 ± 0.02	10 ± 3	0.18 ±0.02	2.03 ±0.10	**172 ±12**
5	INFN	100-300	217.0 ±14.0	2.90 ±0.15	5.2 ±0.26	1.47 ±0.01		0.96 ±0.02	2.14 ±0.07	**102 ±7**
6	INFN	100-300	258.0 ±10	0.30 ±0.06	28 ±1.41	1.16 ±0.01		1.53 ±0.06	2.64 ±0.14	**98 ±6**

Table C. Results of the Optical Stimulated Luminescence (OSL) samples analysis. All errors are at one sigma except for ED (see Fig C for radial plots). See figures 8-11 for locations.

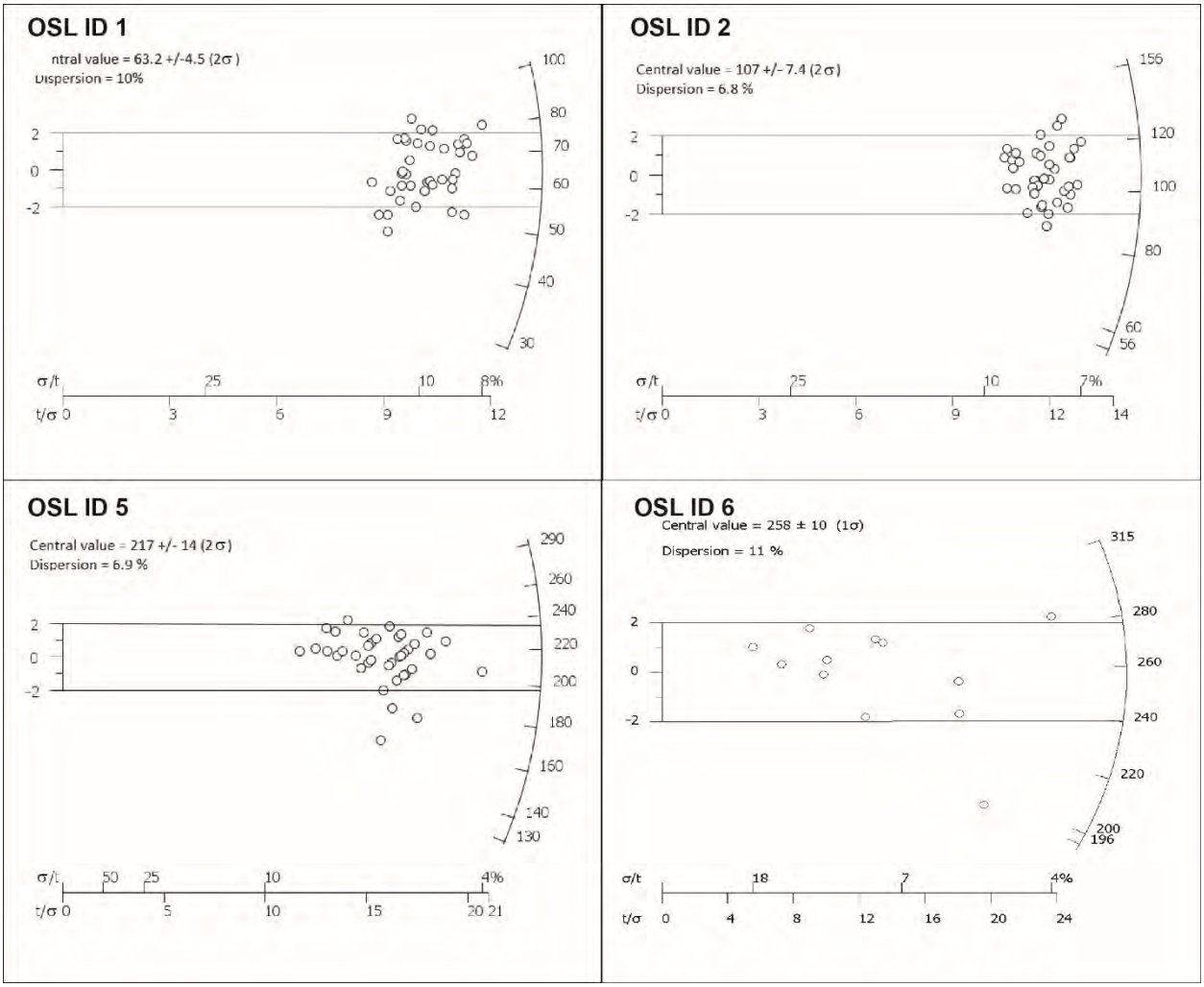

Figure C. Radial plots from the Central Age Model (CAM) used to determine the ED (only for samples analysed at the PH3DRA laboratories).

Appendix D: Terrestrial Cosmonucleid (TCN) dating method and results

We performed a depth profile sampling of a depositional paleosurface (from the surface down to 6 m depth) to determine its age of emplacement with ^{36}Cl cosmogenic nuclide exposure dating, as already done elsewhere (e.g. Le Dortz et al., 2011; Moulin et al., 2016). The sampling was done in a quarry exposure. The deposit is composed of well-rounded pebbles and cobbles with various diameters of up to 30 cm in a sand matrix that represents about 20% of the material. The pebbles and cobbles mainly consist of limestone representative of the lithology of the drained watershed. Moreover, although the initial signs of cementation can be observed on the upper part, the resulting conglomerate is loosely consolidated.

^{36}Cl accumulates in near surface carbonates mostly because of the interactions of Ca with high energetic neutrons and muons from cosmic rays. The samples were crushed, sieved, and chlorine was chemically extracted using AgCl (Schlagenhauf et al. 2010 and references therein). Natural Chlorine (hereafter $Cl_{nat)}$ and ^{36}Cl concentrations were then determined via isotope dilution accelerator mass spectrometry based on the measured $^{35}Cl/^{37}Cl$ and $^{36}Cl/^{35}Cl$ ratio measurements performed at the French national accelerator mass spectrometry (AMS) facility Accélérateur pour les Sciences de la Terre, Environnement, Risques (ASTER) (CEREGE). The ^{36}Cl concentrations were normalized to a ^{36}Cl standard prepared by K. Nishiizumi: KNSTD1600, with a nominal $^{36}Cl/^{35}Cl$ value of $2.11\pm0.06\times10^{-12}$ (Sharma et al., 1990; Fifield et al., 1990). The decay constant of $2.303\pm0.016\times10^{-6}$ yr^{-1} used corresponds to a ^{36}Cl half-life (T1/2) of 3.014×10^{5} years. The analytical uncertainties include counting statistics, machine stability, and blank correction. The measured ^{36}Cl amounts range from ~10^{7} to ~6×10^{7} atoms, 2 order of magnitude higher than that measured in the blanks (10^{5} atoms of ^{36}Cl). The measured amount of Cl_{nat} in the samples is 10 times higher than the amount measured in the blanks. Cl_{nat} concentrations are between 45 and 52 ppm. The ^{36}Cl production rate from spallation of calcium has been calibrated in Sicily by Schimmelpfennig et al., (2011). Because the sampling area is located almost at the same latitude and elevation as this calibration site, we used the calibrated production rate of 42.2±4.8 atoms/g/yr. Scaling with respect to latitude and

elevation was performed considering constant geomagnetic field intensity and using the Stone (2000) scheme. Finally, the Excel spreadsheet provided by Schimmelpfennig et al., (2009) was used to calculate all of the ^{36}Cl production pathways. The density of the deposit was estimated at 2.2 ± 0.3 g/cm^3 (Gruppo di Lavoro MS–AQ, 2010). The ^{36}Cl concentration along the profile depends on the surface denudation rate, the inheritance, and the exposure duration. The concentrations were modelled by varying all three parameters (Braucher et al., 2009) or by fixing some of the parameters to test their respective influences on the resulting CRE ages. The best fit was determined by using a chi-square (χ^2) inversion (e.g., Siame et al., 2004; Braucher et al., 2009).

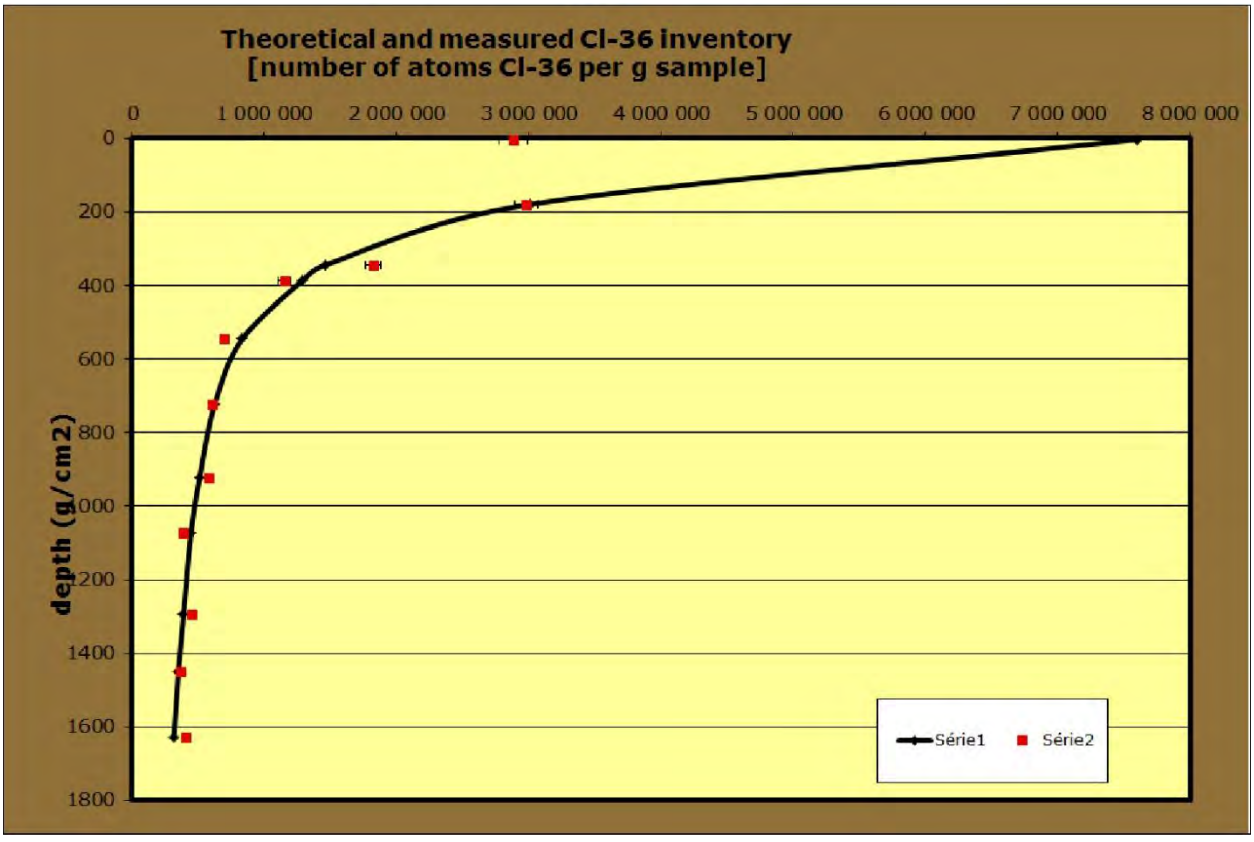

Figure D. Depth profile of the Valle Daria surface. Example of theoretical ^{36}Cl concentration inventory for ~600ka with $\chi^2 = 120$, $\rho = 2.4$ g/cm^3 and denudation rate of 2 m/Ma.

1667

Appendix E: Paleomagnetic field analysis method and results

Since coarse-grained continental deposits do not generally contain sediments or other material suitable for biostratigraphic or radiometric dating, we performed a paleomagnetic sampling of the cemented breccia and conglomerate deposits aiming to analyse their matrix, when present. At each site, cores were drilled with an ASC 280E petrol-powered portable drill and oriented in situ by a magnetic compass. From each core, one to three standard (25 mm, diameter 22 mm height) cylindrical specimens were cut. Paleomagnetic measurements were carried out at the paleomagnetic laboratory of Istituto Nazionale di Geofisica e Vulcanologia (Rome, Italy) on discrete samples using a 2G Enterprises DC SQUID superconducting rock magnetometer. The natural remnant magnetization (NRM) of the samples was analysed by means of both progressive stepwise thermal demagnetization and alternating field (AF) demagnetization. The results indicate that thermal and AF demagnetization are equally effective in isolating the characteristic remanent magnetization (ChRM). Demagnetization data were plotted as demagnetization intensity graphs and Zijderveld (1967) plots. NRM directions were calculated by principal component analysis (Kirschvink, 1980) and plotted on equiareal projections.

Examples of orthogonal projections of demagnetisation data are shown in figure E1. In most of the case we isolate a single magnetization characterized by regular decrease of magnetization with temperature or applied field. The paleomagnetic behaviour is regular in both normal and reverse magnetic polarity samples. The site mean directions are quite well defined, and are better grouped in the geographic reference frame before tilt correction (Fig. E2). This grouping suggests that these units were deposited onto original inclined paleo-surfaces and subsequent tectonic tilting was negligible.

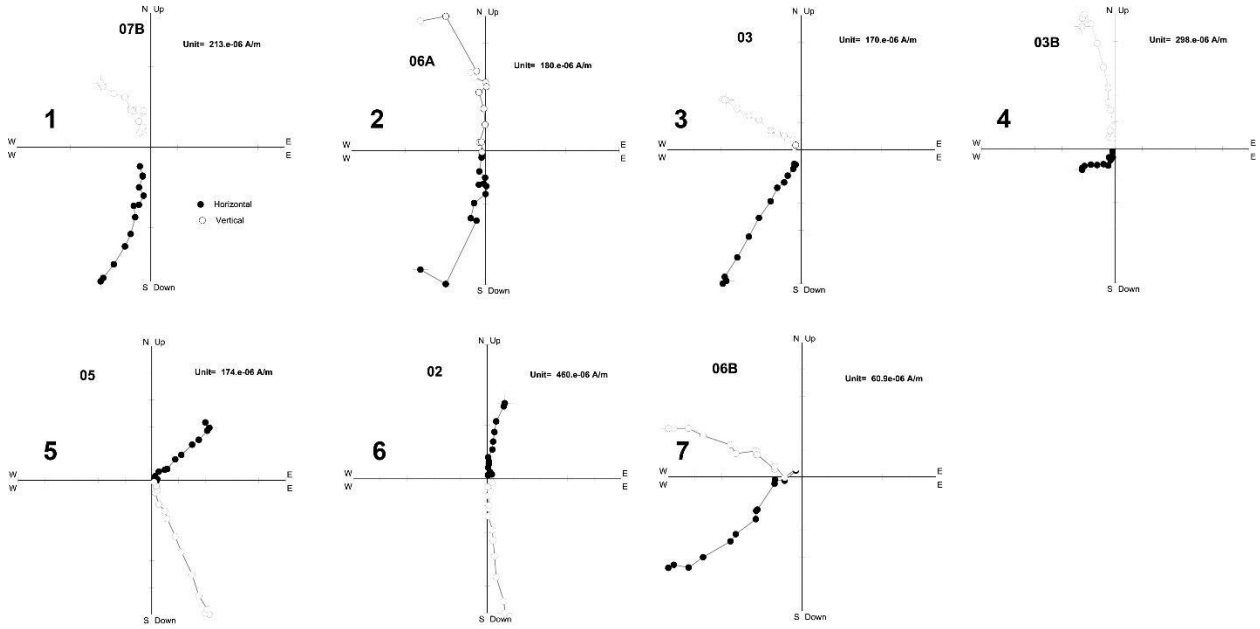

1688

1689 **Figure E1.** Orthogonal diagrams showing a reverse (a) and normal (b) magnetic polarity samples. The first

1690 was thermally demagnetized, whereas the second one was demagnetized by alternate field.

1691

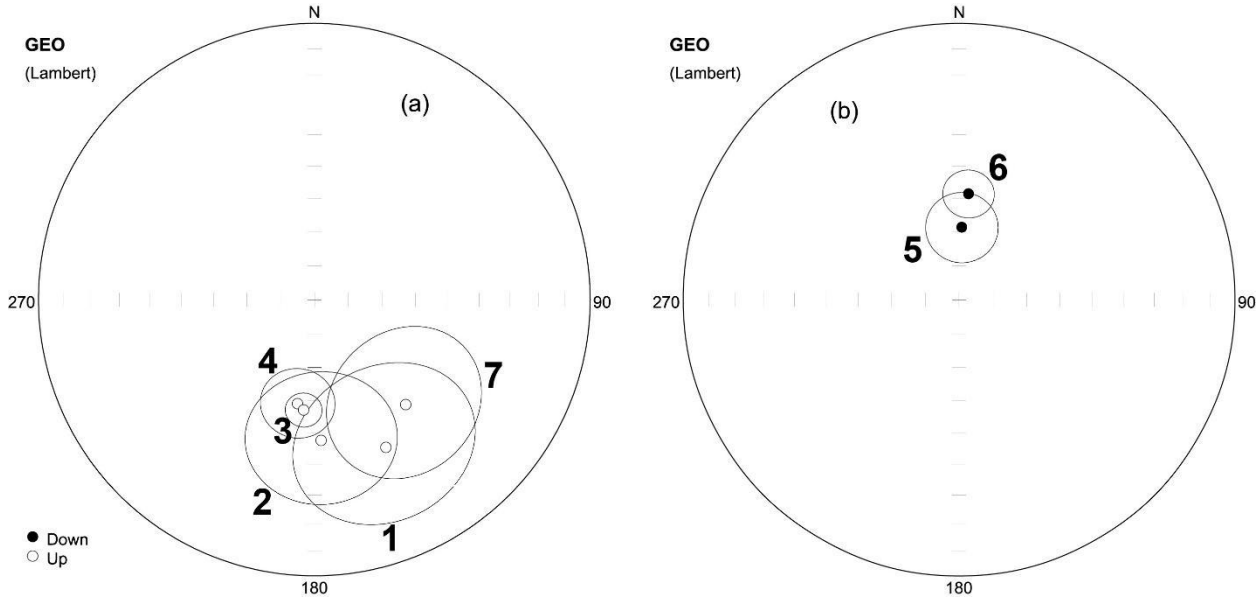

1692

Figure E2. Equal-area, upper hemisphere projections in geographic coordinates of the characteristic component vectors from reverse (a) and normal (b) magnetic polarity sites, with the associated cone of 95% confidence. Red circle, site mean direction, with the cone of 95% confidence. See the text for paleomagnetic mean directions.

Paleomag ID	Lat	Long	Location	n	Dg	Ig	a95	Dt	It	a95	Polarity
1	42,35489	13,4857	Paganica	9	154	-40,3	25,9	166,7	-37,1	23,7	**Reverse**
2	42,34141	13,5142	S. Valentino Valley	5	177	-47,7	21	146,1	-42,3	21,3	**Reverse**
3	42,32993	13,5211	Petogna	19	185,6	-57	5,2	210,4	-65,4	6	**Reverse**
4	42,33041	13,58938	Barisciano Nord	14	189,2	-58,7	10,6	-	-	-	**Reverse**
5	42,19848	13,34789	Vedice Valley outlet	4	2.2°	68.6°	10,5	59.6°	60.2°	10,5	**Normal**
6	42,3297	13,58145	Vedice Valley outlet	10	5	58,4	7,3	45,1	74,2	8,8	**Normal**
7	42,36689	13,5624	La Villa basin	12	138,9	-48,2	22,6	174,1	-46,7	27,6	**Reverse**

Table E. Paleomagnetic samples. Latitude and longitude in CGS and wgs84; n: number of measured samples; Dg, Ig: Declination and Inclination in geographic coordinates; Dt, It: Declination and Inclination after tectonic tilting; a95: 95% ellipse of confidence. See figures 8-11 for locations (except sample 7, localized in Fig. 2).